Dário Bokiló Machado Teca

Licenciado em Engenharia Geológica

Correction of the Anisotropy in Resistivity: Application to Pore Pressure Prediction

Dissertação para obtenção do Grau de Mestre em Engenharia Geológica (Georrecursos)

Orientador: Doutor José António de Almeida

Prof. Associado, Faculdade de Ciências e Tecnologia da UNL

Co-orientador: Engenheiro Tristan Cornu

Pore Pressure and Rock Mechanics Specialist, Empresa Total EP Angola

Júri:

Presidente: Doutor Paulo do Carmo Sá Caetano

Arguente: Doutora Ana Paula Fernandes da Silva

Vogal: Doutor José António de Almeida

FACULDADE DE CIÊNCIAS E TECNOLOGIA
UNIVERSIDADE NOVA DE LISBOA

Julho 2014

Dário Bokiló Machado Teca

Licenciado em Engenharia Geológica

Correction of the Anisotropy in Resistivity: Application to Pore Pressure Prediction

Dissertação para obtenção do Grau de Mestre em Engenharia Geológica (Georrecursos)

Orientador: Doutor José António de Almeida

Prof. Associado, Faculdade de Ciências e Tecnologia da UNL

Co-orientador: Engenheiro Tristan Cornu

Pore Pressure and Rock Mechanics Specialist, Empresa Total EP Angola

Julho 2014

Correction of the Anisotropy in Resistivity: Application to Pore Pressure Prediction

AGRADECIMENTOS

Este trabalho é o resultado do meu estágio com a empresa Total EP Angola, que começou no dia 8 de julho de 2013 e terminou ao 5 de dezembro de 2013. O meu supervisor de estágio foi o especialista em "pore pressure", Eng.º Tristan Cornu da Total EP Angola e o supervisor externo foi o Doutor José António de Almeida da Faculdade de Ciências e Tecnologia - Universidade Nova de Lisboa. O estágio foi realizado no Departamento de Direção de Exploração / subsuperfície da Total EP Angola.

Em primeiro lugar quero agradecer a Total EP Angola pela oportunidade do estágio e finalizar a minha tese de mestrado nas suas instalações. Agradeço ao meu supervisor Eng.º Cornu, que me explicou pacientemente muitos detalhes técnicos e me apoiou nos momentos difíceis do estágio.

Agradeço ao meu grande amigo e colega Erik Ferreira por me ter apresentado a Total EP Angola.

Aos meus pais e irmãos pelo apoio e compreensão pela minha ausência nos momentos em que a minha presença era fundamental.

Agradeço a todos os meus professores no Departamento de Ciências da Terra, pelos ensinamentos, conselhos e pelas oportunidades que me foram dadas durante a formação académica. Destaco os meus agradecimentos ao professor Doutor José Carlos Kullberg por me ter ajudado na conclusão da minha licenciatura e o professor Doutor José António de Almeida pela co-supervisão do meu mestrado e revisão do documento final.

Não posso esquecer de agradecer à minha grande amiga Marisa Manuel, que tanto desejou ver os meus estudos em Portugal concluídos e ansiosamente aguarda pelo meu regresso a Angola.

Há muitas outras pessoas que foram fundamentais nos meus estudos em Portugal para mencionar, mas no meu íntimo eu os agradeço bastante.

RESUMO

A presente dissertação de mestrado baseia-se no estágio curricular feito na empresa Total EP Angola entre Julho e Dezembro de 2013. Os dados apresentados são relativos a um caso de estudo real de um bloco de exploração, que por razões de confidencialidade tem a designação de bloco Michocho.

A medição pressão dos fluidos nas formações rochosas pode ser inferida, a partir dos logs de resistividade das formações. Em poços não perpendiculares às camadas rochosas, as curvas de resistividade apresentam valores mais elevados do que o esperado devido ao efeito anisotrópico das formações, portanto a inferência da pressão dos fluídos a partir destas resistividades pode conduzir a valores irrealistas. A maioria dos poços de desenvolvimento perfurados no bloco Michocho em Angola são altamente desviados, se não forem sub-horizontais, na secção do reservatório. O objetivo deste trabalho é corrigir o efeito anisotrópico da resistividade devido à inclinação do poço em relação as formações atravessadas. A correção da resistividade neste estudo é baseada na fórmula proposta por Moran e Gianzero em 1979 e envolve a inclinação da ferramenta de indução e o coeficiente de anisotropia da formação rochosa.

Para a aplicação desta fórmula nos logs de resistividade dos poços do bloco Michocho fizeram-se, em primeiro lugar, testes de validação. Por falta de dados nos poços de desenvolvimento (poços muito inclinados), o teste de validação foi efetuado em cinco poços de exploração, onde se tem disponíveis logs de resistividades nas duas direções principais. Assumiu-se que a fórmula seria aprovada para a correção da resistividade se a resistividade horizontal obtida pela fórmula tivesse boa correspondência com a resistividade horizontal obtida pela ferramenta de indução de logs. Posteriormente à validação, fez-se a calibração do coeficiente de anisotropia a ser usado na fórmula e corrigiram-se as curvas de resistividades dos poços de desenvolvimento, estes muito desviados em relação as camadas rochosas.

As resistividades corrigidas permitem a previsão da pressão dos fluidos nas formações rochosas, onde o principal objetivo é identificar formações de baixa permeabilidade que são zonas onde a pressão dos fluidos é mais elevada (Overpressure). Para ilustrar esta etapa, escolheu-se uma curva de resistividade de um dos poços de exploração e calculou-se a pressão dos fluidos em formações de baixa permeabilidade utilizando a fórmula proposta por Eaton, 1975. Com estes dados identificou-se uma potencial ocorrência de sobrepressões, situação que deve ser evitada na perfuração de poços.

Palavras-chave: reservatórios petróleo; pressão dos fluidos; logs de resistividade; anisotropia das formações; correção da resistividade.

ABSTRACT

This dissertation is based on a curricular training period done at company Total EP Angola between July and December 2013. The data presented relate to a real case study of an exploration block, which for reasons of confidentiality is designated by Block Michocho.

The fluids pressure measurement in the geological formations can be inferred from the formation resistivity log. In not perpendicular wells to the layers, resistivity curves show higher values than the expected due to the anisotropic effect of the formation thus the inference of the pressure of fluids from resistivity logs can lead to unrealistic values. Most of the developments wells drilled on Block Michocho in Angola are highly deviated, if not sub-horizontal, in the reservoir section. The objective of this work is to correct the anisotropic effect of the resistivity of Block Michocho due to non-perpendicularity of the wells when intersect the geological formations. In this study, the correction of the resistivity is based on the formula proposed by Moran and Gianzero in 1979 and involves the dipping angle of the induction logging tool and the coefficient of anisotropy of the rock formation.

Prior to application of this formula for the corrections of resistivity of the Block Michocho wells logs, a set of validation tests were made. Due to lack of data on development wells (highly inclined wells) the validation test was carried out in five exploration wells where resistivity is available in the two principal directions. It was assumed that the formula would be approved for resistivity corrections if the horizontal resistivity obtained by the formula had a good correspondence with the horizontal resistivity obtained by the induction logging tool. After this validation step, the coefficient of anisotropy to be used in the formula was calibrated as well as the correction of the curves of resistivity of the remaining development wells, those much more diverted regarding the rock layers.

The corrected resistivity can be applied for pore pressure prediction in low permeability rock formations, in which the main objective is to identify regions where fluid pressure is higher than normal pressure, i.e. overpressure regions. For illustration purposes, a resistivity curve from an exploration well was chosen and the pressure of the fluids in low permeability rocks was computed by using the formula proposed by Eaton in 1975. With this well data, a potential overpressure region was identified and should be avoided in drilling activities.

Key-words: oil reservoir; fluids pressure; resistivity logs; geological formation anisotropy; correction of resistivity.

INDEX

INDEX OF FIGURES

INDEX OF TABLES

ACRONYMS

API Units: American Petroleum Institute Units.

c: Is the compaction constant in 1/m or 1/ft.

Computed RH: computed horizontal resistivity ohm-m (equation 5)

GR: Gamma ray, API units.

ILD: Depth Induction Log.

LM: Lower Miocene formation.

LWD: Logging While Drilling.

LW: Logging Wireline

M: Miocene formation.

M1: Middle Miocene formation.

MSL: Measurement sea level, meters units.

MWD: Measurement while drilling.

NCP or NTC: Normal compaction profile or normal compaction trend.

OBG: Overburden stress.

OL: Oligocene formation.

PPP: Pore Pressure Prediction.

Pshale: Pore Prediction in the shale formation.

Ra or Rt: apparent resistivity from the tool, Ohm-m units.

Rh: Horizontal resistivity from the tool, Ohm-m units.

Rn: Shale resistivity in normal compaction condition, Ohm-m units.

Ro: Shale resistivity in mudline Ohm-m units.

RTE: rotary table, meters units.

Rv: Vertical resistivity from the tool, Ohm-m units.

TEPA: TOTAL EP ANGOLA.

TVD: True vertical depth, meter units.

UUM: Upper upper Miocene formation.

UM: Upper Miocene formation.

WD: Water depth, meters units

Z: True vertical depth below the mudline, meters units

SYMBOLS

α: Apparent dip angle formed between the borehole and line normal to the bedding plane, degrees.

ϕ: Porosity (dimensionless)

ϕ_0: Porosity in the mudline (dimensionless)

λ: Coefficient of anisotropy, dimensionless.

1. INTRODUCTION

The resistivity is a measure used to infer pore pressures lithology in depth, once it is not possible to measure the pressure directly from the rock formations. In deviated wells, due to the lack of logs data available in the non-reservoir zones, it is difficult to follow-up continuously the pressure.

The resistivity and gamma ray are both usually some of the available well logs, and those data are often used for reservoir characterization and modelling (Luis & Almeida, 1996; Da Costa e Silva et al, 1997; Almeida, 2010; Quental et al, 2012; Kuznetsova et al, 2014; Alves et al, 2014). But resistivity measurements are affected by wells deviations mainly in the low permeability zones. Hence, to use resistivity for pressure predictions, it is necessary to correct the anisotropy generated by the deviation of the wells and make use of an apparent angle.

The correction of anisotropy in the resistivity must be done just in low permeability rock formations, such as mudstone and shale.

If corrections are not made to resistivity, anisotropy and dip may cause erroneous induction log interpretation (Klein, 1993).

The first and main objective of the work is to test a methodology to correct resistivity from anisotropy generated by the apparent angle of intersection between the wells and the geological formations (dip plus deviation). In order to validate the proposed method of correction of anisotropy, a set of wells with logs data from log while drilling (LWD) and wireline (WL) were used. The study is addressed to real data from a block renamed to Block Michocho, and were tested and validated with five exploration wells closer to the operated fields.

The methodology proposed for correction of the anisotropy is based on a model given by Moran and Gianzero (1979) in the paper “Induction Log Anisotropy Corrections” written by James D.Klein (Klein, 1993).

This model assumes a laminated sand-shale sequence inclined to the wellbore with isotropic sand layers and anisotropic shale layers, and includes two levels of anisotropy at macroscopic and microscopic scale. The model assumes that the thicknesses of the individual sand and shale beds are lower than can be captured by induction logging tools. The parameters of the model are dip angle, sand resistivity, volume of laminar shale, shale longitudinal resistivity, and shale coefficient of anisotropy.

The deviation of the geological structure in vertical wells can also generate erroneous i.e. this deviation is relative. The model applies only to laminated formations with bed thicknesses less

than the tool resolution. The preferred lithologies for pore pressure interpretation are shale and mudstones because they are more responsive to overpressure than most rock types.

In this study, the corrected resistivity logs will be used in the pore pressure prediction to find along depth water reservoir, oil reservoir, overpressures zones, and it will help in the design of the well, and in the determination of the mud weight to drill, once there is a hazard associated to the drilling in overpressure zones.

The hazards of pore pressure concern in pressure fluids within low permeability rock formations higher than normal pressure (hydrostatic) which can be termed overpressure. Abnormal pressures, particularly overpressure, can greatly increase drilling non-productive time and cause serious drilling incidents (e.g., well blowouts, pressure kicks, and fluid influx) if the abnormal pressures are not predicted before drilling and while drilling. Pressure prediction is fundamental for drilling activities.

The pore pressure gradient is used in drilling engineering due to the convenience of determining mud weight as is shown in Figure 1.1. The pore pressure gradient at a given depth is the pore pressure divided by the true vertical depth (TVD). The mud weight should be appropriately selected based on pore pressure gradient, wellbore stability and fracture gradient prior to setting and cementing a casing.

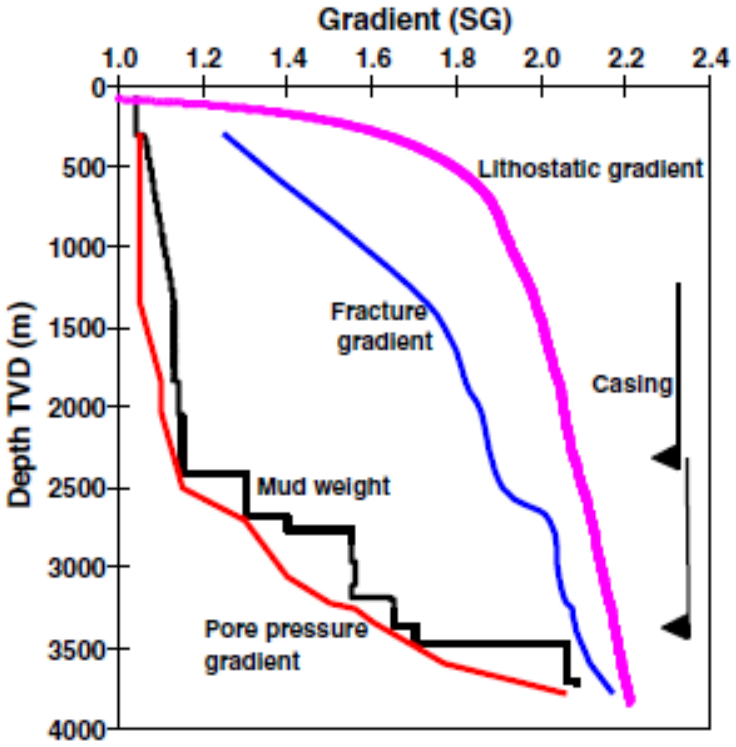

Figure 1.1 Pore pressure gradient, proper mud weight to stabilize the wellbore, fracture gradient, overburden stress gradient and casing shoes with depth.(Source: Zhang, 2011)

The drilling fluid (mud) is applied in the form of mud pressure to support the wellbore walls and for preventing influx and wellbore collapse during drilling. In order to avoid fluid influx, kicks and wellbore instability in an open hole section, a heavier mud pressure than the pore pressure is needed. When mud weight is higher than the fracture gradient of the drilling section, it may fracture the formation, causing losses or even lost circulation. To prevent wellbore from hydraulic fracturing by the high mud weight , as needed where there is overpressure , casing needs to be set to protect the overlying formations from fracturing, as illustrated in figure 1.1.

First, predictions are usually done from sonic or velocity logs, which are data available before and during drilling in order to determine the pressure in depth, particularly in low permeability rock formations.

Resistivity is the measure used to infer fluid pressures in this study. However, resistivity from a high deviated well must be corrected due to its anisotropic effects. Most of development wells are highly deviated, if not sub-horizontal, in the reservoir section. and A proposed correction of anisotropy is presented in Figure 1.2 below, in which a hypothetical corrected resistivity of a development well termed Dona 761 was performed through the equation given by Moran and Gianzero (1979).

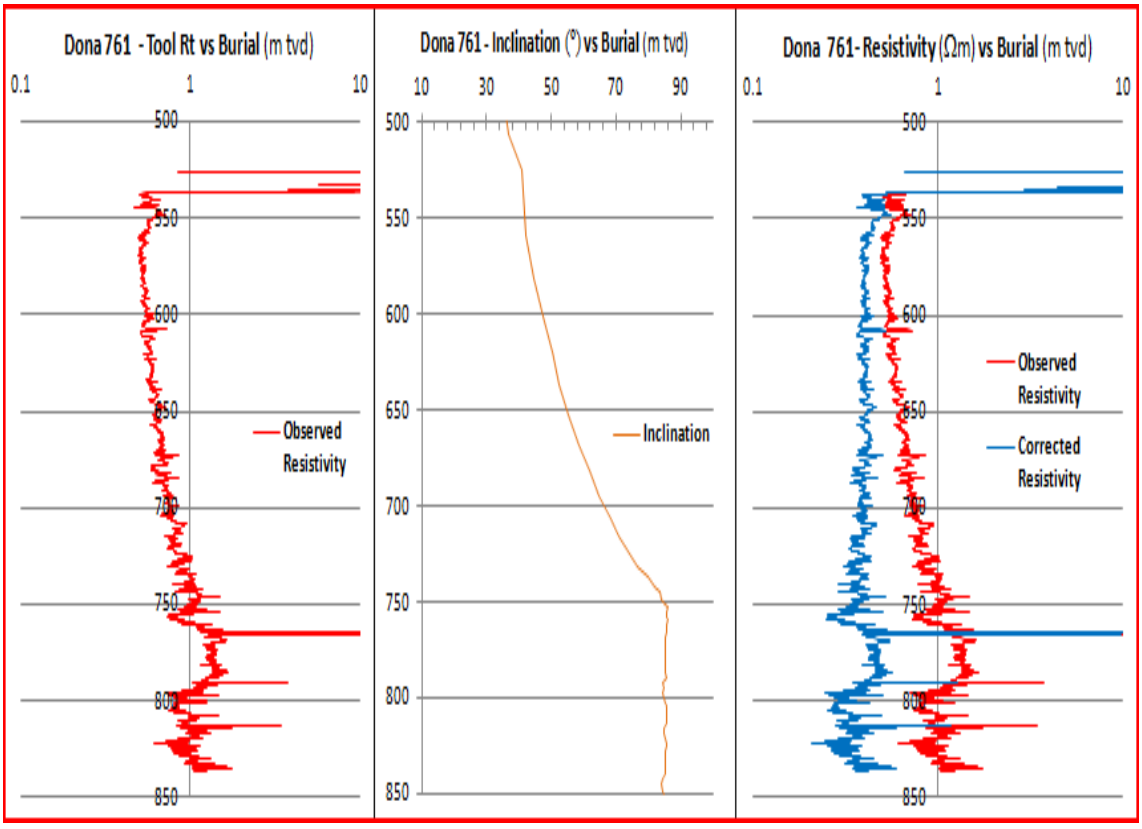

Figure 1.2 The first plot (left) shows the observed resistivity and its trajectory with burial. The second plot (middle) represents the inclination of the well vs burial around 90º. A correction of resistivity is represented in the third plot (right), as well as the comparison with the observed resistivity.

Dona 761 well is a development well with 80º deviation. The inclination angle of the well has an impact upon the observed resistivity values as it can be seen in Figure 1.2. It appears that the hypothetical corrected resistivity is the more appropriate method to infer pressure prediction attenuating the anisotropy effect observed in tool resistivity.

This work is based on this type of correction, through a prior validation step using logs of data of five exploration wells with different inclination angles.

This study is divided into five chapters:

- The first chapter presents a bibliography synthesis that addresses overpressure, normal compaction trend, pore pressure prediction, anisotropy and its correction, and an explanation of the induction of gamma ray and resistivity logs. This chapter shows shortly the problem of resistivity corrections from log well data and relate all these terms to the case study.
- Second chapter presents the method of correction of the anisotropy and the test of validation of the correction on exploration wells. It also quantifies and qualifies the influence of anisotropy on Block Michocho. In order to validate test findings, this chapter also explains how the equation of correction of the anisotropy in the fields of the block is checked.
- Third chapter discusses the possibility of calibrating the coefficient of anisotropy using the normal compaction of the fields of Block Michocho and the application of correction on deviated development wells.
- Fourth chapter addresses the application of the pore pressure prediction method in the Lango well and a discussion of benefits and disadvantages of the using corrected resistivity.
- Finally, fifth chapter presents conclusions about the work and recommendations about using the study's method to correct anisotropy.

As to the parameters implied in this work, this study refers to the technical reports of the respective exploration wells from TEPA, in order to understand the lithology of Block Michocho.

2. METHODS

This section details from a theoretic point of view a set of concepts to introduce the problem and the solutions proposed for correction of resistivity in the present case study.

2.1 Overpressure

The overpressure is a problematic issue during drilling in the petroleum's industry. It can be understood as an abnormal pressure, which concerns in a pressure higher than normal or hydrostatic pressure in the formations as we can see in Figure 2.1. Normal pressure is defined as the weight of the water column that comes from surface. Pressure below hydrostatic is called underpressure and it will not be discussed in this report.

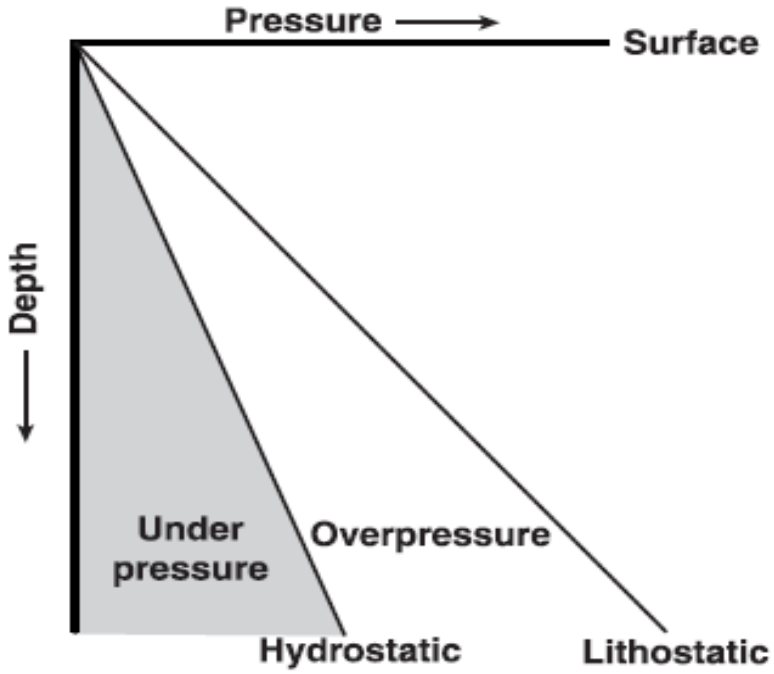

Figure 2.1 Hydrostatic pressure vs depth, underpressure and overpressure. (source: Swarbrick and Osborne, 1998)

In terms of dynamics of the subsurface fluid flow, overpressure is defined as inability of the formation fluids to escape. This retention of fluids can result in disequilibrium states of pressure, and to control that phenomenon it is very important to check the permeability and behaviour of rock seal.

There are many basins in the world containing overpressured reservoirs and the age of the rocks in which overpressures have been recognized ranges from Pleistocene to Cambrian (Swarbrick

and Osborne, 1998). The carbonated rocks and clastic reservoirs are materials in which overpressure is found and it is in rocks deposited too deeper the sedimentary basins.

The hydrostatic line in Figure 2.1 corresponds to single overburden stress, and pressure increases linearly with depth. The mechanisms responsible for overpressure are undercompaction, fluid expansion, lateral transfer and tectonic loading (Bowers, 2002); compaction disequilibrium or undercompaction and fluid volume expansion during gas generation are the ones with more magnitude.

Undercompaction results from low permeability rocks (high sedimentation rates). Increase in vertical stress during loading can lead to incomplete dewatering of the sediment when part of the weight of the load is added to the pore-fluid pressure. This is commonly termed "undercompaction".

Overpressure due to compaction disequilibrium is often recognized by higher porosity than expected at a given depth. Porosity can be considered as a function of the overburden stress and the effective stress. If all the fluid is retained the porosity and effective stress remain constant with depth. Conditions that favour compaction disequilibrium are rapid burial and low permeability rocks.

Compaction disequilibrium is therefore likely to be found in thick clay and shale successions during continuous rapid burial (England et al, 1987). Overpressure in adjacent, high permeability reservoir rocks will result from isolation of the reservoir within the low-permeability section.

To characterize compaction disequilibrium, we must study the plots of pressure vs depth through fluid retention depth where overpressure begins and increases downwards along a gradient, which can closely follow the lithostatic (overburden) gradient.

Fluid expansion creates overpressure in low permeability rocks, where pore fluid volume increases with minimal change in porosity and a rate which does not permit effective dissipation of fluids.

Overpressure can be generated within the pore space by fluid expansion mechanisms such as heating, hydrocarbon maturation, and the expulsion/expansion of intergranular water during clay diagenesis (Bowers, 1995). When such events occur, overpressure results from the rock matrix constraining the pore fluids as the fluids try to increase in volume. Fluids pressure within rock formation cannot be measured directly, but it can be inferred.

Some log parameters allow the inference of pore pressures within rock formation. These log parameters are density, sonic velocity and resistivity. Just as in an overpressure situation, which appears in rock formations with low permeability, log parameters can infer pressure indirectly

identifying shale layers. When pore pressure in shale formations using log parameters are inferred, the trend of the normal curve increases with depth. At a certain depth of the normal curves of these parameters that, is supposed to increase with depth, the pressure decreases. This means that pore pressure in this zone is higher than normal pressure, which corresponds to the normal curve. The subchapter 2.4 discusses this method in more detail.

2.2 Normal Compaction Trend

The compaction trend is related to the normal behaviour of porosity with depth. Normally with depth, the weight above sediments, that is termed overburden stress, increases and the compaction of the sediments increases, too.

Porosity usually decreases with depth due to compaction. This occurs when the sedimentation rate is slow i.e., the equilibrium between increasing overburden and the reduction of pore fluid volume due to compaction or ability to expel fluids is maintained (Mouchet and Mitchell, 1989). This usual compaction generates hydrostatic pore pressure in the formation. Therefore, the deeper the sediment is buried, the higher the overburden stress and the associated compaction.

During burial of sediments, if compaction increases continuously and porosity decreases, fluids dewater with burial, this behaviour can be a linear trend, which is called by normal compaction trend line. When normal compaction is increasing with depth, there are zones in which sedimentation does not undergo the same process: porosity does not decrease as would be expected. In such zones, a phenomenon called compaction disequilibrium or undercompaction occurs. In zones characterized by compaction disequilibrium, fluids are trapped in low permeability formations with pressure higher than hydrostatic pressure.

For in a given log, representative of porosity, the normal compaction trend is used to deduce abnormal pressure zones in the shale. In order to predict pore pressure build-up in sediments due to compaction disequilibrium, it is necessary to establish a trend curve for porosity versus depth due to normal compaction. One commonly approach is based on porosity versus depth relationship Athy (1930):

$$\phi = \phi_0 e^{-cz} \qquad (1)$$

Where ϕ is porosity; ϕ_0 is the porosity in the mudline; z is the true vertical depth below the mudline; and c is the compaction constant in 1/m or 1/ft.

As with porosity, resistivity is also used to infer fluids. As porosity, decreases with burial, resistivity increases in the shale along depth. The function of the normal compaction trend line

acts as a reference in the measuring resistivity to help to make a better interpretation on the study of pore pressure prediction being resistivity a parameter of control.

It should be noted that pore pressure in the formation near the wellbore is affected by drilling-induced stresses (Zhang and Roegiers, 2005). Therefore, in order to obtain formation pore pressure the deep resistivity is also required for calculations of the pore pressure. Figure 2.2 demonstrates the normal compaction trend line.

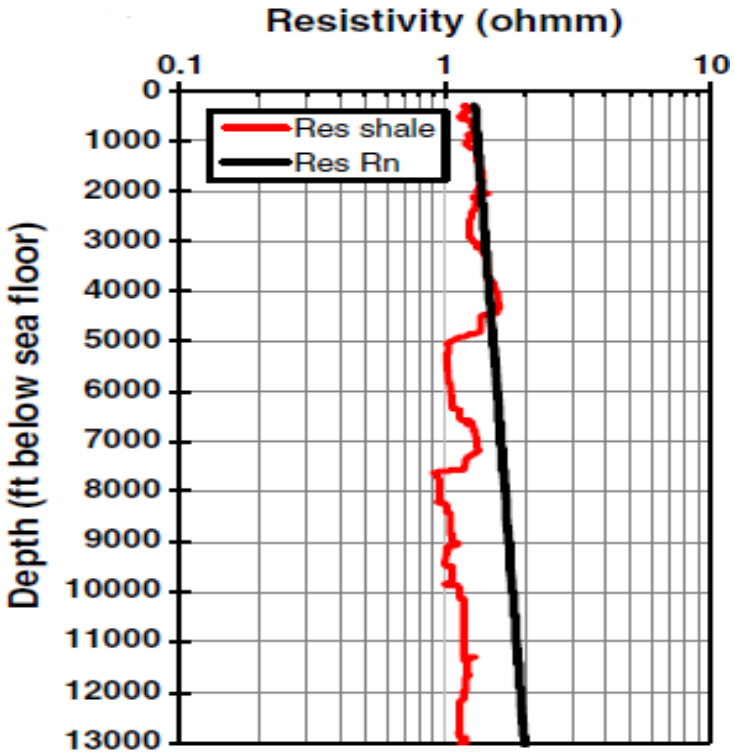

Figure 2.2 Normal compaction trendline according to resistivity versus depth. Red line is shale resistivity and black line is normal resistivity (*Rn*) (Source: Zhang, 2011).

The resistivity varies according to depth as can be seen in Figure 2.2. At depths less than 4900ft below the sea floor the formation is in normal compaction. From 4900 to 7600ft, the formation is slightly under-compacted with lower resistivity than the normal compaction trend, implying that the pore pressures increases according to Eaton's theory. From 7600 to 13000ft, the formation is further under-compacted and more elevated pore pressures exist. Figure 2.2 also demonstrates that the adapted Eaton's resistivity method gives a good result in pore pressure calculation.

It is difficult to determine normal shale resistivity or shale resistivity in the condition of hydrostatic pore pressure. One approach is to assume that normal shale resistivity is a constant, but this does not work in most cases. However, normal resistivity (*Rn*) is a function of the burial

depth, as shown in Figure 2.2. Hence, the normal compaction trendline needs to be determined for pore pressure prediction.

Based on the relationship of measured resistivity and burial depth in the formations with hydrostatic pressures, the following equation of the normal compaction trend of resistivity can be used:

$$Rn = R_0 e^{bz} \qquad (2)$$

Where Rn is the shale resistivity with normal compaction condition; R_0 is the shale resistivity in the mudline; b is the constant; and z is the depth below the mudline.

2.3 Pore Pressure Prediction

Pore pressure is also known as formation pressure and is related to interstitial fluids that percolate within the rocks formations. Hydrostatic pressure occurs when the pressure within the formations is equal to the pressure in the column of water that extends to the surface. When the fluid pressure in the sediment with low permeability (shale or mudstones) is greater than normal pressure, overpressure zones are present.

For a driller's geologists, it is important to know pore pressure within formations to determine the mud weight required to drill future wells safely.

The fundamental theory for pore pressure prediction is based on Terzaghi's and Biot's effective stress law (Biot, 1941; Terzaghi et al, 1996). This theory argues that pore pressure in the formation is a function of total stress (overburden stress) and effective stress. The overburden stress, effective vertical stress and pore pressure can be estimated by:

$$p = \frac{\alpha_v - \alpha_e}{\alpha} \qquad (3)$$

Where p is the pore pressure; α_v is the overburden stress; α_e is the vertical effective stress; and α is the Biot effective coefficient. It is conventionally assumed that α=1.

When overburden stress and effective stresses are known, pore pressure can be calculated from equation (3). Overburden stress can be easily obtained from bulk density logs, while effective stress can be correlated to well log data, such as resistivity, sonic velocity, bulk density and drilling parameters.

The pore pressure profile is similar to many geologically young sedimentary basins where undercompaction is the major cause of overpressure that can be encountered at a certain depth.

In Figure 2.3, hydrostatic pressure, formation pore pressure, overburden stress and vertical effective stress with the true vertical depth (TVD) are displayed for a typical oil and gas exploration well.

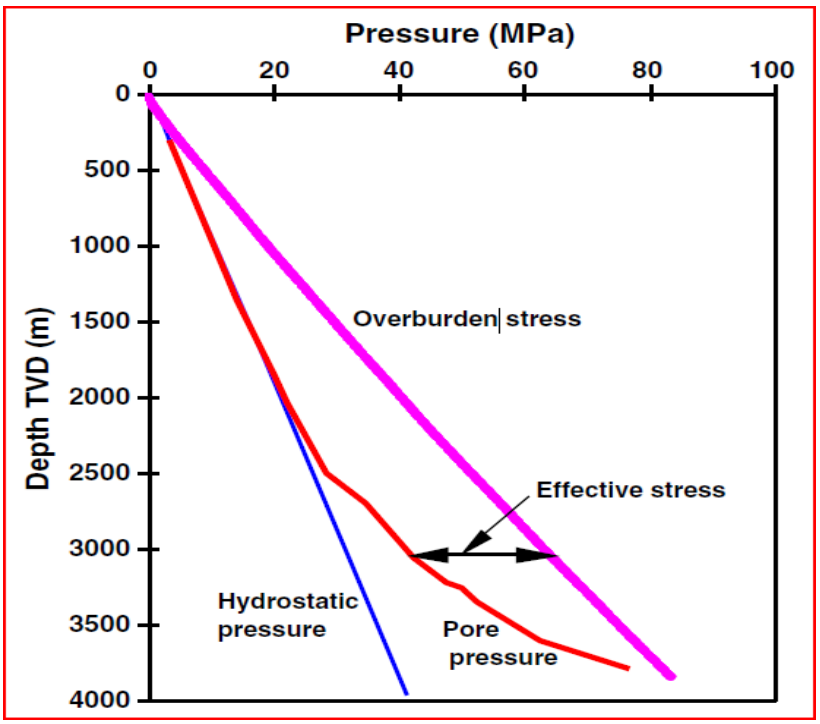

Figure 2.3 Variations of hydrostatic pressure, formation pore pressure, overburden stress and vertical effective stress with the true vertical depth (TVD) in a typical oil and gas exploration well. (Source: Zhang, 2011)

At relative shallow depths (less than 2000m) pore pressure is hydrostatic, indicating a continuous interconnected column of pore fluid that extends from the surface to a certain depth. Overpressure starts deeper than 2000m, where pore pressure increases rapidly with depth, implying that deeper formations are hydraulically isolated from shallower ones. By 3800m, pore pressure reaches to a value close to the overburden stress, a condition referred to as hard overpressure. According to the equation (3), the increasing in overpressure causes reduction in the effective stress.

Pore pressure analyses include three steps:

- Pre-drill pore pressure prediction;
- Pore pressure prediction while drilling;
- Post-well pore pressure analysis.

The pre-drill pore pressure can be predicted by using the seismic interval velocity data in the planned well location as well as using geological, well logging and drilling data in the offset wells. The pore pressure prediction while drilling generally uses the logging data while drilling (LWD), measurement while drilling (MWD), drilling parameters, and mud logging data for analyses. Finally, the post-well analysis intends to analyse pore pressures in the drilled wells using all available data to build pore pressure model, which can be used for pre-drill pore pressure predictions in the future wells. The well-log-based resistivity method serves to predict pore pressure formation, in order to identify reservoir and fluids pressures.

Eaton (Eaton, 1975) proposes an equation to predict pore pressure gradient in shales using resistivity log. This equation, presented below is more applicable for young sedimentary basins, and requires that the normal shale resistivity is properly determined.

$$P_{pg} = OBG - \left(OBG - P_{ng}\right)\left(\frac{R}{R_n}\right)^n \quad (4)$$

Where P_{pg} is the formation pore pressure gradient; OBG is the overburden stress gradient; P_{ng} is the hydrostatic pore pressure gradient (normally 0.465psi/ft or 1.03MPa/km, dependent on water salinity); R is log the shale resistivity; R_n is the shale resistivity normal compacted trend, n is the exponent constant ranging from 0.6 to 1.5, and normally n=1.2 (Zhang, 2011).

2.4 Pore Pressure Estimation in Real Time

The estimation of pore fluids is a method that helps detect overpressure. It consists of the observation of the trend of resistivity (as study parameter) according to depth within low permeability rock formations such as shale and mudstones. Because resistivity increases with depth in the shale zones, we infer that fluids pressure also increase in a linear fashion.

In Figure 2.4 below, resistivity versus depth is plotted in shale zones in order to predict fluid pressure. The blue line represents the linear trajectory of resistivity under normal conditions. At a certain depth in shale zones, the trend of resistivity decreases as yellow line shows. That sometimes happens; can be interpreted this as being overpressure due to a phenomenon related to undercompaction. The green line represents the top of overpressure.

The estimation of pore pressure inferred in the resistivity log data can be performed in real-time or in the office, but the values of resistivity must be accurate and unaffected by the effects of anisotropy. Rather than resistivity, the method of pore pressure estimation in real-time can also be performed using parameters such as sonic velocity or density logs.

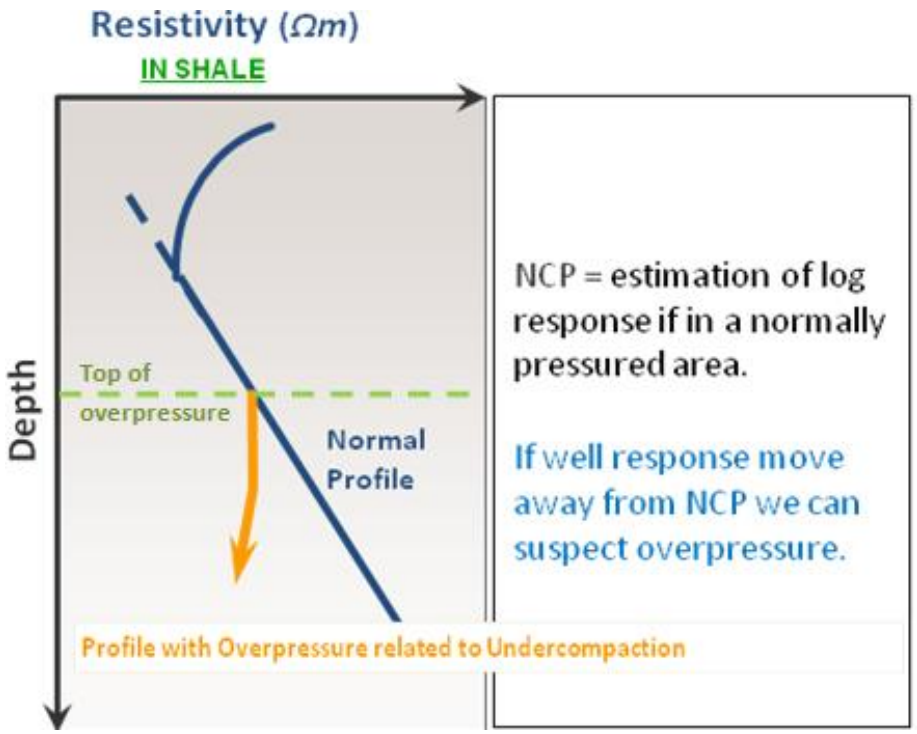

Figure 2.4 Interpretation of the pore pressure prediction in real time. Overpressure detection from compaction profile with LWD. (Source: KSI PPP training).

2.5 Electrical Anisotropy

Electrical anisotropy consists of the dependence of resistivity on the direction of current flow within a rock. The measure resistivity in the induction logging tool in a vertical wellbore with horizontal bedding gives the longitudinal resistivity, which corresponds to current flow parallel to the bedding. Whether bedding has a significant inclination angle relative to the wellbore or dip angle of the well is deviated relatively to the bedding it is possible to obtain high resistivity values due to anisotropy. It means that horizontal induction logs crossed more than one formation or different materials in a certain depth of investigation.

A rock is isotropic if it has same value of resistivity independent of its direction. If the measurement of resistivity in a given direction is greater than measurement of resistivity in another two directions, this rock is termed anisotropic rock.

There are two types of anisotropy – microscopic and macroscopic. Microscopic anisotropy is related to the fabric of the rock itself. Microscopic anisotropy can be both mica or clay grains. Such anisotropy could originate during primary deposition and compaction, during later cementation or diagenesis, or by stress from tectonic forces long after deposition (Klein, 1993). To the naked eye, rocks with microscopic anisotropy can appear homogenous. Macroscopic anisotropy consists in homogenous rock layers divided in parallel sequences; each layer contains distinct electrical properties. In scale, the layering can vary from fine to coarse grain,

but the sequence of beds seen in part or whole behave in an anisotropic manner. Current flowing that passes through to the bedding perpendicularly have more difficulty due to resistance of the rock than when current flowing occurs parallel to the bedding. Macroscopic resistivity will affect measurement of resistivity when the scale of the bedding is less than the resolution of the measurement tool (Klein, 1993).

The combination of microscopic (from individual beds) and macroscopic (from beds with different electrical properties) anisotropy results in total anisotropy that exists in a given bedding. The coefficient of anisotropy and the apparent angle (dip plus deviation) are responsible for the effect of the increasing resistivity, which does not correspond to the real reading of resistivity.

Anisotropy in a wellbore with high angle relatively to the bedding can have huge impact on the resistivity. One interpretation of this resistivity log of specific material can lead to erroneous estimates of hydrocarbon (Klein, 1993). Hence, resistivities from wells in which anisotropy have a big impact must be corrected to improve interpretation of the formation and fluids that percolate in its interstitials.

The influence of the anisotropy in resistivity (Rv/Rh) of wellbore highly deviated is shown below in Figure 2.5, where several curves of apparent resistivity having different coefficients of anisotropy vary as the relative inclination increases.

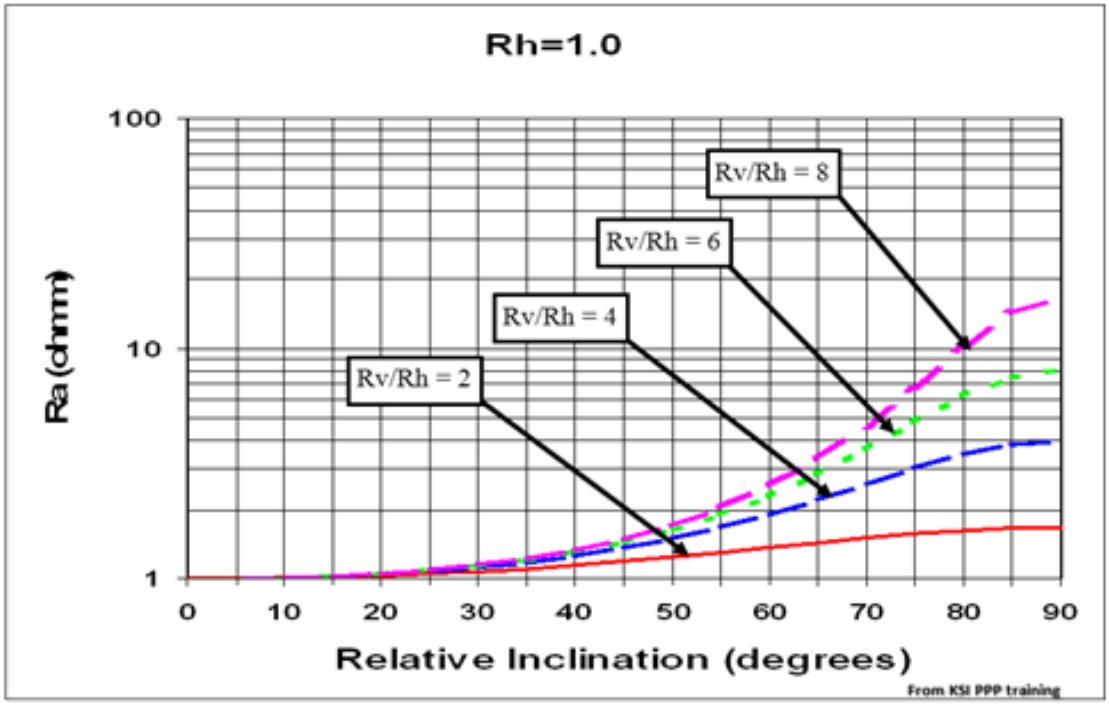

Figure 2.5 Influence of the relative inclination in resistivity measurement when different values of anisotropy (Rv/Rh) within the formations are considered. (Source: KSI PPP Training)

Initially, all curves have 1ohm of apparent resistivity and until a certain point of relative inclination start to increase. Each curve of apparent resistivity with the respective coefficient of anisotropy increases with inclination relative to the bedding. The first curve (in red) has a coefficient of two (2), starts to increase clearly after 30º. The same occurs to the remaining curves, but the increasing gradient of the apparent resistivity is greater for higher orders of anisotropy magnitude. Without any doubt, higher coefficients of anisotropy correspond to higher gradients of apparent resistivity increasing. In addition, there is minimum value of inclination on the graph (around 40º) that anisotropy starts to have a significant impact on resistivity.

2.6 Correction of the Anisotropy

The main objective of this study is to propose a methodology to attenuate the effects of the anisotropy in the resistivity, using the equation proposed by Moran and Gianzero (1979):

$$R_t = \frac{\lambda R_h}{\sqrt{(sin^2\,\alpha + \lambda^2\,cos^2\,\alpha)}} \quad (5)$$

$$\lambda = \frac{R_v}{R_h} \quad (6)$$

Where:

- R_t – True resistivity
- R_v – Vertical resistivity
- R_h – Horizontal resistivity
- α – Angle between the tool axis and a vector normal to the bedding plane (figure 2.6).

This equation must be validated for the field or block that resistivity curves will be corrected. The criteria of validation consists of correlate the measure resistivity to the calculated resistivity. The acquisition of the logs are made by two tools:

- arcVision Array Resistivity that provides just the true resistivity;
- Rt Scanner Triaxial that provides resistivity of the three principal directions;

The corrected resistivity is parallel to bedding plane as well as horizontal resistivity.

If the calculated horizontal resistivity using the true resistivity from Rt Scanner tool has correspondence to the measure horizontal resistivity from the same tool, in all study wells, the validation of equation (5) is done. Therefore, using the true resistivity from arcVision tool (where we do not have horizontal resistivity) in the equation (5), the horizontal resistivity can be calculated.

Figure 2.6 shows both arcVision and Rt Scanner tools. The first tool is used in log acquisitions of development wells, which are highly deviated. The second tool is

more expensive and is used just in log acquisitions of exploration, which are the first's wells of each field.

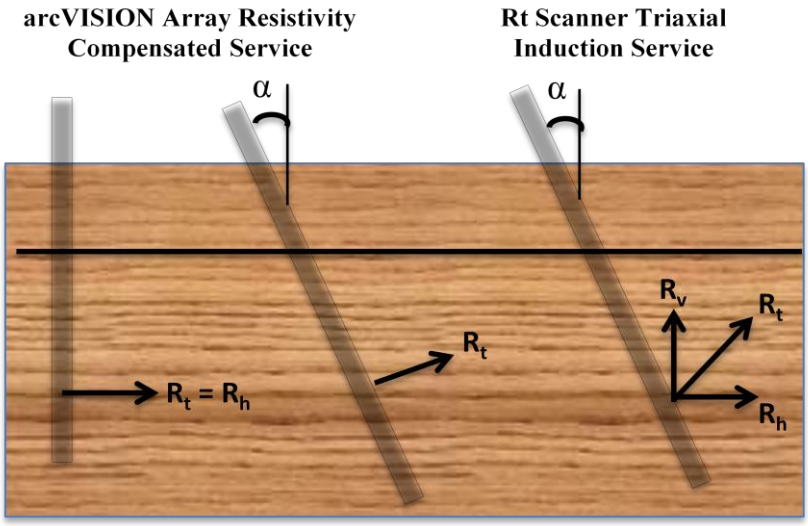

Figure 2.6 Interpretation of the apparent angle.

Both vertical and horizontal resistivities derive from the tool RT SCANNER TRIAXIAL INDUCTION SERVICE, and their ratios give the recorded coefficient of anisotropy with depth (λ). According to Moran and Gianzero (1979), making correction using this equation is necessary to assume a laminated sequence of sand-shale, that has an inclination relative to the wellbore, and consider that material of sand are isotropic and low permeability rocks, such as shale is anisotropic.

For a reservoir composed by intercalated layers of sand and shale that are sufficiently thick to be resolved by Depth Induction Log (ILD), only the microscopic anisotropy of the individuals layers are important.

2.7 Induction Logs

2.7.1 Gamma ray

Nuclear well logging is fundamentally based on natural and induced gamma ray measurements and the results of neutron or gamma ray interactions with atoms and their components. Gamma ray includes natural gamma radioactivity, gamma ray emission resulting from bombardment and the different types of interactions with the elements.

Gamma ray is the most important radiation involved in nuclear logging because they have a high power of penetration and consequently can be recorded even if they have to cross the mud column or a casing.

Gamma ray is used to measure the radioactivity of a rock formation. Natural gamma ray is related to the radioactivity intrinsic to rock formation, whilst induced gamma ray consists of the emission of energy to the rock formation to get a response of the lithology, which can be high or low gamma ray. The responses of the rocks formation are detected in a gamma ray detector installed in the logging tool.

Clay minerals have a crystalline structure that can contain more radioactive elements than sandstones. Therefore, gamma ray data in well logs can be used to separate shale intervals from other lithologies. The step required to separate shale from other rocks is drawing base lines in gamma ray data, as shown in figure 2.7.

A simple interpretation of the plot of the gamma ray versus depth is to consider that a measurement of above 75API (counts per second) of gamma ray, indicates a rock formation with huge radioactivity material and low permeability, such as mudstone and shale. Below 75API of gamma ray, indicates a lithology with less radioactivity material and high permeability such as sandstones.

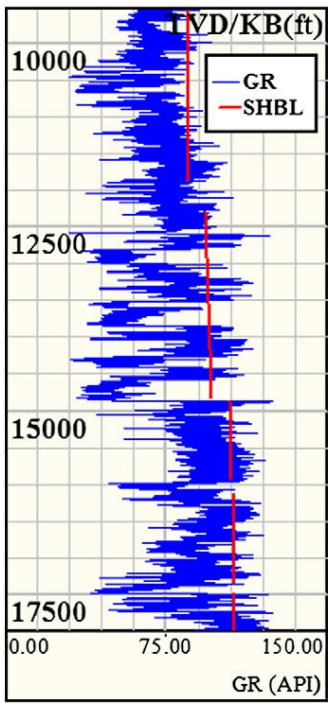

Figure 2.7 Gamma ray variations with depth. (Source: Zhang, 2011)

2.7.2 Resistivity

Resistivity is the inverse of conductivity. The electrical resistivity of a substance is its ability to block the flow of electrical current through it. The unit of resistivity is ohm-m and it is a fundamental inherent property of substance (metal, rock or fluid).

The measurement of formation resistivity is of particular importance for the evaluation of hydrocarbon saturation in the non-invaded portion of the reservoir. Combination of the resistivity data with porosity measurements and formation-water resistivity knowledge allows the computation of the water saturation in both shallow and deep zones. Comparison of these two saturation values indicates the amount of the fluid mobility and, consequently, allows the evaluation of the reservoir productivity.

There are several of techniques or tools in use for measurement of the formations resistivity, but all are variations of a common system:

- One emitter (electrode) sends a signal (electrical current) into the formation.
- One receiver (electrode) measures the response of the formation to this signal at a certain distance from the emitter.

Generally, an increase in the distance between emitter and receiver (called spacing) results in an improved depth of investigation (and a reading nearer to R_t), at the expense of vertical resolution.

Resistivity trends are often used in pore pressure determination. This technique relies upon accurate determination of shale resistivity as an indication of elevated pore pressure.

According to Hottmann and Johnson (1965), well-compacted shale rock with less quantity of water (less porosity) is more resistive than a less compacted shale rock. They concluded that a sequence of normally compacted sediments should have a normally increasing shale resistivity trend. Then, any shale resistivity decrease from the normal trend indicates the presence of overpressure.

The techniques used to determine the shale points of the rock formation consist of trace a cut off in the a gamma ray plot and read the correspondent resistivity curve at the same depth (Figure 2.8).

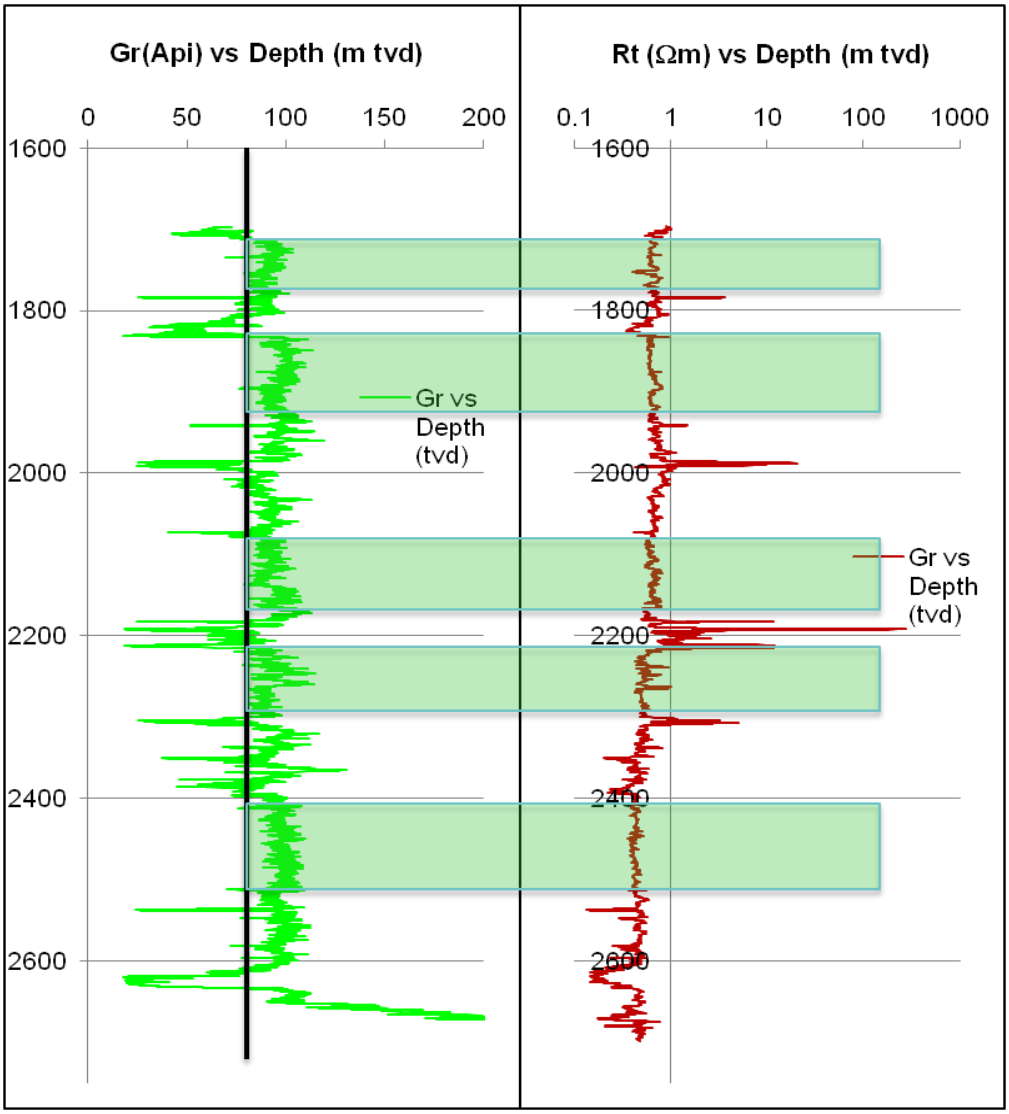

Figure 2.8 Classification into shale rock. Values above black line in the left plot define shale points. Right plot is resistivity. The boxes represent some shale intervals.

2.8 Types of Wells

2.8.1 Exploration Wells

The exploration well is the first well drilled in an area identified by survey data as having potential for oil or gas production. Enough accurate data from the field exists about the nature, size and viability of the reservoir and its contained gas. For this reason, it uses wireline logging to get more details (parameter) of the area. If an exploration well is well succeeding in terms of hydrocarbons production, it can be modified for production. An unsuccessful well is decommissioned and the area rehabilitated.

"An exploratory well represents a risk for the company drilling it, because it is not known, before investing in the well, how much oil or natural gas it might contain. The well may turn out to be a profitable new source of fossil fuel, or it may contain noncommercial quantities of fuel that aren't worth extracting; in the latter case, the well may be plugged and abandoned." (Source: www.investopedia.com/terms/e/exploratory-well.asp).

In summary, an exploration well is drilled to:

a) Find oil or gas in an area previously considered unproductive;

b) Find a new reservoir in a known field, i.e., one previously producing oil and gas from another reservoir;

c) Extend the limit of a known oil or gas reservoir

2.8.2 Development Wells

Development wells are wells drilled within the proved area of an oil or gas reservoir to the depth of a stratigraphic horizon known to be productive, to maximize the chances of success. In order arrive to the reservoir horizontally, development wells generally are highly deviated.

Development wells do not need much log data, hence log data acquisitions are made by logging-while-drilling (LWD) mainly true resistivity and gamma ray exist.

2.9 Description of the Logging Tools

This study uses two techniques to produce the acquisition of logging data: (1) Logging While Drilling (LWD); and (2) Wireline logging (LW).

Logging While Drilling is the technique of transmitting well logging tools into a well borehole downhole as part of the bottom hole assembly (BHA). Wireline logging is an expensive technique that consists of continuously collecting and recording data from a borehole during the drilling process.

The LWD – arcVISION is a compensated array resistivity tool developed by Schlumberger for medium to large boreholes (Figure 2.9). The 6.75 inch (17 cm) diameter tool makes multiple, borehole-compensated phase shift and attenuation resistivity measurements at two frequencies: 2MHz and 400 kHz; With arcVision, which usually uses 2MHz. At 2 MHz, phase-shift and attenuation can be measured between two antennas with negligible induction. Borehole compensation cancels the differences between the two receivers.

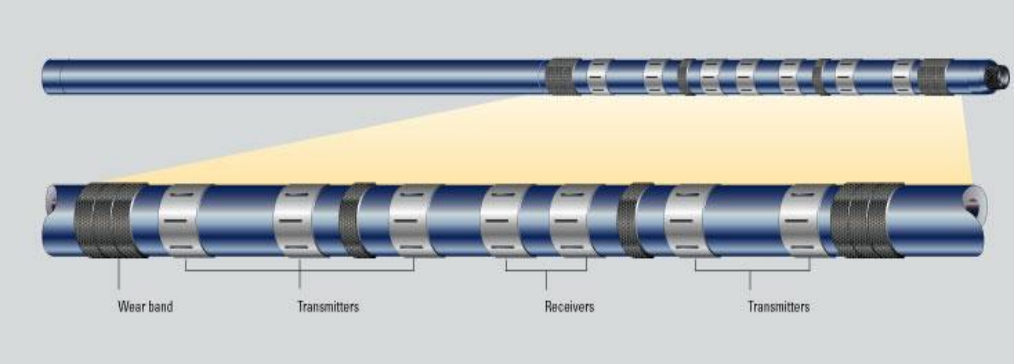

Figure 2.9 arcVISION tool and devices: wear band, transmitters and receivers. (Source: Schlumberger)

The tool's antenna array consists of five transmitters and two receivers to achieve both a range of depths of investigations as well as borehole compensation. This tool provides gamma ray, resistivity, inclination and annular pressure–while–drilling measurements (APWD) that help to produce and evaluate reservoirs.

To differentiate between borehole effects, anisotropy, invasion and shoulder beds are useful for multiple depths of investigation (DOI). Borehole compensation is important because it significantly reduces the effects of borehole rugosity.

The arcVISION tool can operate in memory mode or in real-time mode in combination with the TeleScope MWD tool; it can also be combined with any other LWD tool.

Three factors have a considerable influence in depth of investigation (DOI):

- Distance from transmitter (T) to receiver (R) (as greater is the distance T/R, the deeper is the DOI);
- Signal frequency (the lower the frequency the deeper the DOI);
- Type of measurement (phase shift reads are more shallow than attenuation).

Mode of operation (see Figure 2.10 and Figure 2.11):

- The current from the top transmitter induces an electromagnetic field within the formation;
- This propagates away from the transmitter;
- The wave induces a current at the receivers;
- The phase and amplitude of the wave are measured and converted to resistivity.

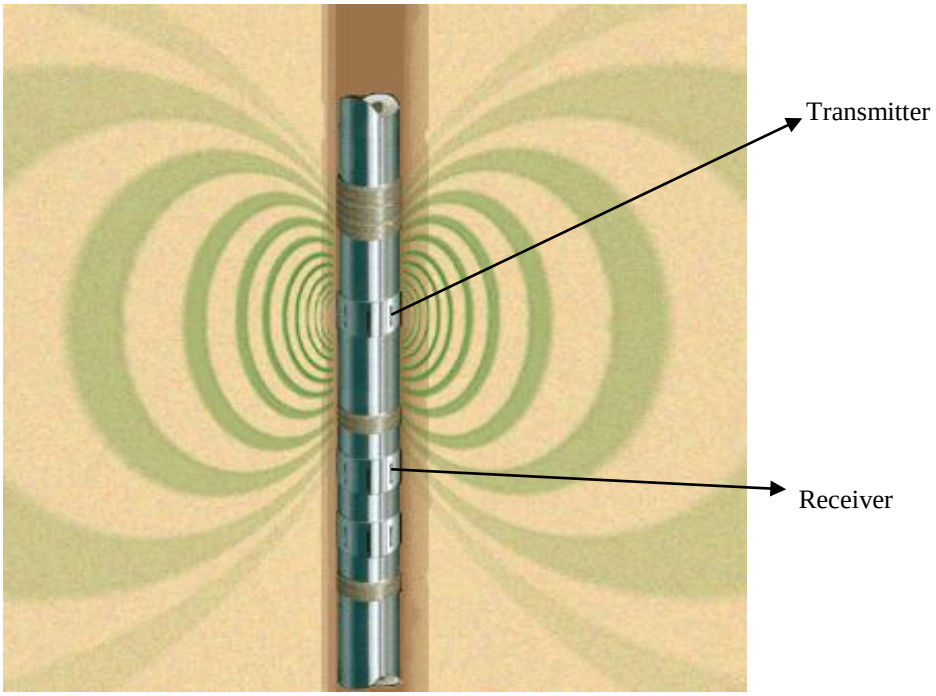

Figure 2.10 Model of operation of the logging tool.(Source: Schlumberger)

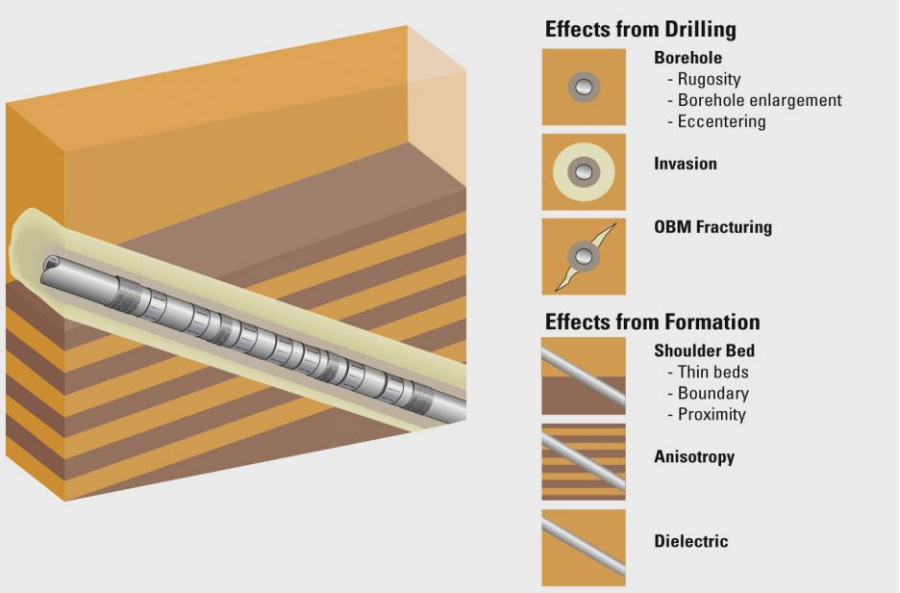

Figure 2.11 arcVISION resistivity environmental effects: from drilling and from formation.(Source: Schlumberger)

The RT Scanner triaxial induction device (figure 2.12) calculates both vertical and horizontal resistivity (R_v and R_h) from direct measurements while simultaneously solving for formation dip at any well deviation (1D inversion); R_h runs parallel to the bedding plane and R_v is orthogonal to the R_h. As with arcVISION Tools, RT Scanner provides resistivity in a given depth of investigation (DOI).

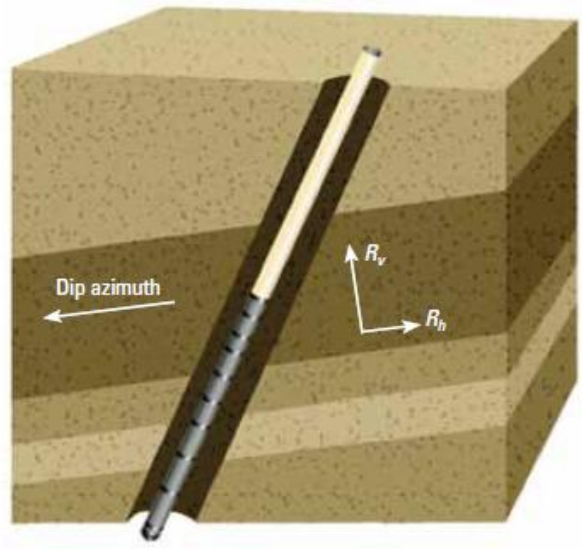

Figure 2.12 The 1D inversion of the Rt Scanner measurements obtained by the collocated coils produces both dip and resistivity information. (Source: Schlumberger)

3. CASE STUDY

This study investigates a block and five exploration wells whose names have been changed in order to keep certain privileged information confidential. This section describes the geographical and geological characteristics of the Block Michocho and the wells available.

3.1 Geographical and Geological Settings of Block Michocho

3.1.1 Geographical Settings

Block Michocho is an exploration and production block located in the West of the Luanda province, in the region of the capital of Angola. The main operator of these fields is the Company Total EP Angola. A set of wells closer to the operated fields were chosen to characterize anisotropy in the Block Michoho. Figure 3.1 shows location of the five exploration as well as a set of development wells named "Dona".

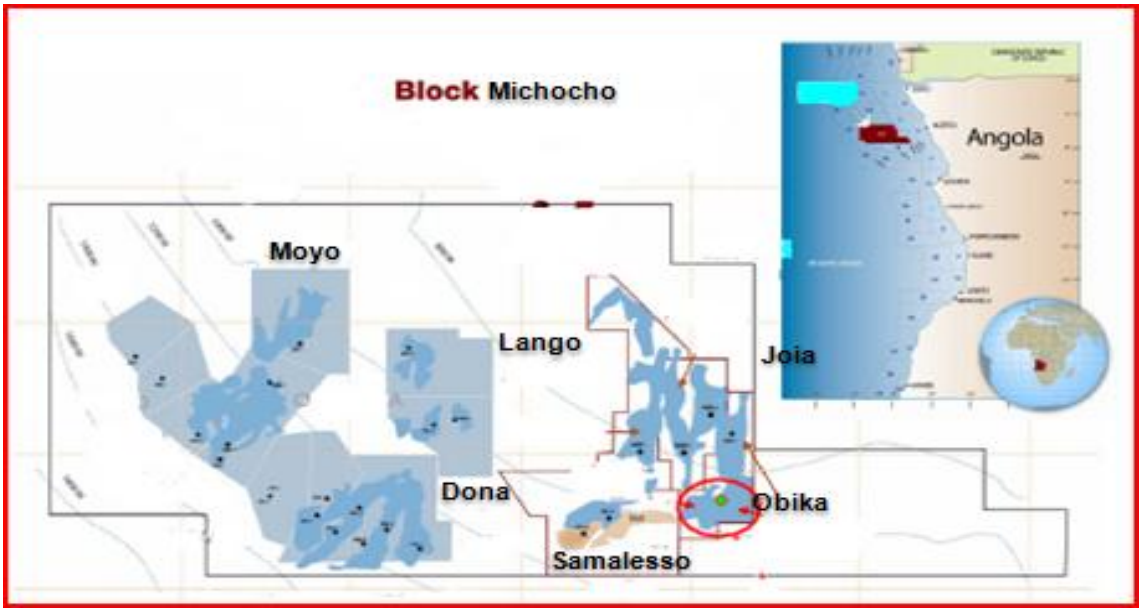

Figure 3.1 Location of Block Michocho in the offshore of Angola and location of the Joia, Obika, Moyo, Samalesso, Lango and Dona wells under study. (source: TEPA)

3.1.2 Geological Settings

The Block Michocho is located at the SouthWestern edge of the huge Lower Congo Basin, mainly of Tertiary Period. The structural evolution is attributed to a westward regional thin-skinned extension that has been affecting the Upper Cretaceous to current sedimentary cover since the Albian.

The Aptian "Loeme" salt layer corresponds to the basal detachment level which permitted the westward gravity gliding of the sedimentary cover above a pre-Aptian passive deposits.

From east to west, the Block Michocho's passive margin is divided into four main tectonic domains with contrasted deformation styles (Figure 3.2): (1) stable, (2) proximal extensional (3) transitional and (4) Compressional.

The Middle Miocene – Upper Miocene (M-UM) area is located in the proximal-extensional domain marked by numerous listric and normal faults separating some tectonic rafts of Cretaceous, Eocene and Oligocene series separated by huge compensation graben (as the NW-SE oriented Oligocene E Graben) which are unfilled by Miocene to actual series.

During the Pliocene Period, the area was characterized by a significant increase in tectonic sliding activity that created a typical turtleback anticline westward and a thick Plio-Pleistocene depot-centre above the M-UM area and eastward (graben).

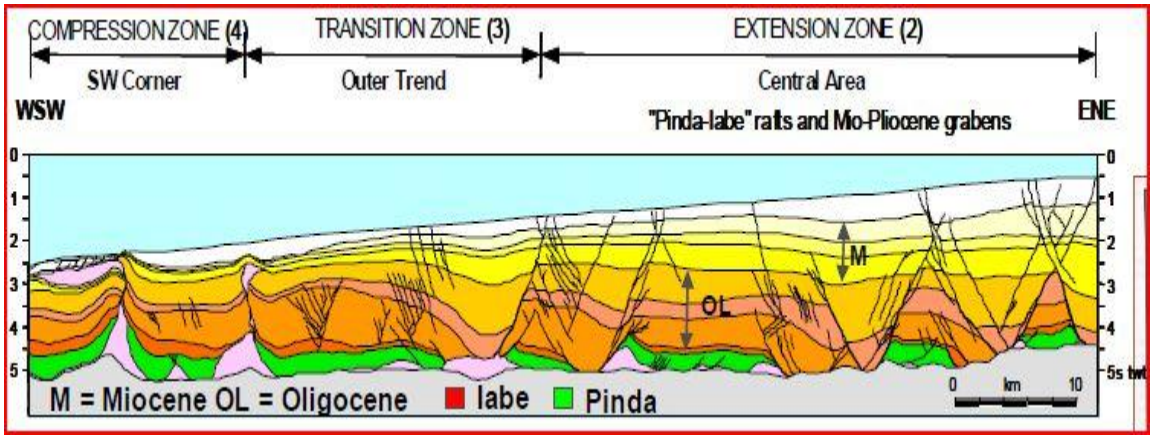

Figure 3.2 Location of block Michocho (Source: TEPA).

According to the combination of numerous faults and sand levels overall, the sedimentary series (Lower Miocene, Middle Miocene, Upper Miocene) M and UM present the same source rocks, pathway and timing migration.

According to a technical report of TEPA, the Middle Miocene interval is constituted of channel-levee turbidity complexes and initial lobe deposits. Lower Miocene interval is constituted by sand lobes and slightly erosive sandy channels, which are more or less canalized by graben axis.

The lithology of the Block Michocho is composed predominantly of sand, shale, laminations of sand-shale and turbidity's sequences from the Oligocene series. (see Figure 3.3).

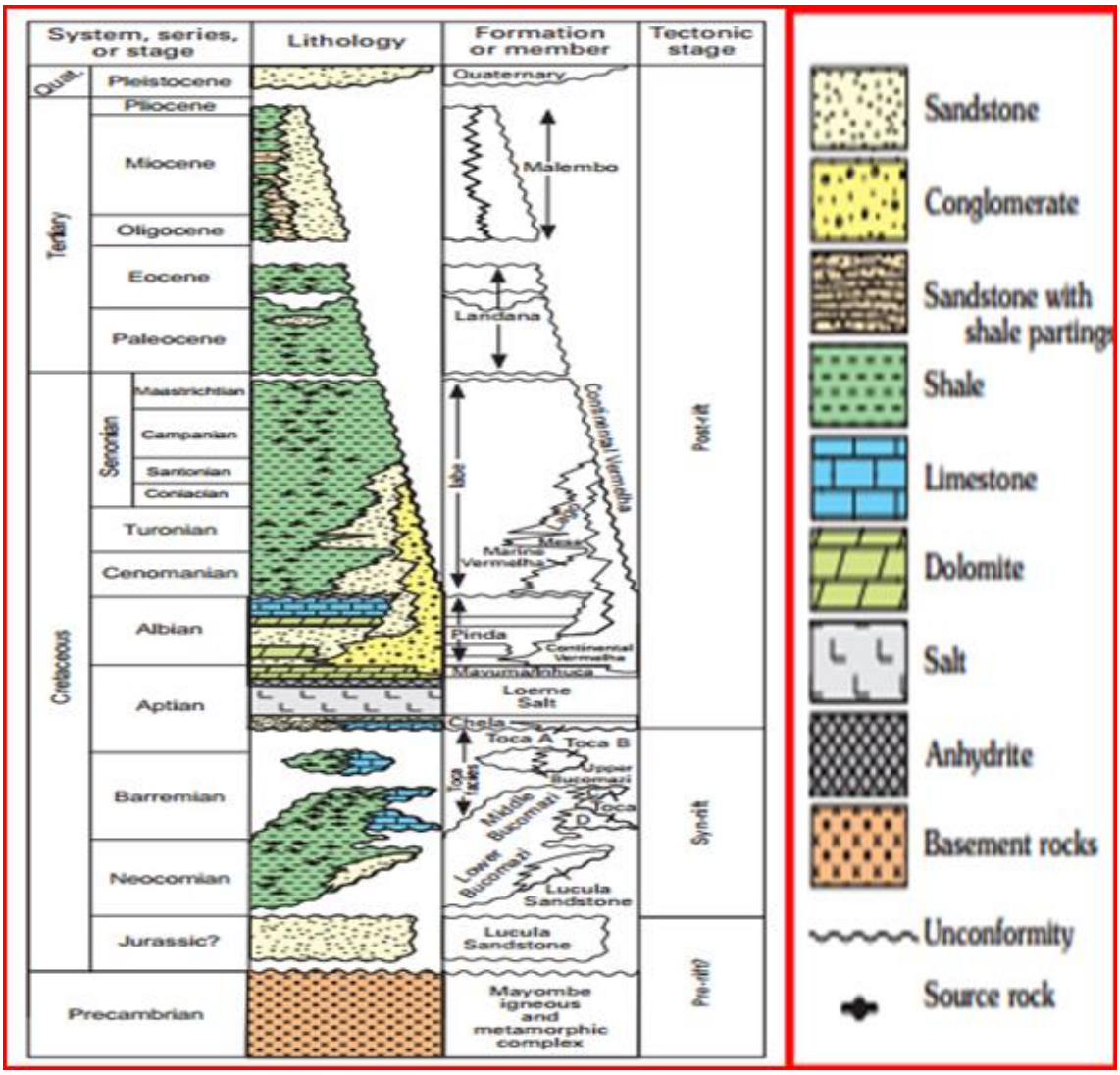

Figure 3.3 Lithostratigraphic column of the Lower Congo Basin (source: Brownfield and Charpentier, 2006).

3.2 Exploration Wells of Block Michocho

The following table describes the operational features of the five exploration wells (Joia, Obika, Moyo, Samalesso and Lango) in this study. As the block name, the wells were also renamed due to confidentiality reasons.

Table 3.1 Features of the wells.

PARAMETERS	WELLS				
	Joia	**Obika**	**Moyo**	**Samalesso**	**Lango**
RTE (m/MSL)	26	19	26	38	19
WD (m)	481	902	900	1015	1056
Burial Start (m tvd)	814.6	528.9	709.1	1705.0	621.9
Burial End (m tvd)	1860.2	1128.9	1243.1	2323.3	1624.1
Stratigraphy	Upper Miocene & Middle Miocene	Upper Miocene & Miocene	Lower Miocene	Miocene and Oligocene	Miocene
Max. deviation(º)	23.8	0	1	50	3

3.3 Application of the Method on the Wells

Figure 3.4 below outlines the workflow conducted in this study. Figure 3.5 and 3.6 provides the same template to describe worked data and investigated parameters for each well. This study was carried out in Excel®. Table 3.2 lists the parameters of the template sheet.

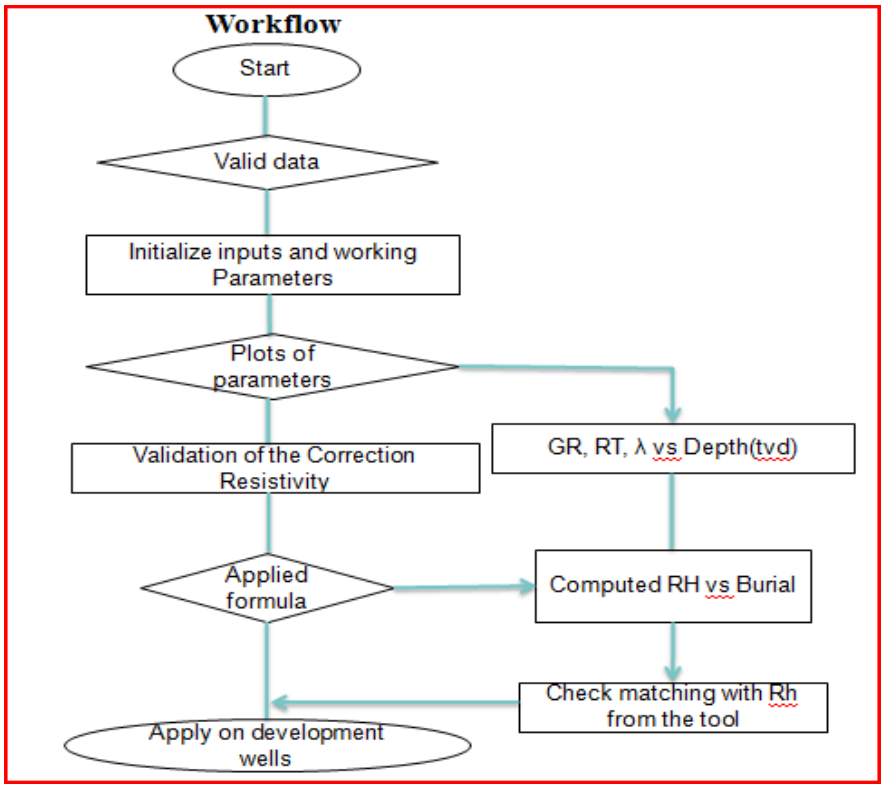

Figure 3.4 Workflow of the case study.

A	B	C	D	E	F	G	H	I	J	K
WELL							Rt	26	WD	481
DEPTH(m tvd)	TVD (m)	GR (Api)	Rt (Ωm)	Rv (Ωm)	Rh(Ωm)	Rv/Rh	Burial (m tvd)	Deviation (°)	Computed RH	Error (Rh vs RH)
1311.0209	1321.6603	66.7417	0.7856	-999.25	-999.25	1	814.6603096	1.484845637	0.7856	1.7560566
1311.0971	1321.731	71.4835	0.7958	3.5038	0.8096	4.327816206	814.7310192	1.48793623	0.795320137	0.99938747
1311.1733	1321.8017	71.4835	0.795	3.548	0.8097	4.381869828	814.8017288	1.491026823	0.794519956	0.999387427
1311.2495	1321.8724	67.8614	0.7836	3.5848	0.8097	4.42731876	814.8724384	1.494117416	0.783126308	0.99938746
1311.3257	1321.9431	67.8614	0.7782	3.6108	0.8097	4.459429418	814.943148	1.49720801	0.77772921	0.999387493
1311.4019	1322.0139	68.8726	0.7614	3.625	0.8097	4.476966778	815.0138576	1.500298603	0.760939182	0.999387525
1311.4781	1322.0846	68.8726	0.7806	3.6274	0.8096	4.48048419	815.0845672	1.503389196	0.780127523	0.999387634
1311.5543	1322.1553	68.521	0.7848	3.6188	0.8094	4.470966148	815.1552768	1.506479789	0.784325087	0.999387818
1311.6305	1322.226	68.521	0.7989	3.5999	0.8091	4.449264615	815.2259864	1.509570382	0.798416804	0.999388077

Figure 3.5 Excel® template of the worked data.

S	T	U	V
Depth (m tvd)	TVD (m)	Inclination (°)	Burial (m tvd)
1606.59	1606.5783	0.14	680.578336
1632.87	1632.8583	0.04	706.8583147
1666.95	1666.9383	0.00	740.9383119
1694.65	1694.6383	0.06	768.6383069
1751.27	1751.2583	0.04	825.2582944
1779.92	1779.9083	0.06	853.9082889
1808.01	1807.9983	0.06	881.9982823

Figure 3.6 Survey of one well. Interpolation to get the inclination of other points of the depth.

Table 3.2 List of parameters used in the Excel® template of the worked data.

List and description of parameters taken into account	
Depth (m tvd)	Measured depth with RT and WD
TVD (m)	True vertical depth
GR(Api)	Gamma ray
Rt(Ωm)	True resistivity
Rh(Ωm)	Horizontal resistivity
Rv(Ωm)	Vertical resistivity
Rv/Rh	Coefficient of anisotropy
Burial (m tvd)	Measured depth without RT and WD
Deviation (º)	Inclination between the wellbore and the bedding
Computed RH(Ωm)	Horizontal resistivity from the equation (5)
Error(Rh vs RH)	Error of Computed RH regarding horizontal resistivity
RT(m)	Rotary table
WD(m)	Water depth

Equation 5 (page 14) was rewritten into equation (6) to enable calculation of horizontal resistivity (R_h) from the remaining parameters.

$$Computed\ RH = R_t\sqrt{\frac{sin^2\alpha}{\lambda^2} + cos^2\alpha} \qquad (6)$$

One study objectives is to check in each well (table 3.1) if the computed horizontal resistivity (R_h) matches with horizontal resistivity measured with the logging. If the matches verify in the five wells, we can conclude that Equation (5) serves to make correction of the anisotropy in resistivity. It is very important to know the coefficient of anisotropy that we have to use in that formula.

3.4 Validation of the Formula and Results Well by Well

The same procedure was applied for the five exploration wells as mentioned. The results are present in a sequence of graphics subdivided by well and stratigraphy to better understand the behaviour of the formation anisotropy in the resistivity.

First, to restrict the shale points, a gamma ray versus depth graph was plotted. A threshold of 75API was used to separate shale. It is important to take into account that neither all gamma ray above 75API is shale, as it is possible to find micro-carbonaceous specks, organic matter and other materials with high radioactive. Second, boxes of intervals of shale from the plot of

gamma ray versus depth were selected and correlated with resistivity and anisotropy in the same depth to produce an expedited interpretation.

3.4.1 Joia Well

Figure 3.7 displays the plot of gamma ray, inclination, resistivity log and anisotropy by depth for Joia; stratigraphic units are showed at the left part of the graphic.

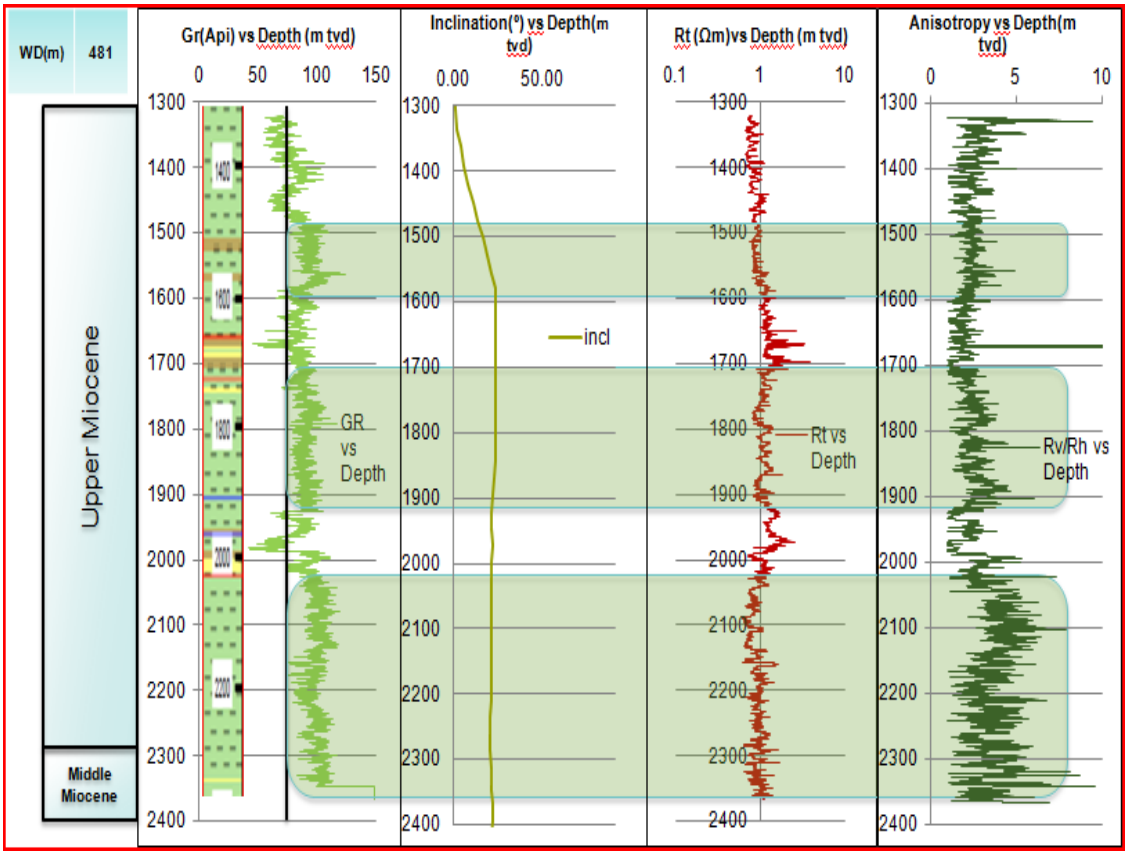

Figure 3.7 Joia well: plot of gamma ray, inclination, resistivity log and anisotropy with depth separated by stratigraphy.

Concerning Joia well:

- The depth is more in Upper Miocene and the material is turbidity.
- Shale points (were gamma ray are above 75API, black line) are delimited by green boxes to better visualize the correspondent values in resistivity and anisotropy.
- The inclination of Joia well increases until 24º and stabilize. Therefore, the impact of deviation on the anisotropy with depth is insignificant.

- Within the depth range between 1480m and 1590m (first box) resistivity is around 0.85Ωm representing a massive claystone interval (TEPA technical report).
- Between depths 1650m and 1700m, gamma ray decreases abruptly and becomes almost proportional to the increase of resistivity. This interval is predominantly sandstone; by correlation with the plot of resistivity in that zone, an expedited interpretation reveals that it corresponds to on oil reservoir. A similar situation occurs at depths between 1900m and 2000m.
- The righter plot of the Figure indicates an increase of anisotropy with depth. The Figure 3.8 shows that increase with more detail.

Figure 3.8 Joia well: plots of gamma ray and recorded coefficient of anisotropy with depth. Red lines represent trends of anisotropy within the shale intervals.

- From the correlation between the plot of gamma ray (green boxes) and anisotropy in depth, it is observed an increase of anisotropy in the low permeable rock formation (shale) (red lines). Fortunately, that evolution of anisotropy will not cause major changes in the resistivity.
- The peak of gamma ray at around 1670m corresponds to the sequence of sand-shale, and a high peak of anisotropy in that depth was observed. That abrupt transition of lithology creates locally high anisotropy.

Figure 3.9 demonstrates the result of Equation (5) modified to Equation (6) using the recorded coefficient of anisotropy for each point of depth and the error between the matches of the horizontal resistivity from the tool and computed horizontal resistivity.

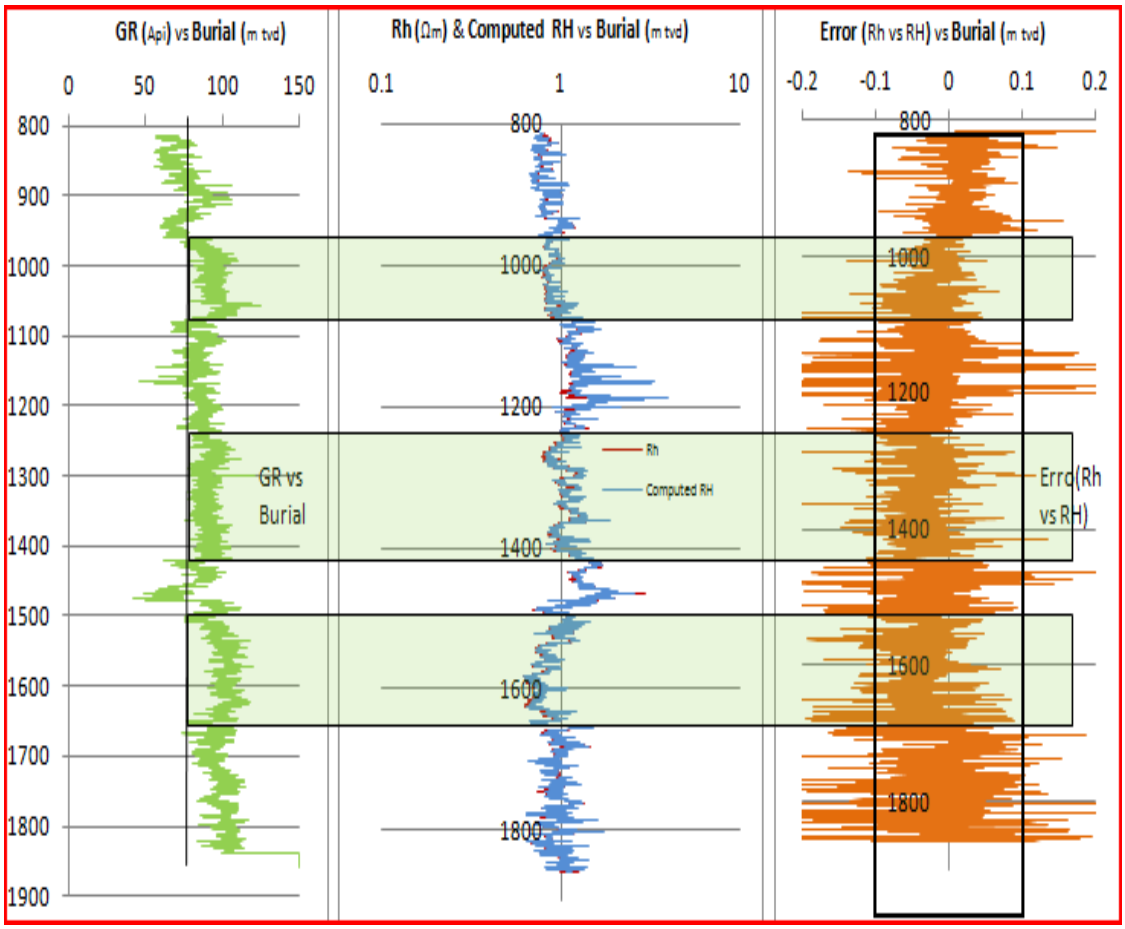

Figure 3.9 Joia well. Application and validation of Equation 5 using recorded coefficient of anisotropy. Left track: gamma ray; middle track: computed horizontal resistivity (blue line) matching with horizontal resistivity (red line) from the tool; right track: error associated with the matching between computed Rh and measured Rh.

The plot on the right shows the error, or the difference between the computed resistivity and the logging tool resistivity. Within the green boxes (shale points) errors are below 10%, which can be acceptable for the validation of the Equation (5).

The plot of anisotropy versus depth (see Figure 3.7 and 3.8) demonstrates a range of anisotropy between 2 and 6. Besides the use of recorded values for coefficient of anisotropy in the equation 5, in a second test and for sensitivity purposes three constant values for coefficient of anisotropy were used in the equation 5 in order to check if the results are similar. In figure 3.10, results are of coefficient of anisotropy equals to 3. The others plots with coefficient of anisotropy 2 and 6 are in the annex.

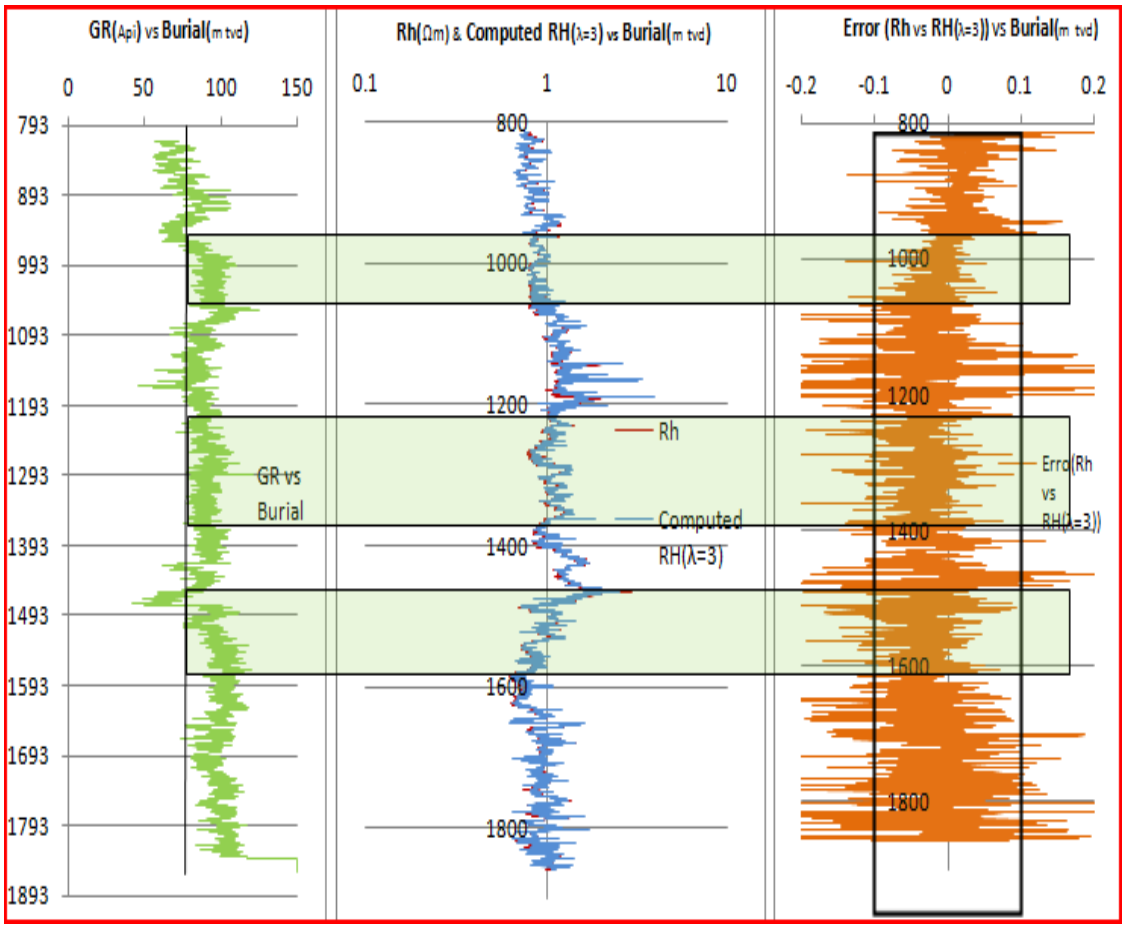

Figure 3.10 Joia well. Validation of the equation 5 using constant coefficient of anisotropy equals to 3 and computed error.

The results show that there is no substantial difference between the plots with recorded or constant coefficient of anisotropy of Equation 5 and the error associated is almost the same in the shale points. Similar results are obtained for the remaining coefficient of anisotropy values 2 and 6 (see annex).

In order to understand the evolution of anisotropy and its relationship with gamma ray in depth, Figure 3.11 displays a scattergram of those two variables in three intervals of shale.

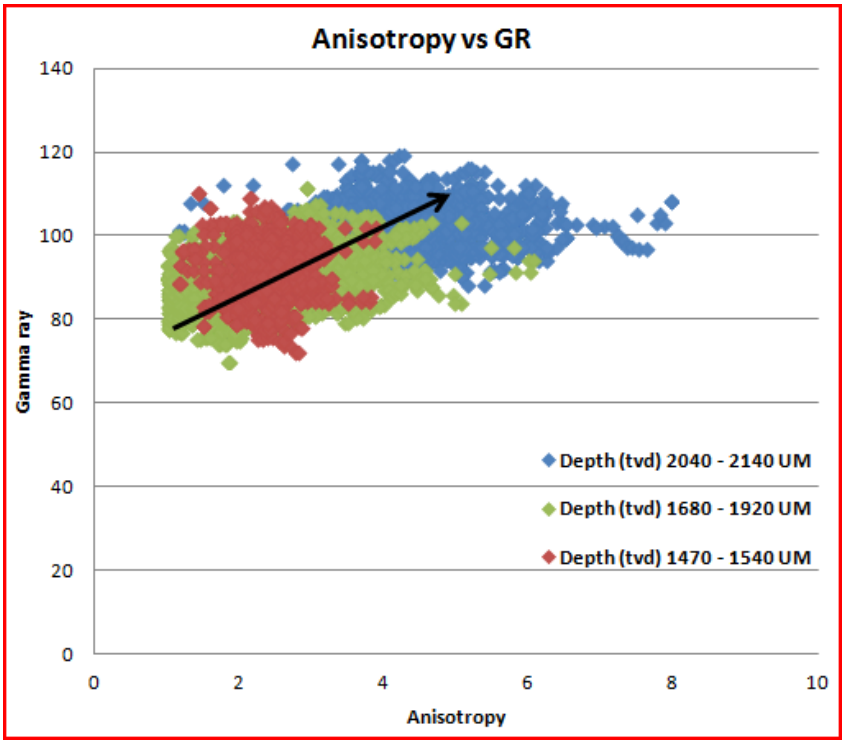

Figure 3.11 Joia well. Scattergram between anisotropy (x-axis) and gamma ray (y-axis) within shale intervals.

Despite a strong dispersion of values, Figure 3.11 enables to observe that the anisotropy increase with GR and both increases in depth, due to compaction of material, where sediments are undergoing to reorganization and they create laminations of different materials.

3.4.2 Obika well

Figure 3.12 displays a plot of gamma ray, inclination, resistivity log and anisotropy by depth; stratigraphic units are showed at the left part of the graphic.

Concerning Obika well:

- Obika well stratigraphy sits in Upper Miocene with predominance of sand and shale.
- A gamma ray cut-off of 75API (black line) to get shale points was also applied, which are identified by grey boxes.
- Obika well is vertical; therefore, anisotropy will not have impact in the resistivity.

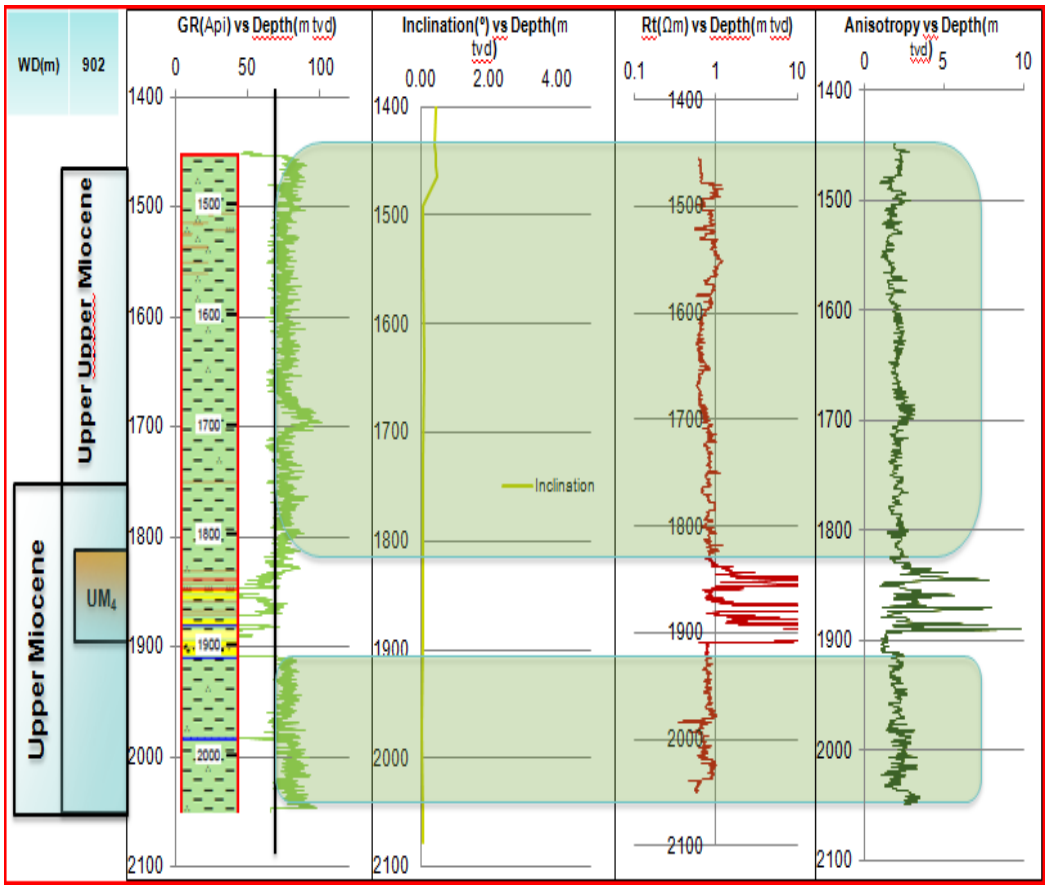

Figure 3.12 Obika well: plot of gamma ray, inclination, resistivity log and anisotropy with depth separated by stratigraphy.

- At the interval between 1480m and 1800m, (selected box) a massive claystone is identified (TEPA technical report).
- Between depth 1800 and 1900m gamma ray decreases abruptly, and becomes almost proportional to the increase of resistivity. This interval contains predominantly sandstone; the behaviour of resistivity in that zone suggests a correspondence to an oil reservoir.
- After the oil reservoir, at a depth between 1900m and 2500m a massive claystone occur again.

Figure 3.13 shows the application and validation of the equation (5) using recorded coefficient of anisotropy for each point of depth and the error (differences) between the values of the horizontal resistivity from the logging tool and the computed horizontal resistivity.

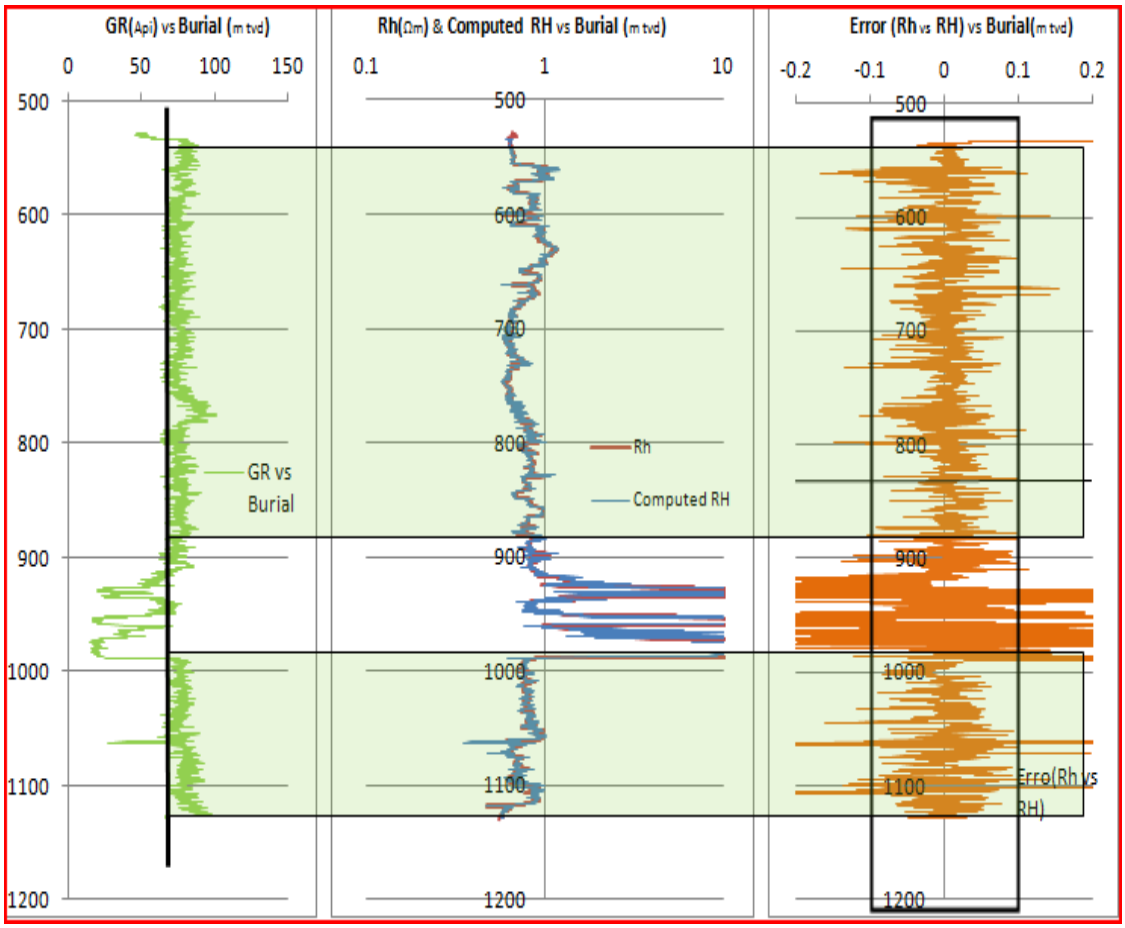

Figure 3.13 Obika well. Application and validation of equation 5 using recorded coefficient of anisotropy. Left track: gamma ray; middle track: computed horizontal resistivity (blue line) matching with horizontal resistivity (red line) from the tool; right track: error associated to the matching between computed Rh and measured Rh.

The center plot shows Computed Horizontal Resistivity (blue line) matching with Horizontal Resistivity (red line) from the tool. From the selected box, the error matching between the computed horizontal resistivity and the horizontal resistivity from the logging tool is quite always below 10%.

Again, in the figure 3.14, the computed horizontal resistivity uses a coefficient of anisotropy of 3. In annex plots with coefficient of anisotropy of 2 and 6 are presented. Both plots using record or constant coefficient of anisotropy on equation (5) get the same results and the error associated are almost the same in the shale points. The plot of validation of the equation (5) using coefficient of anisotropy 2 and 6 present the same results (see annex).

Finally, figure 3.15 displays a scattergram of anisotropy and gamma ray in the intervals of shale.

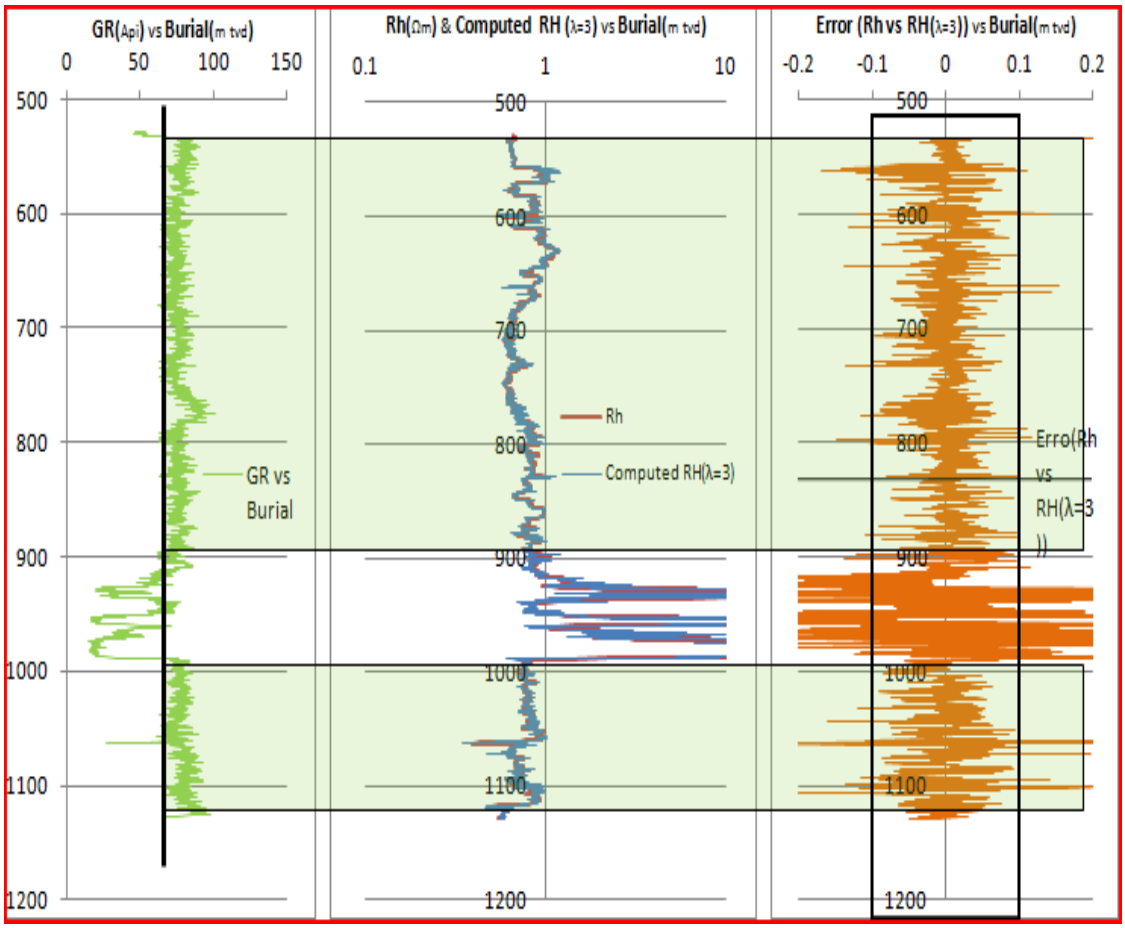

Figure 3.14 Obika well. Validation of the equation 5 using a constant coefficient of anisotropy equal to 3 and error associated.

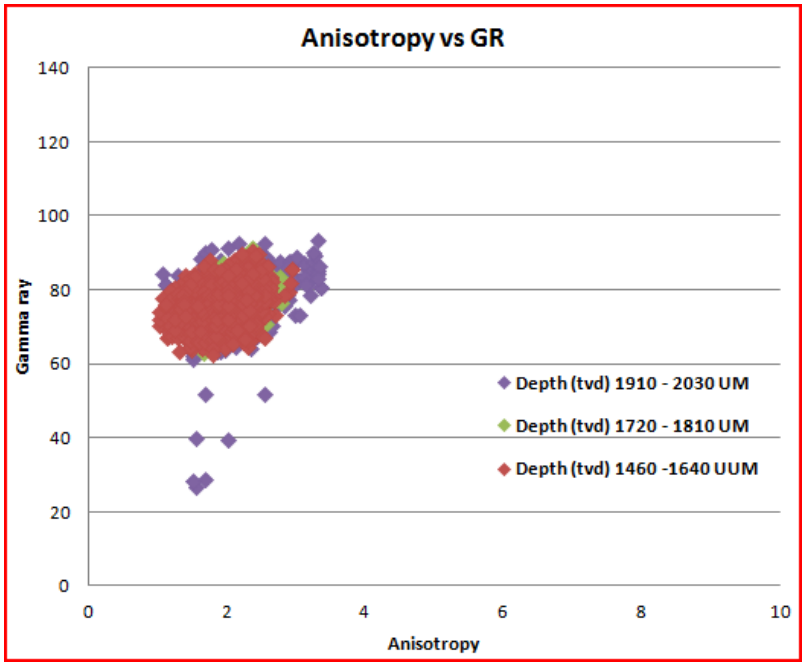

Figure 3.15 Obika well. Scattergram between anisotropy (x-axis) and gamma ray (y-axis) within shale intervals.

Obika well is vertical and it is a shallow well hence, anisotropy has a lower range interval when compared for instance with Joia well. The scattergram between anisotropy and gamma ray in these three intervals of shale points does not give good answers about the behaviour of both parameters in depth. There is a small increase in anisotropy but it is not expressive to support the idea that anisotropy increase with depth due to compaction.

3.4.3 Moyo Well

Figure 3.16 displays a plot of gamma ray, inclination, resistivity log and anisotropy by depth; stratigraphic units are showed at the left part of the graphic.

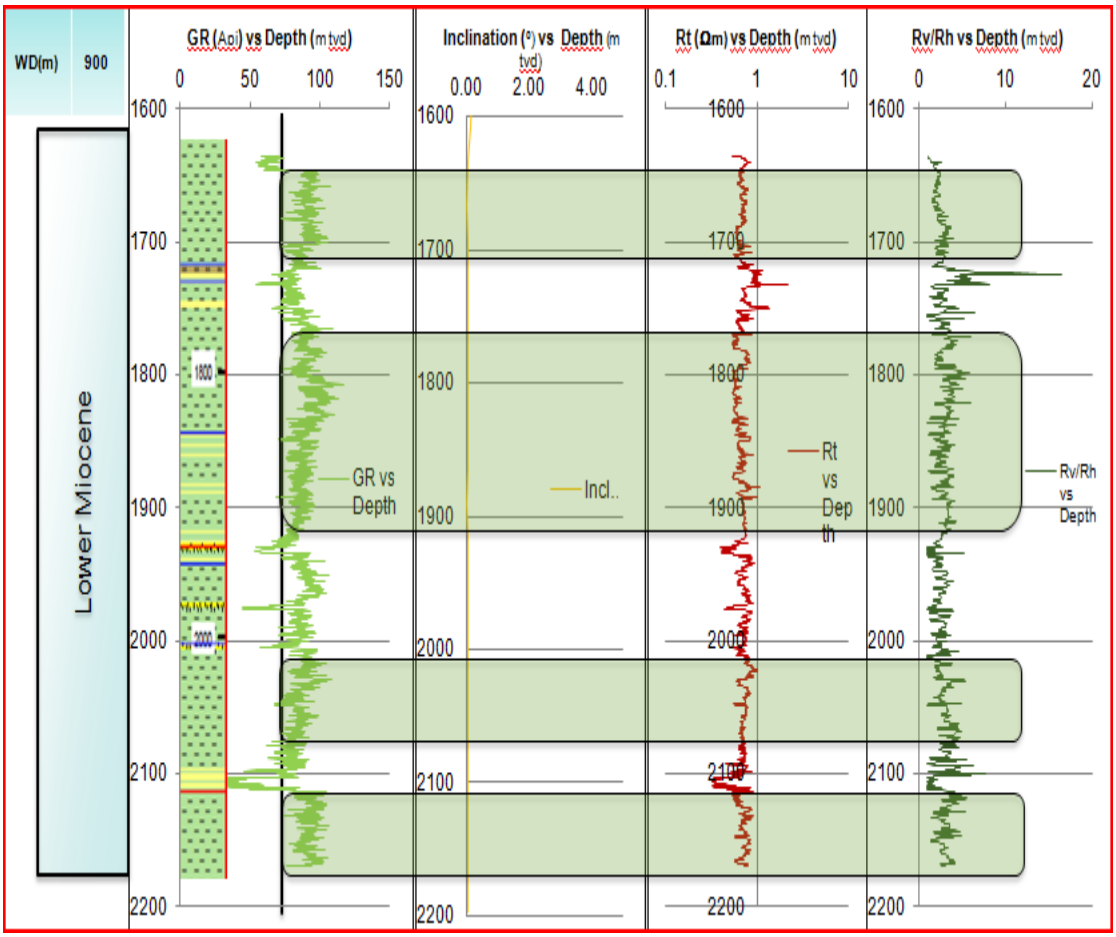

Figure 3.16 Moyo well. Plot of gamma ray, inclination, resistivity log and anisotropy with depth separated by stratigraphy.

Concerning Moyo well:

- Moyo well sits in Lower Miocene shale, sand and laminations of sand-shale occurs.

- A gamma ray cut-off of 75API (black line) was made to get shale data, which are identified by green boxes.
- Moyo well is vertical; therefore, anisotropy will not have an impact on resistivity.
- From depth 1600m to 1700m, (selected box) resistivity represents claystone (TEPA technical report).
- At depth 1730m there is an interval in which gamma ray decreases, indicating the presence of sand sediment and resistivity increases indicating the presence of an oil reservoir.
- Gamma ray presents many peaks below 75 API. Those peaks represent sequences of sand-shale.
- At depth of 2100m gamma ray is very low which indicates a sand interval. The same depth presents decreasing resistivity, which indicates the presence of a water reservoir.
- Moyo well is vertical; but the behaviour of anisotropy is unlike Obika well. That happens because of the sand-shale sequence. The transitions of lithology are macroscopically anisotropic.

Once again, Figure 3.17 demonstrates the application and validation of Equation (5) using the recorded coefficient of anisotropy for each point of depth and the error (differences) between the values of the horizontal resistivity from the logging tool and the computed horizontal resistivity.

The plot in the center shows a good match between both true and computed horizontal resistivity (respectively the red and the blue lines). From the green box, the error or differences in resistivity are below 10% in shale zones.

Figure 3.18 shows the computed horizontal resistivity with the constant 3 as coefficient of anisotropy. The plots with coefficient of anisotropy 2 and 6 are included as attachments to this paper.

There is no substantial difference between the plots using record or constant coefficients of anisotropy on Equation (5); the error associated is almost the same in the shale points. The plot of validation of Equation 5 using coefficient of anisotropy 2 and 6 present the same results (see annex).

Finally, figure 3.19 displays a scattergram of anisotropy and gamma ray in the intervals of shale.

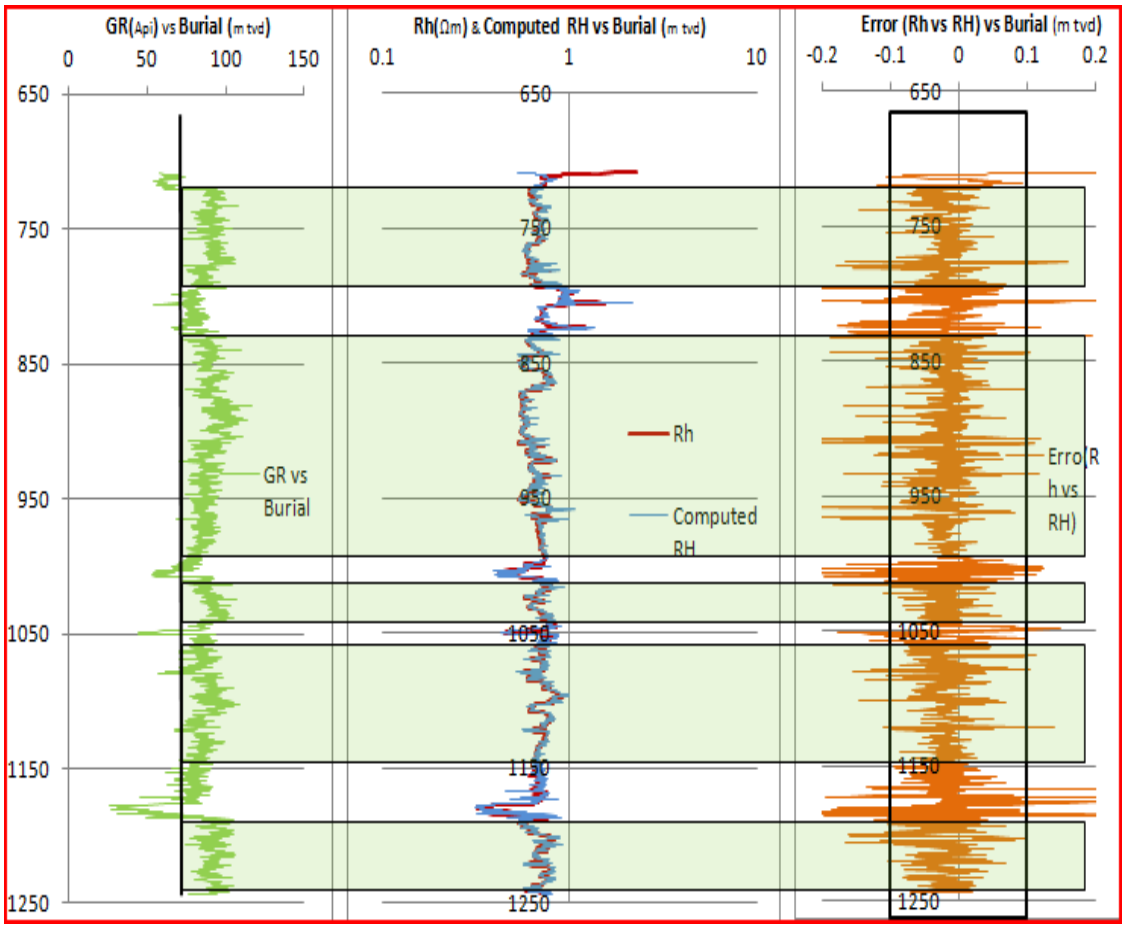

Figure 3.17 Moyo well. Application and validation of equation 5 using recorded coefficient of anisotropy. Left track: gamma ray; middle track: computed horizontal resistivity (blue line) matching with horizontal resistivity (red line) from the tool; right track: error associated to the matching between computed Rh and measured Rh.

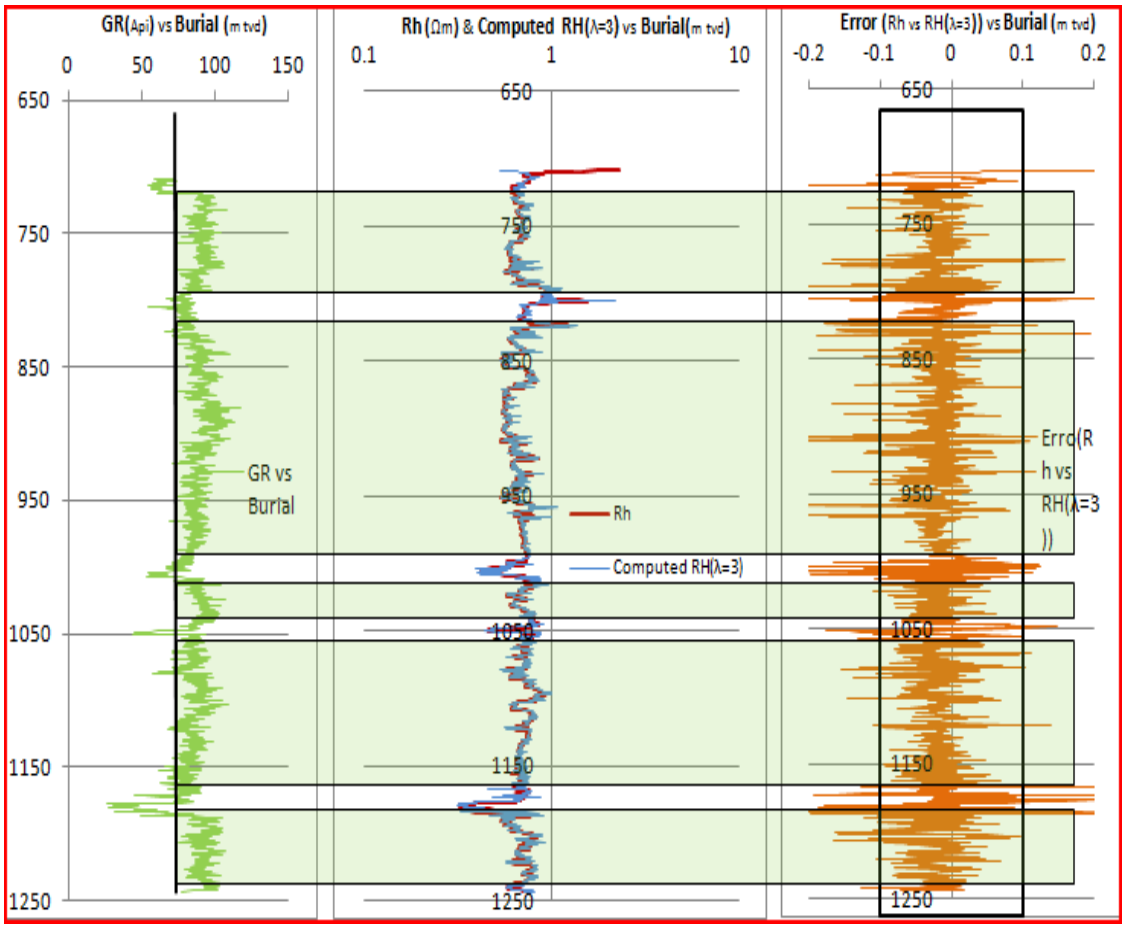

Figure 3.18 Moyo well. Validation of the equation 5 using a constant coefficient of anisotropy of 3 and error associated.

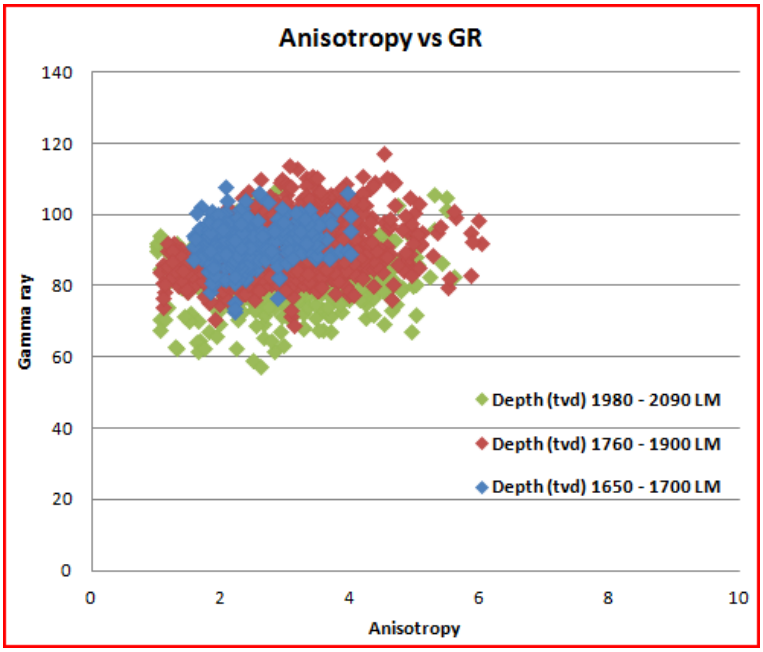

Figure 3.19 Moyo well. Scattergram between anisotropy (x-axis) and gamma ray (y-axis) in shale intervals.

The Moyo well is vertical and shallow hence, anisotropy has a low expression. The crossplot between anisotropy and gamma ray does not provides a good reading concerning to the behaviour of anisotropy with depth in shale intervals.

3.4.4 Samalesso well

Figure 3.20 displays a plot of gamma ray, inclination, resistivity log and anisotropy by depth; stratigraphic units are showed at the left part of the graphic.

Concerning Samalesso well:

- The Samalesso well sits in Miocene and Oligocene formations, and consists of predominantly shale, sand and trace micro carbonaceous specks, that is occasionally sub-laminated with organic matter, slightly to very dolomitic.
- Gamma ray presents high values in both Miocene and Oligocene formations. This probably occurs because of the presence of organic matter.
- We define a gamma ray cut-off of 80API (black line) to select shale points. The gamma ray box includes shale intervals to verify what happens in the evolution of the plots of resistivity versus depth.

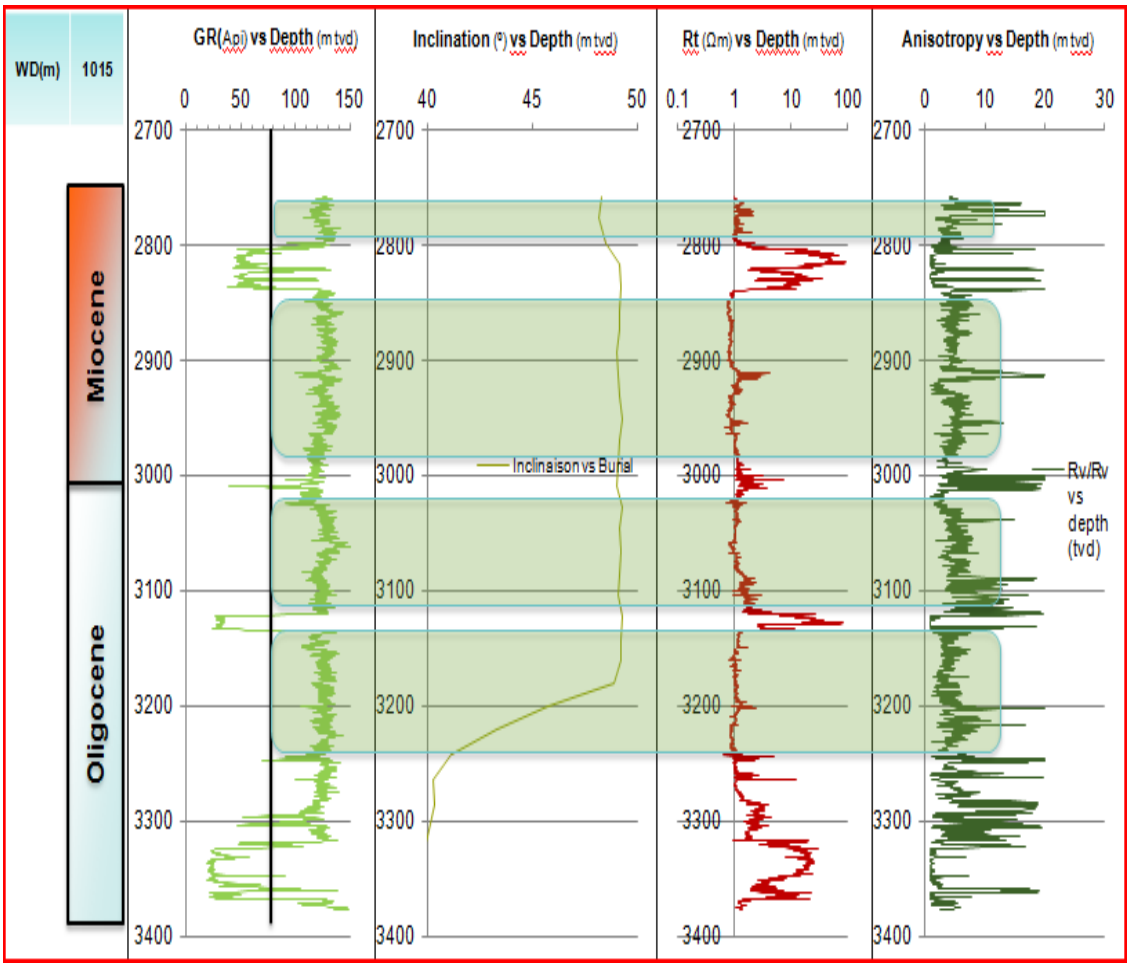

Figure 3.20 Samalesso well. Plot of gamma ray, inclination, resistivity log and anisotropy with depth separated by stratigraphical units.

- According to the plot of gamma ray versus depth, intervals from depths of 2800m to 2840m, from 3120m to 3140m and 3270m to 3380m indicate a large amount of sand. The correlation of these intervals with the plot of resistivity indicates an oil reservoir.
- The Samalesso well has an inclination of 50º; therefore, anisotropy will have a impact on the resistivity.
- Anisotropy presents many high peaks in both formations because of the variation of the lithology along the depth.
- The plot of anisotropy versus depth reveals many high peaks in the zones of a change of sediments, for instance, a sequence of sand-shale.

Figure 3.21 plots the application and validation of Equation (5) using a recorded coefficient of anisotropy for each point of depth and the error between the matches of the measure horizontal resistivity and computed horizontal resistivity.

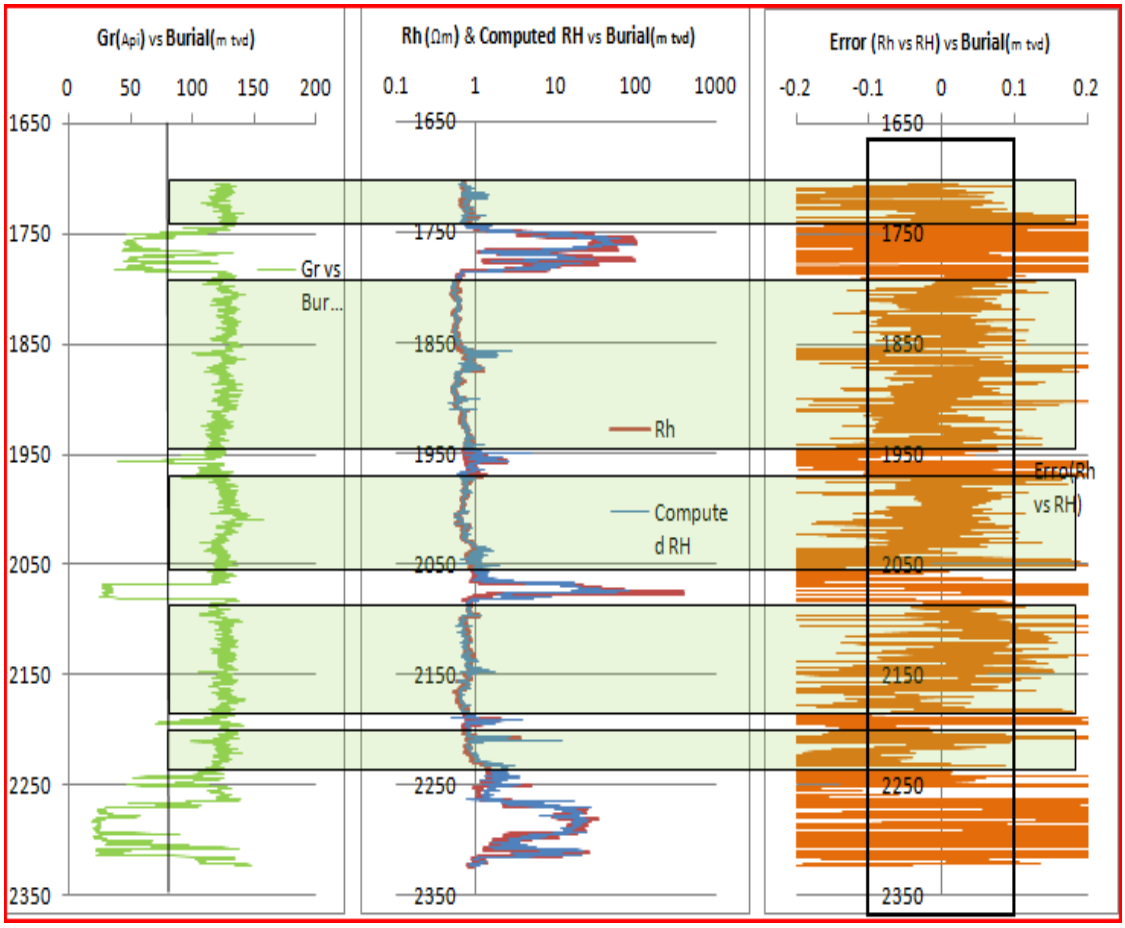

Figure 3.21 Samalesso well. Application and validation of equation 5 using recorded coefficient of anisotropy. Left track: gamma ray; middle track: computed horizontal resistivity (blue line) matching with horizontal resistivity (red line) from the tool; right track: error associated to the matching between computed Rh and measured Rh.

The plot in the center shows computed horizontal resistivity (blue line) matching well with horizontal resistivity (red line) from the logging tool. From selected box, the matching error between computed horizontal resistivity and horizontal resistivity from the tool is below 10% in shale zones.

Figure 3.22, the computed horizontal resistivity uses a coefficient of anisotropy 3. The plots with coefficients of anisotropy 2 and 6 are included in the annex. There is no substantial difference between the plots using record or constant coefficients of anisotropy in Equation (5) and the error associated is almost the same in the shale points. The plot of validation of Equation (5) using coefficients of anisotropy 2 and 6 present the same results (see annex).

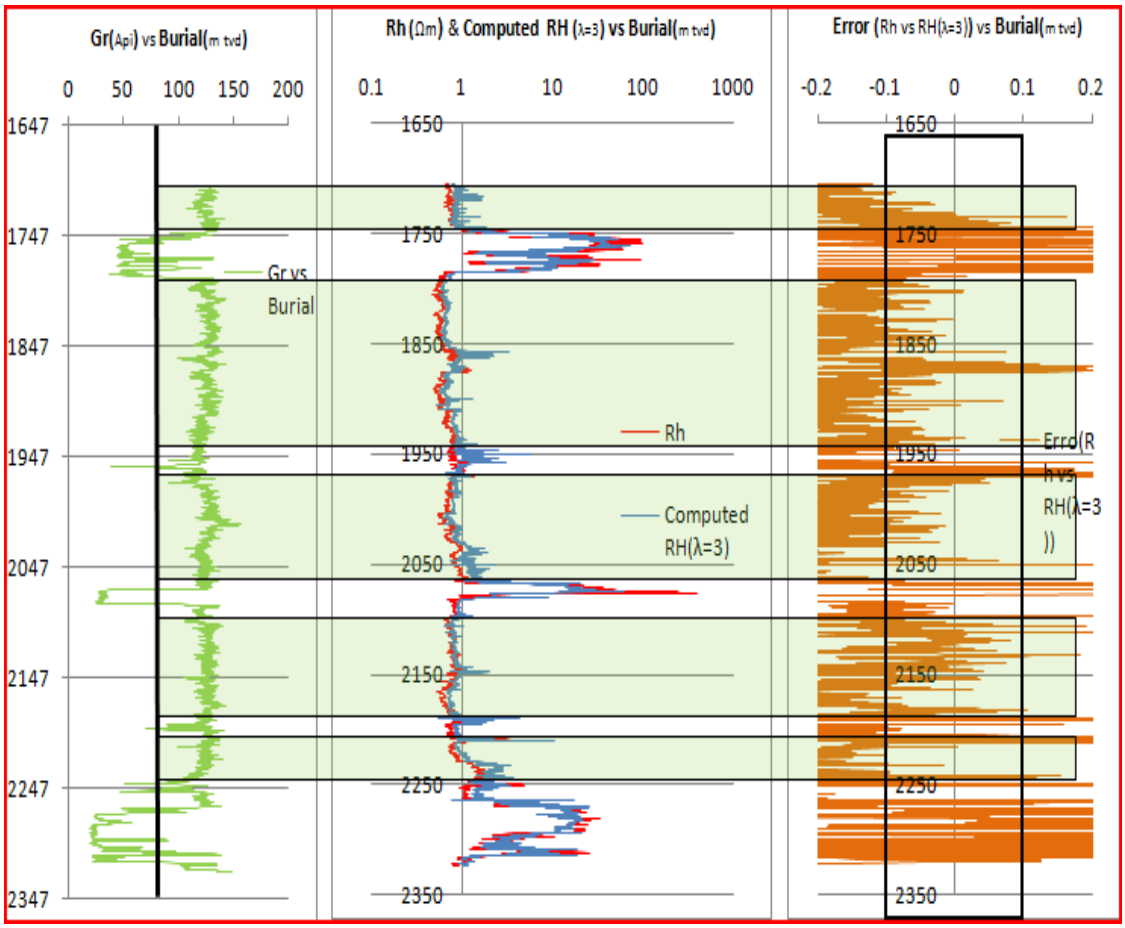

Figure 3.22 Samalesso well. Validation of the equation 5 using constant coefficient of anisotropy of 3 and error associated.

Finally, Figure 3.23 displays a scattergram of anisotropy and gamma ray in the intervals of shale.

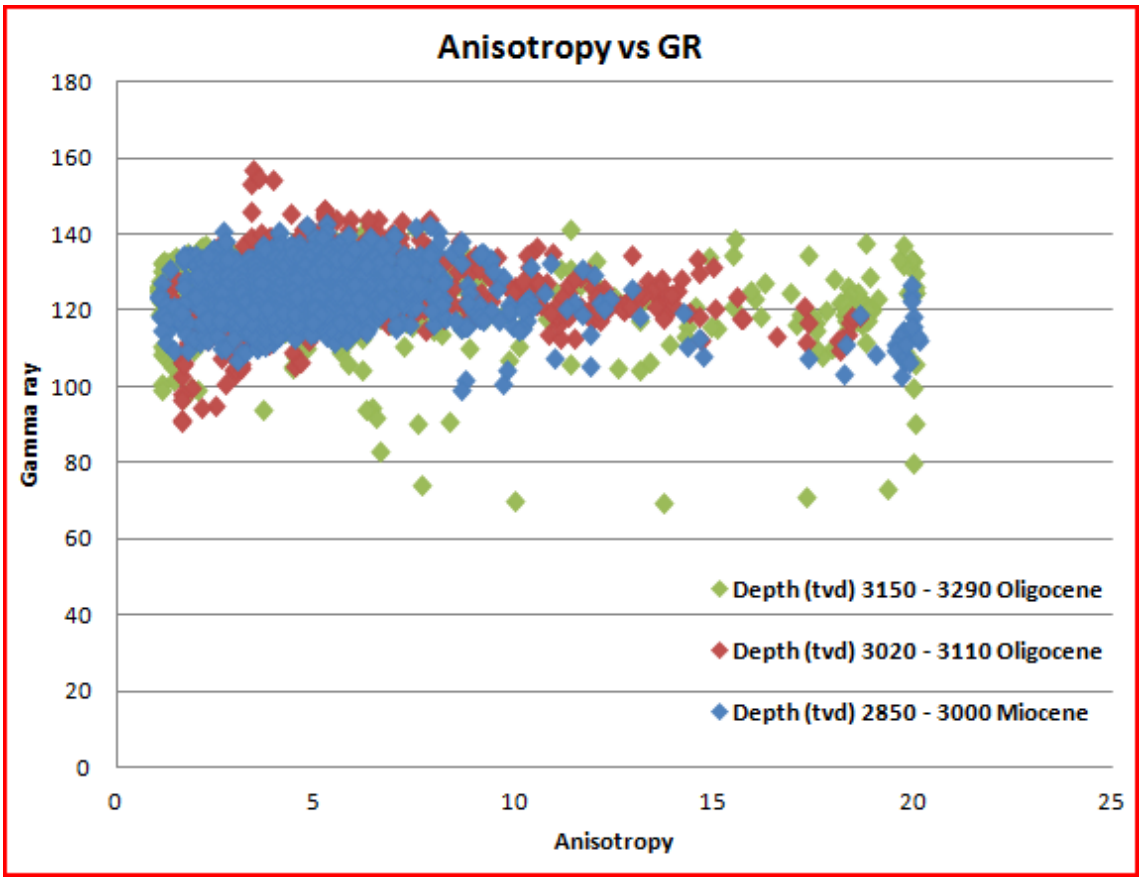

Figure 3.23 Samalesso well. Scattergram between anisotropy (x-axis) and gamma ray (y-axis) in shale intervals.

In the scattergram, anisotropy is disseminated in every part of both formations; it is very high. The Samalesso well has a high deviation and it is deeper than all wells; hence, anisotropy will produce huge impact on resistivity.

3.4.5 Lango well

Figure 3.24 displays a plot of gamma ray, inclination, resistivity log and anisotropy by depth; stratigraphic units are showed at the left part of the graphic.

Concerning Lango well:

- The Lango well sits in a Miocene formation, and consists of predominantly shale, sand and many sequences of sand-shale.
- Gamma ray presents many peaks of low values that represent sequences of sand-shale. The correlation of these peaks in the plot of resistivity corresponds to the presence of oil reservoirs.

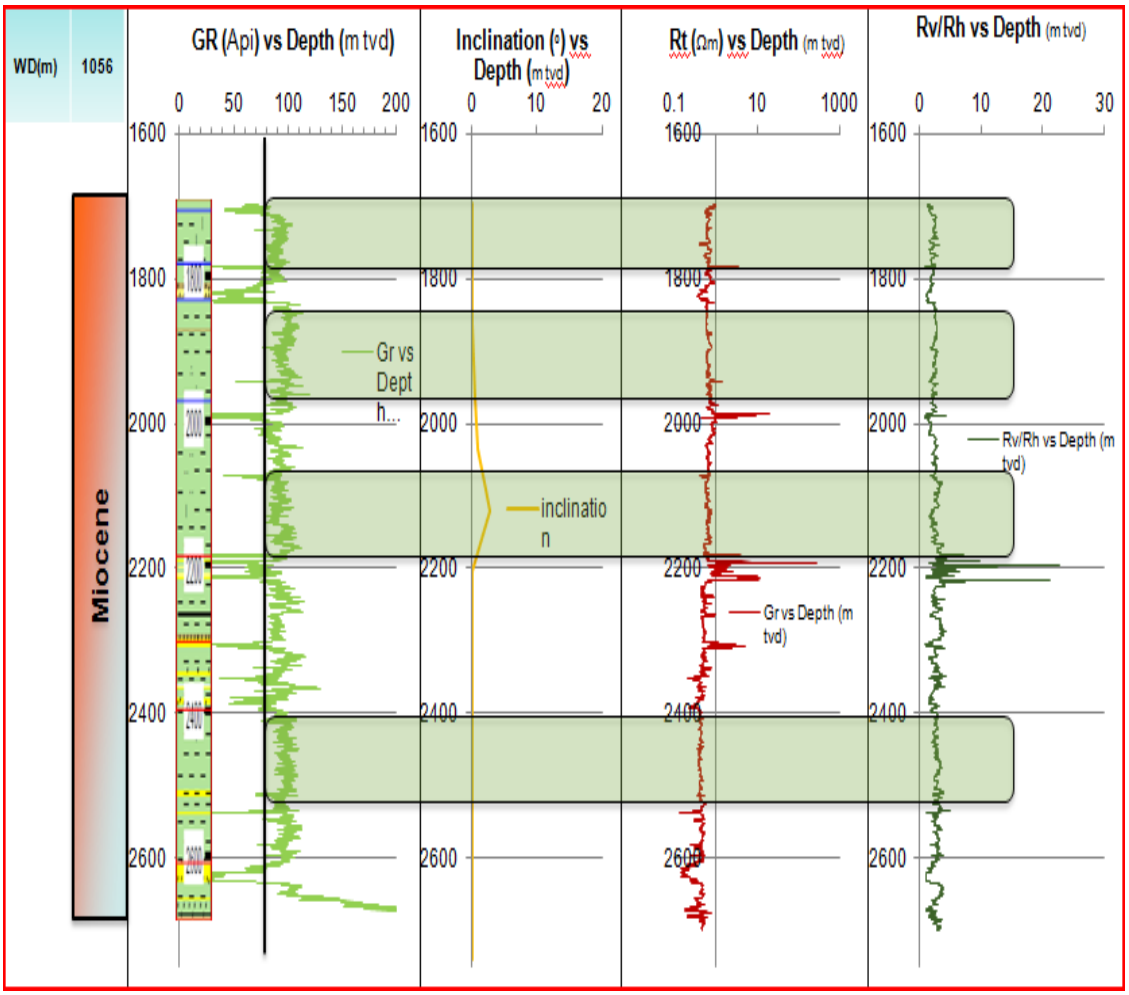

Figure 3.24 Lango well. Plot of gamma ray, inclination, resistivity log and anisotropy all with depth separated by stratigraphy.

- A gamma ray cut-off of 80API (black line) was defined to select shale points. From gamma ray the boxes shows shale intervals to verify what happens in the evolution of the plots of resistivity versus depth.
- The depths below 1800m low values of gamma ray are observed, which corresponds to sandstone. When correlating it in the plot of resistivity, that zone shows the presence of a water reservoir. We can find the same scenario in depth of 2600m.
- The depth below 2200m presents a similar situation in gamma ray but the resistivity shows the opposite behaviour corresponding to the presence of an oil reservoir.
- Anisotropy reveals some high peaks in the zones of change of sediments for example, sequences of sand-shale. The depth 2200m is the best example of the presence of a sequence of sand-shale.

Figure 3.25 plots the application and validation of Equation 5 using recorded coefficient of anisotropy for each point of depth and the error between the matches of the measure horizontal resistivity and computed horizontal resistivity.

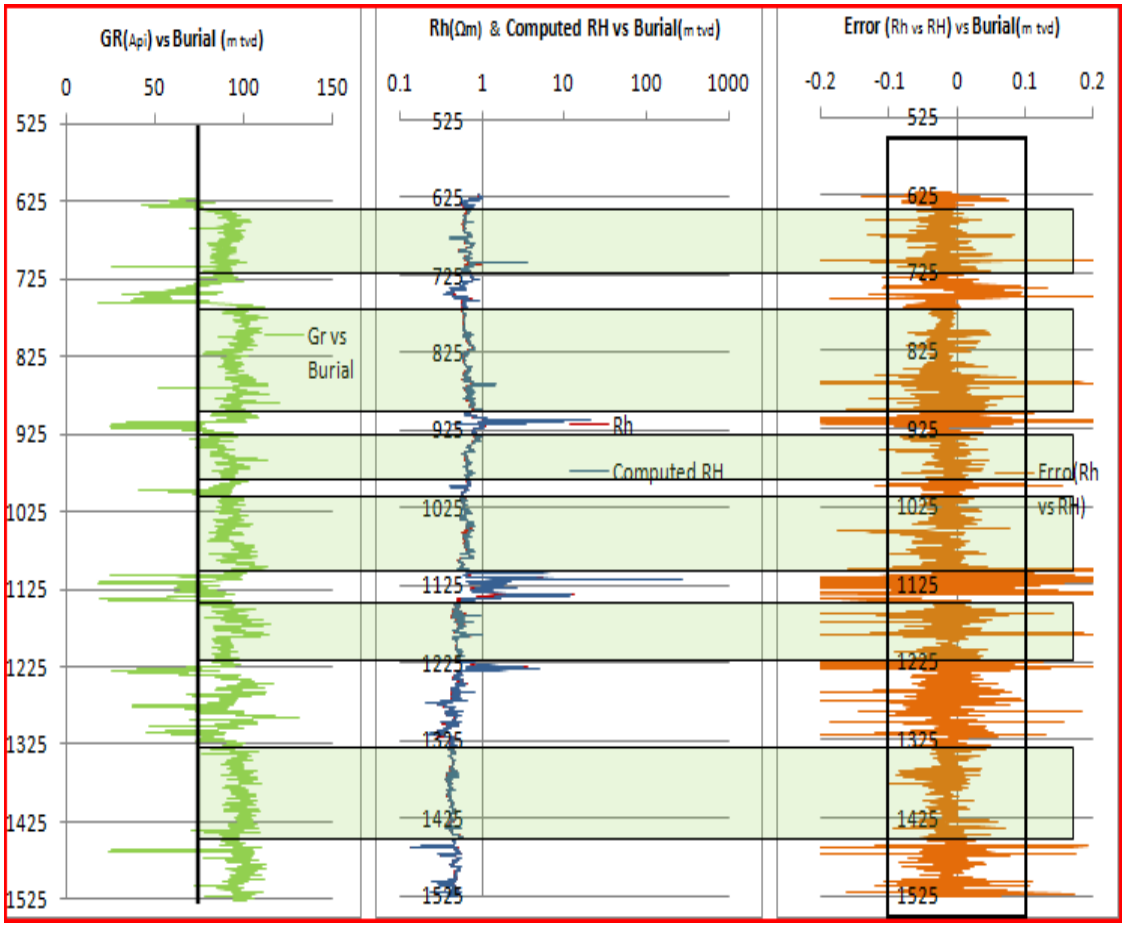

Figure 3.25 Lango well. Application and validation of equation 5 using recorded coefficient of anisotropy. Left track: gamma ray; middle track: computed horizontal resistivity (blue line) matching with horizontal resistivity (red line) from the tool; right track: error associated to the matching between computed Rh and measured Rh.

The plot in the center shows computed horizontal resistivity (blue line) matching with measure horizontal resistivity (red line). In the green box, we see the error of the matching between computed horizontal resistivity and horizontal resistivity from the tool is below 10%.

Figure 3.26, the computed horizontal resistivity has in its coefficient of anisotropy the constant 3. The plots of equation (5) with coefficients of anisotropy 2 and 6 are included in attachments to this paper.

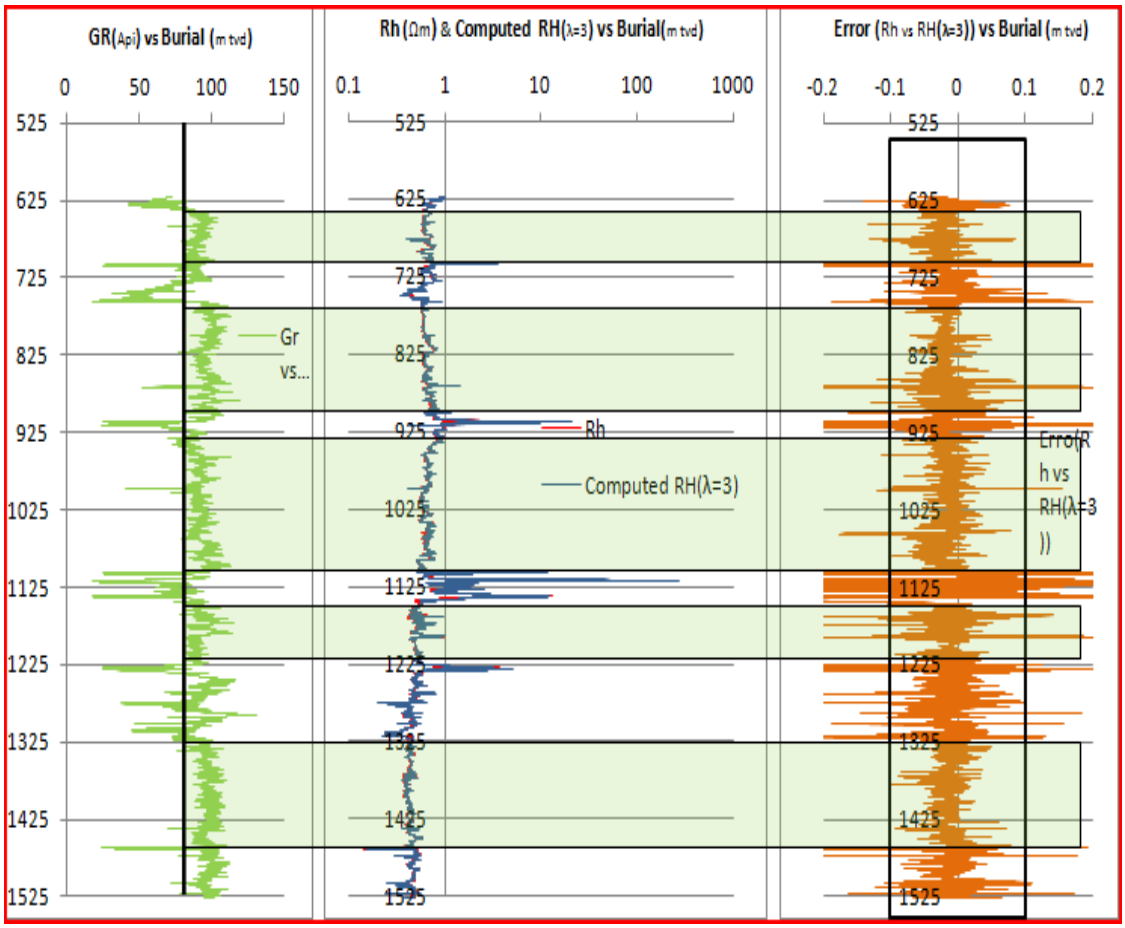

Figure 3.26 Lango well. Validation of Equation 5 using constant coefficient of anisotropy 3 and error associated.

As the previous wells, there is no substantial difference between the plots using record or constant coefficient of anisotropy in Equation (5) and the error associated is almost the same in the shale points. The plot of validation of equation (5) using coefficient of anisotropy 2 and 6 present the same results (see annex).

Finally, Figure 3.27 displays a scattergram of anisotropy and gamma ray in the intervals of shale.

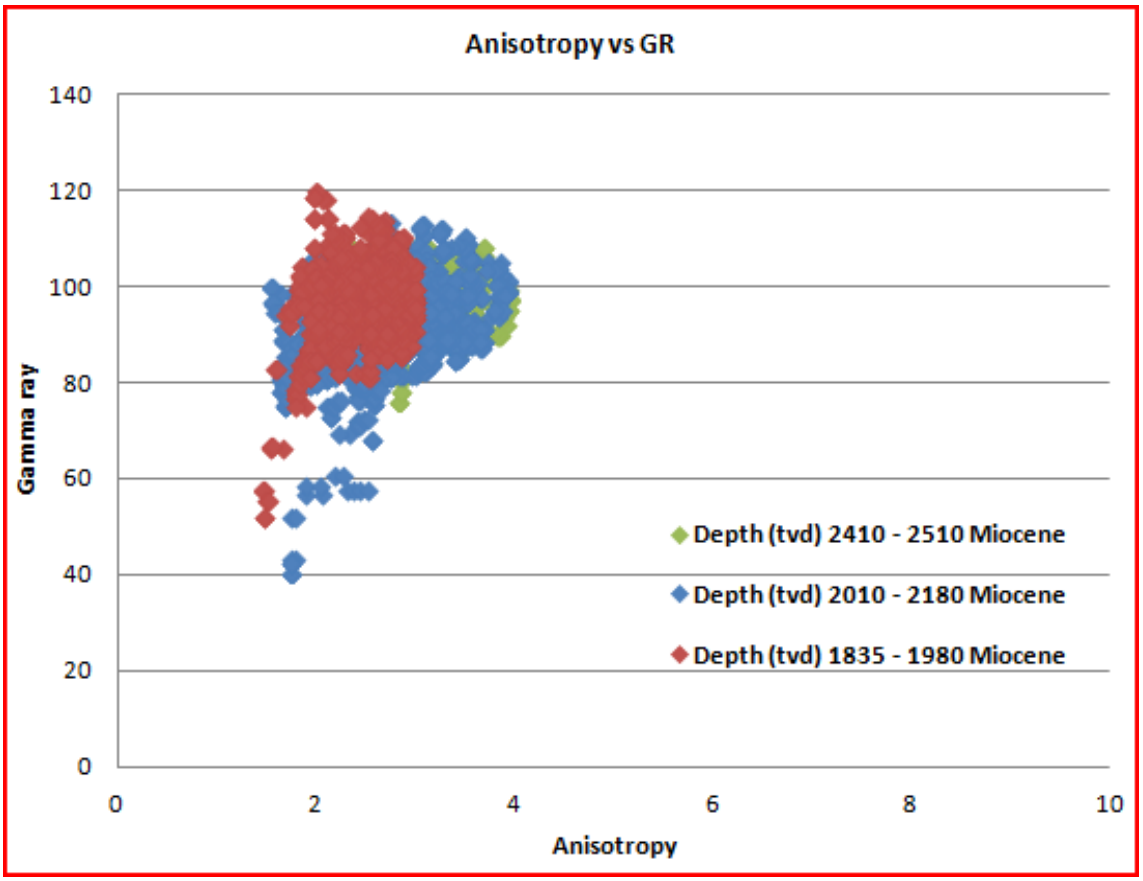

Figure 3.27 Lango well. Scattergram between anisotropy (x-axis) and gamma ray (y-axis) in shale intervals.

The Lango well is vertical and shallow hence, anisotropy is not expressed. The scattergram between anisotropy and gamma ray does not provide a good explanation for the behaviour of anisotropy with depth in shale intervals.

3.5 Characterization of the Anisotropy

Figure 3.28 shows the trend of anisotropy with depth in the five exploration wells simultaneously. The global visualization clearly exhibits an increasing trend of the anisotropy with depth in the five exploration wells of Block Michocho.

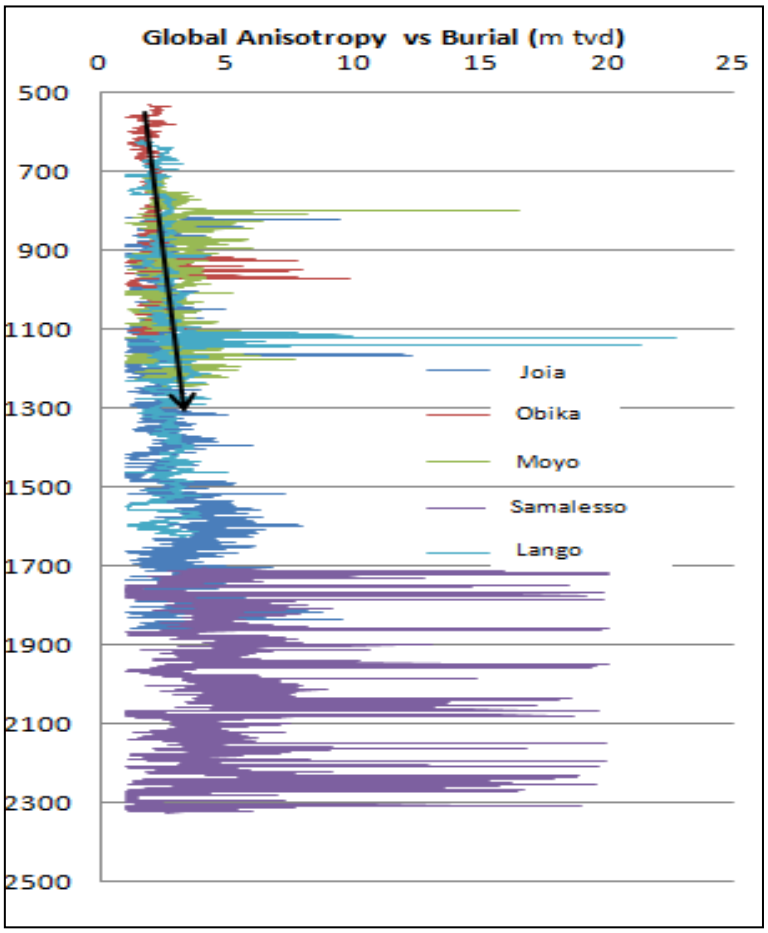

Figure 3.28 Global trend of anisotropy with depth.

Figure 3.29 explain the increase of anisotropy in depth. Along the depth, sediments are compacted and they reorganized themselves, creating laminations of material with different properties. Because of that, the logging tool reads vertical resistivity greater than the horizontal resistivity when cross over different layers along the depth. As the anisotropy is the ratio between vertical and horizontal resistivity, the greater the depth the greater anisotropy will be.

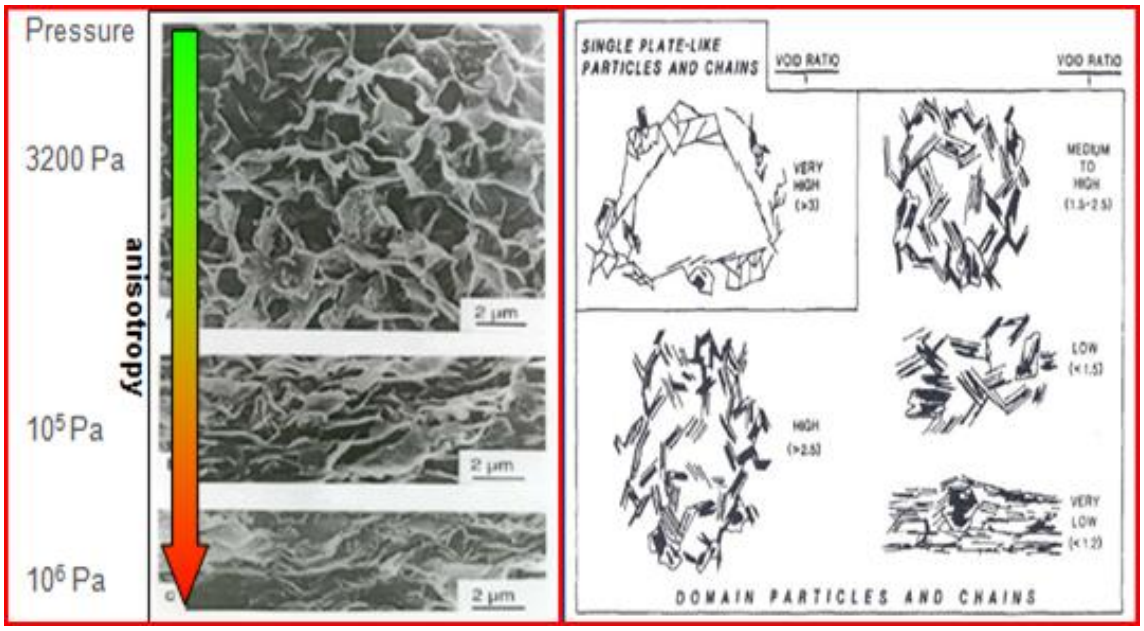

Figure 3.29 Explanation of the increase of anisotropy in depth. (Source: KSI PPP training)

3.6 Global Results of the Wells

Table 3.3 synthesizes the geological and operational parameters of the five exploration wells.

Table 3.3 Geological and operational parameters of the five exploration wells.

Parameters/Wells	Joia	Obika	Moyo	Samalesso	Lango
RTE(m/MSL)	26	19	26	38	19
WD(m)	481	902	900	1015	1056
Burial – Start (m tvd)	814.6	528.9	709.1	1705.0	621.9
Burial – End (m tvd)	1860.2	1128.9	1243.1	2323.3	1624.1
Max. Deviation (º)	23.8º	0º	1º	50º	3º
Anisotropy range	**2 – 6**	**2 – 4**	**2 – 6**	**2 – 6**	**2 – 4**
Error (Rh vs RH) (%)	**<10**	**<10**	**<10**	**<10**	**<8**
Impact of λ on Rt	**Reasonable**	**Very low**	**Very low**	**High**	**Very low**

From the plots of the five wells, a range of anisotropy values with depth was obtained being possible to quantify and qualify the impact of the anisotropy on resistivity. Of the five exploration wells, Samalesso is the well most affected well by the anisotropy due its high inclination.

The shale of the Oligocene formation is very anisotropic as shown in Table 3.4. A simple explanation for this is that Oligocene is a deeper formation than Miocene. Therefore, resistivity in that formation will be affected manly in high deviated wells.

Table 3.4 Influence of anisotropy in the stratigraphic series.

Parameters/Units	**Upper Miocene**	**Middle Miocene**	**Lower Miocene**	**Oligocene**
Impact of λ on Rt	Low	Low	Very low	High
λ on the shale points	Low	Reasonable	Reasonable	High

4. APPLICATION OF THE CORRECTION ON A DEVELOPMENT WELL

4.1 Dona 761 Well

The Dona 761 is one of a set development wells that sit between Middle Miocene and Lower Miocene series. Dona 761 has a maximum deviation of 80º and the measure resistivity is unrealistic due to the anisotropy effect. Hence, it is important to correct the resistivity acquired at Dona 761 well, in order to make a better interpretation in the pore pressure prediction. Figure 4.1 shows the correction of the observed resistivity using different constants coefficients of anisotropy of 2, 3 and 6.

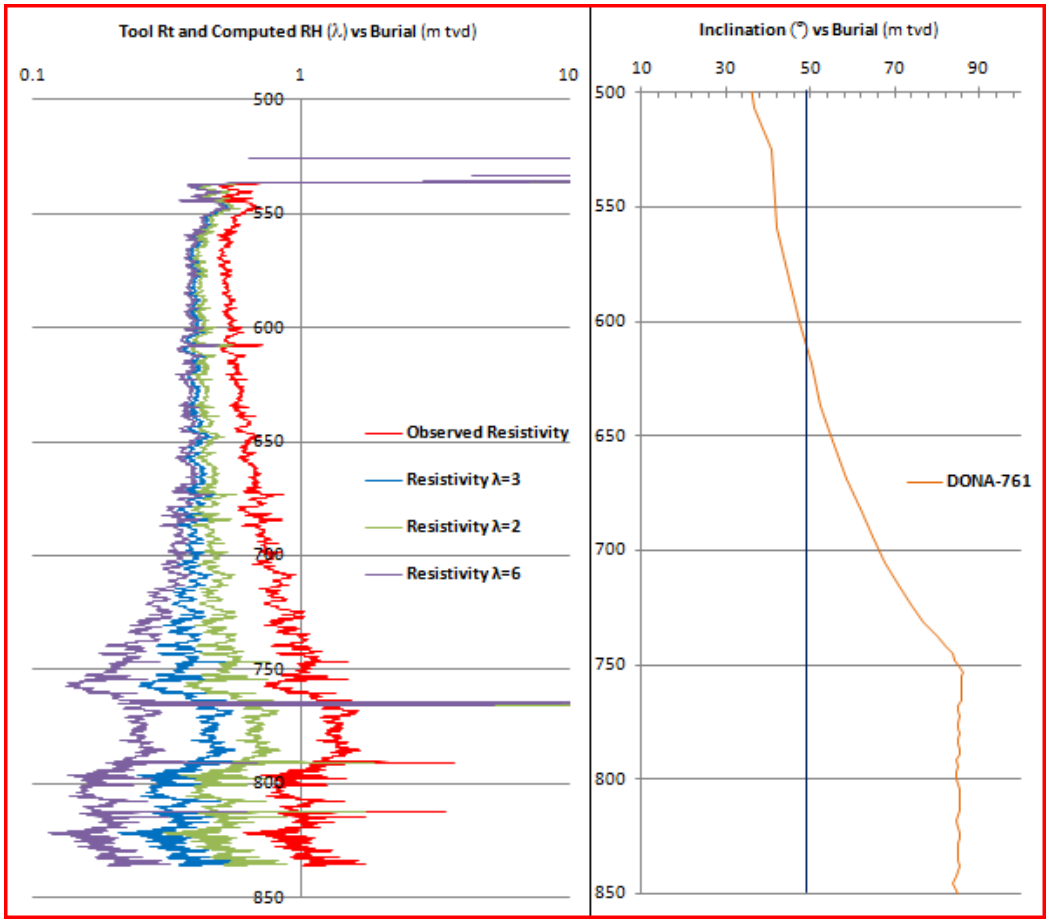

Figure 4.1 Dona development well. Plot on the left shows correction of the observed resistivity (red line) using minimum, mean and maximum coefficient of anisotropy. Plot on the right shows the inclination of Dalia well with depth.

The application of Equation (5) to correction of resistivity of this development well presents different curves for different coefficients of anisotropy. From that plot, it is difficult to know which curve is the proper curve to use in the pore pressure prediction. Therefore, Equation (5) cannot be used with a constant coefficient of anisotropy. The solution found for the calibration of the coefficient of anisotropy based in the normal compaction trend of shale resistivity.

4.2 Calibration of the Coefficient of Anisotropy

According Eaton, the normal resistivity (Rn) is a function of the burial depth. Therefore, it is possible to calibrate the coefficient of anisotropy using the normal compaction condition of both vertical and horizontal resistivity.

$$\mathrm{Rn} = \mathrm{R_0 e^{bz}} \qquad (7)$$

Where Rn is the shale resistivity with normal compaction condition; R_0 is the shale resistivity in the mudline; b is the constant; and z is the depth below the mudline.

We calculate the constant *b* through the global trend of both vertical and horizontal resistivity of the five exploration wells applying a value of z (z=5000m) greater than all the wells of Block Michocho. Once we have the constant b, we calculate both vertical and horizontal normal shale resistivity for the five exploration wells.

From the ratio between vertical and horizontal resistivity (Equation 8), it is possible to get the coefficient of anisotropy in the normal compaction condition.

$$\mathrm{Rn}\,(R_h) = \mathrm{R_0 e^{bz}} \quad ; \quad \mathrm{Rn}\,(R_v) = \mathrm{R_0 e^{bz}} \quad ; \quad \lambda = \frac{R_v}{R_h} \qquad (8)$$

Figure 4.2 shows the application of Equation (8) to obtain a global trend of both horizontal and vertical normal shale resistivity and the global trend of anisotropy in depth.

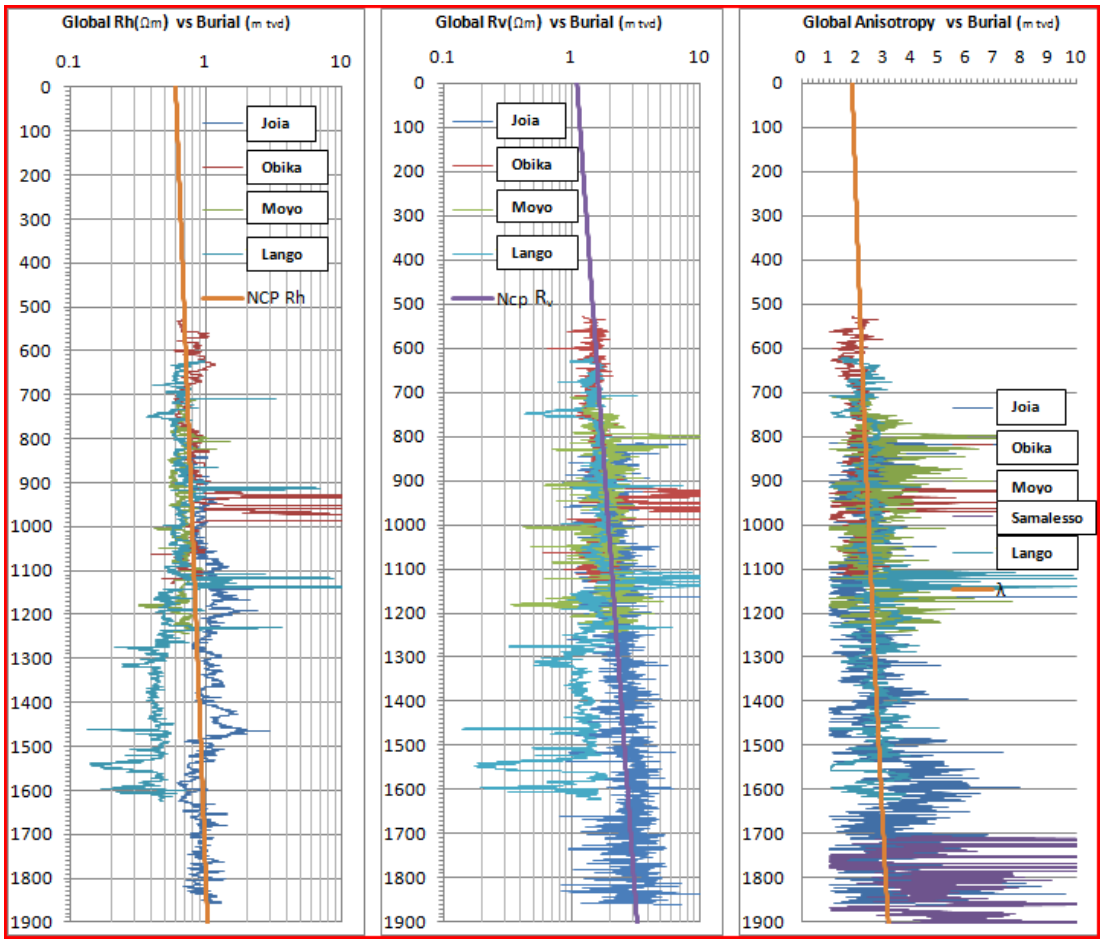

Figure 4.2 Horizontal and vertical resistivity of the wells. The lines showing the trend of resistivity resulted from equation 2. The line in the global resulted from the ratio between vertical and horizontal resistivity. Righ plot shows the calculated trend for anisotropy.

4.3 Impact of the Anisotropy in Resistivity

The presence of an anisotropic formation in deviated wells or in wells in which bedding is inclined relative to the wellbore can result in significant deviations in induction log response.

Three exploration wells with different relative dip to the bedding were chosen to evaluate the impact of the anisotropy on their apparent resistivity (see Figure 4.3).

We get the impact of the anisotropy by comparing the corrected resistivity curve (blue line) regarding to the measure true resistivity (red line) of the three exploration wells as the slope of the wells increases.

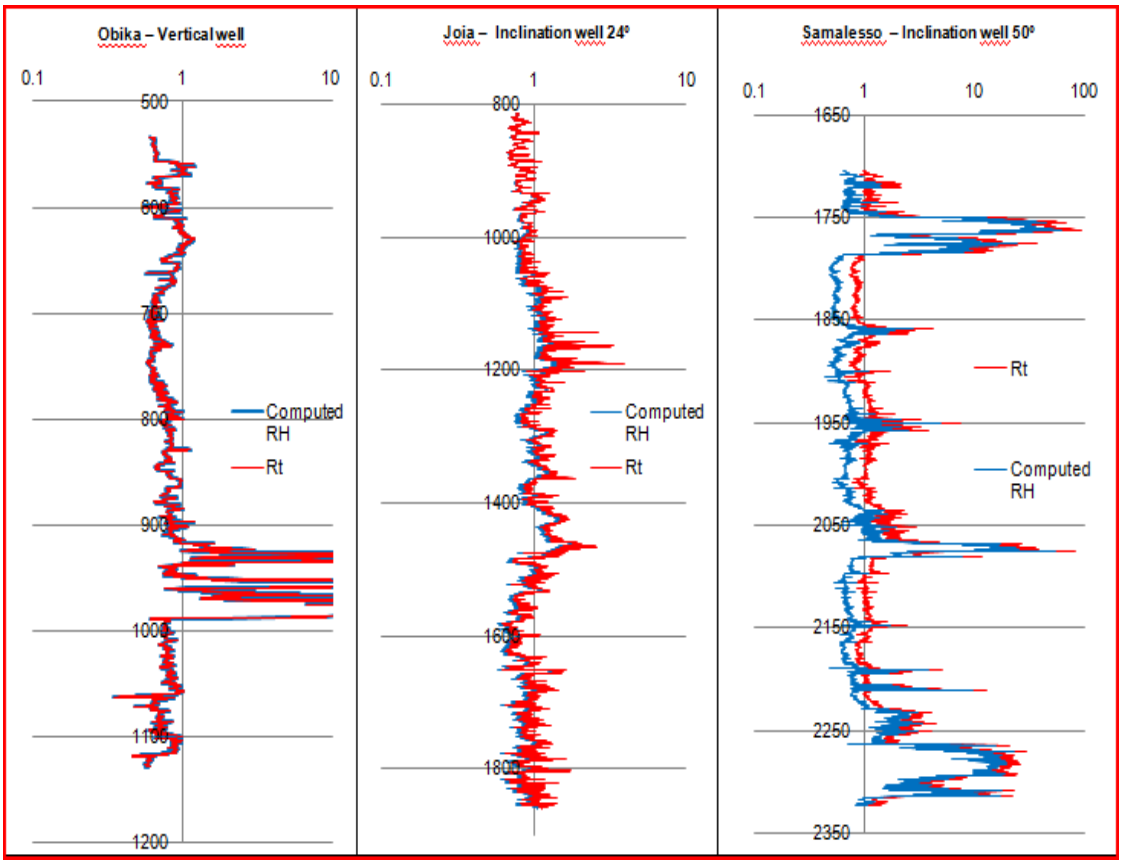

Figure 4.3 Log plots of observed resistivity and corrected resistivity for three wells with different deviation. The corrected resistivities in the more highly deviated wells are generally consistent with the resistivities recorded in the nearly vertical well, which is nearly perpendicular to the bedding.

According to Figure 4.3, the first track is a vertical well, in which both observed and corrected resistivity have the same result. This means that, in the vertical wells it is not necessary correct the anisotropy.

The second track of the Joia well presents a well with 24º inclination. In that well, anisotropy has an insignificant impact and is observed recorded corrected resistivity that differ from recorded observed resistivity at a certain depth.

The third track is Samalesso well, which has a 50º inclination, and corrected resistivity lower than the observed resistivity. That formation is very deep and anisotropic; therefore, we have values of the deep induction log that are significantly larger in deviated wells than in vertical wells.

That corrected resistivity is correct measurement to use to estimate of pore pressure. Figure 4.4 below demonstrates the impact of the anisotropy in a set of curves of resistivity of development wells. All these wells have high inclination and give unrealistic resistivity values. Even in the Figure 4.4, on the right track are the respective corrections of these curves, which are more

coherent, with resistivity values closer to the resistivity values of vertical wells, which are resistivity's parallel to the bedding plane.

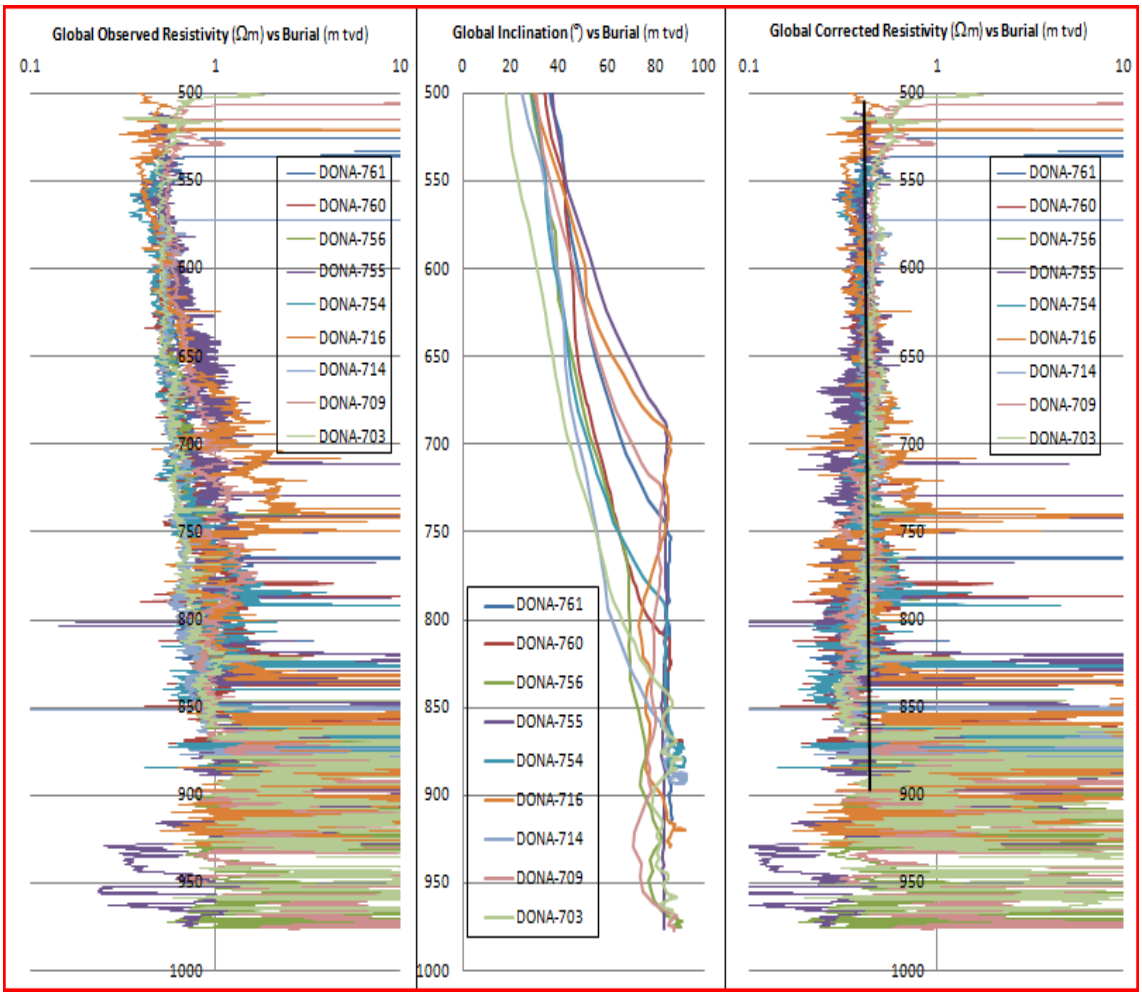

Figure 4.4 Development wells. On the left track: observed resistivities; on the middle track: inclination of the wells; on the right track: corrected resistivity of the development wells.

The high inclination of the development wells changes completely the observed resistivity due to the anisotropy environment. Equation (5) corrects the global trend of the resistivity to the vertical direction. The present corrected resistivity is appropriate for use in pore pressure prediction.

5. AN EXAMPLE OF PORE PRESSURE PREDICTION

5.1 Lango Well

Lango is a vertical well hence, it is not necessary to correct its resistivity. Lango resistivity is ready to be used in the pore pressure prediction.

The log resistivity of Figure 5.1 is only from shale points, and fluids in these formations are under much pressure. Pore pressure prediction was performed using the Equation (4) given by Eaton (1975). That requires calculating the pressure in a rock formation with low permeability such as shale.

$$P_{pg} = OBG - \left(OBG - P_{ng}\right)\left(\frac{R}{R_n}\right)^n \qquad (4)$$

Where P_{pg} is the formation pore pressure gradient; OBG is the overburden stress gradient; P_{ng} is the hydrostatic pore pressure gradient (normally 0.465psi/ft or 1.03MPa/km, dependent on water salinity); R is log the shale resistivity; R_n is the shale resistivity normal compacted trend, n is the exponent constant ranging from 0.6 to 1.5, and normally n=1.2 (Zhang, 2011).

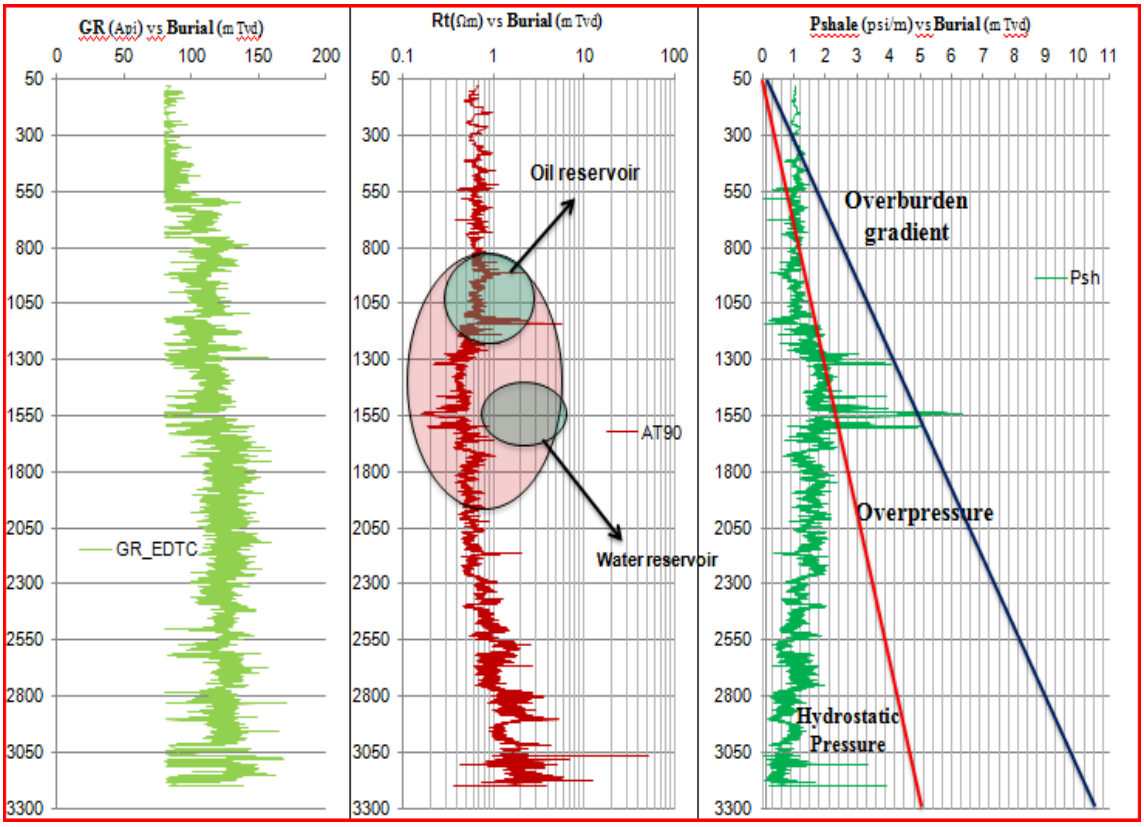

Figure 5.1 Sidetrack of Lango well. (left): gamma ray with cut-off 75API; (middle) resistivity; (right) pore pressure prediction.

From gamma ray and resistivity, shale points were filtered. Therefore, the pressure inferred in the resistivity of the Lango well is all from low permeability formation. At lower depths the pressure is normal but at a certain depth the pressure increases more than the normal pressure. The selected area on the resistivity plot shows oil reservoir and water reservoir under much pressured. An overpressure can be identified in the right track of Figure 5.1. The track on the right demonstrates pore pressure in the shale. From the normal pressure of the water and the (respectively, 1.525psi/m and 3.28psi/m), we calculate the pressure until depth 3300m. Hydrostatic pressure is under redline. The phenomenon of overpressure is between the hydrostatic pressure and the overburden gradient. Overpressure is what we want to avoid in drilling activity. Hence, we have to report the above situation to the department of the company that will design future wells in the Block Michocho.

5.2 Benefits and Disadvantages of the Correction of Resistivity

The correction of anisotropy in resistivity from wells with high relative dips serves to obtain the resistivity parallel to a bedding plan; that resistivity is appropriate in pore pressure prediction.

Although the details of the logs are different, corrected resistivity recorded are more consistent than observed resistivity. Anisotropy correction gives results more closely resemble to logs from vertical wells.

Application of Equation (5) requires horizontal resistivity logs, which are logs obtained with wireline induction tools that are very expensive. Before using Equation (5) to correct resistivity, the Equation must be validated for the field that we want to investigate. That requires to have available all log data of the parameter involved in the Equation.

For this study, the calibration of the coefficient of anisotropy did not utilize a unique coefficient. We have to use a mean of the normal resistivity shale of the field.

The correction of anisotropy reduces resistivity logs used to estimate reserves.

Corrected resistivity curves from Equation (5), when validated are appropriate for pore pressure prediction.

6. FINAL REMARKS

6.1 Conclusion

Whenever anisotropy is present in a formation and a wellbore performed in that is not perpendicular to the bedding, having high relative dip angle, the measured induction log resistivities will be too large. The higher the coefficient of anisotropy, the higher the increase of apparent resistivity.

In addition, there is a minimum angle of the relative well inclination required to see a significant impact of the anisotropy on the apparent resistivity.

The resistivity of anisotropic rock formations relies on the horizontal resistivity of the specific rock formation (resistivity measured by an induction tool normal to the bedding), the coefficient of anisotropy, and the angle between the wellbore and a vector normal to the bedding plane.

Shales or thinly laminated sand-shale sequences are the cause of anisotropy. In the shale materials in all five exploration wells, anisotropy increases with burial due to compaction, which reorganizes the sediments.

Block Michocho presents an Oligocene formation more anisotropic than Miocene. The increase of anisotropy with compaction is the more likely explanation for this situation.

The formula of correction of the anisotropy in resistivity was validated, with 10% as global error associated, which can be seen as acceptable when working with resistivity logs.

This formula computes horizontal resistivity, the closest property measured by wireline induction logs, for the five exploration wells.

In the Block Michocho, the coefficient of anisotropy reached a global range between two and six along the depth. This required us to use the Equation (5) with different constants of coefficient of anisotropy in resistivity curves of the development well highly deviated. But we realized during this study that making a correction with Equation (5) using a constant coefficient of anisotropy gives us different curves i.e for this block, there is no appropriate constant coefficient of anisotropy that would produce a better correction.

It is important to calibrate the coefficient of anisotropy correctly, in order to predict/estimate the right shale pressure; therefore, we used the normal compaction condition (applying Eaton's equation) of both vertical and horizontal shale resistivities to produce the global trend of coefficient of anisotropy for Block Michocho.

From the set of curves of development wells, we see the correction of anisotropy putting vertical trend to the curves, and also see that the values of corrected resistivity are more

coherent and relatively close to the values resistivities of vertical wells, which is nearly normal to the bedding.

The application of the method of pore pressure prediction in shale resistivity was performed successfully, which allowed us to verify that the behaviour of resistivity log with depth permits us to infer the pressures of the fluid within formations. From the resistivity curve, we infer the pressure on the well under study and could find an overpressure situation starting at depth 1050m. We could check the overpressure using Eaton's Equation (4) of pore pressure in shale.

6.2 Recommendations on the use of the Method Developed

To use the correction of anisotropy in pore pressure prediction is important to filter resistivity to select the shale points (regions).

In the other blocks or fields, equation (5) must be validated before using to correct resistivity logs. A better way to make validation of equation (5) is to compare horizontal resistivity from induction log tool with computed horizontal resistivity for the wells where this information is available.

It is not necessary to apply the correction of anisotropy in resistivity of wells that intersect perpendicular to the bedding because the induction logs tool gives the true resistivity, which is equal to horizontal resistivity.

To correct more accurately the curves of resistivity it is better to calibrate the coefficient of anisotropy using the normal compaction condition.

7. REFERENCES

Almeida, J.A. (2010) Stochastic simulation methods for characterization of lithoclasses in carbonate reservoirs. Earth-Science Reviews 101 (3), 250-270.

Alves, F., Almeida, J.A., Ferreira, A. (2014) Geostatistical Inversion of 3D Post-stack Seismic and Well Data for the Characterization of Acoustic Impedance in Oil Fields. Mathematics of Planet Earth, Lecture Notes in Earth System Sciences, 689-693.

Athy, L.F (1930) Density, porosity and compaction of sedimentary rocks. AAPG Bulletin. 14(1): 1-24.

Biot, M.A. (1941) General Theory of Three- Dimensional Consolidation. Journal of Applied Physics (American Institute of Physics, USA), 12 (2), 155-164.

Bowers, G.L. (1995) Pore Pressure Estimation From Velocity Data: Accounting for Overpressure Mechanisms Besides Undercompaction. SPE Drilling and Completions, 10(2): 89-95. SPE-27488-PA. DOI: 10.2118/27488-PA.

Bowers, G.L. (2002) Detecting High Pressure. The Leading Edge 21 (2): 174-177. DOI:10.1190/1.1452608.

Brownfield, Michael E. and Charpentier, Ronald R.(2006) Geology and Total Petroleum Systems of the West-Central Coastal Province (7203), West Africa. U.S. Geological Survey, Reston, Virginia.

Da Costa e Silva, AJ, Soares, A., Almeida, J., Ramos, L., Carvalho, J (1997) A multi-step approach for modelling oil reservoir lithologies and petrophysical attributes based on the integration of geostatistics and geology. Geostatistics Wollongong 96, vol. 1, Eds. Baafi, E.Y. & Schofield, N.A., 327-336.

England, W.A., Mackenzie, A.S., Mann, D.M. and Quigley, T.M. (1987) The Movement and entrapment of petroleum fluids in the subsurface. Journal of the Geological Society, 144(2), 327-347, DOI:10.1144/gsjgs.144.2.0327.

Eaton, B.A. (1975) The equation for Geopressure prediction from well logs, SPE 01/1975; 5544:1-11. DOI:10.2118/5544-MS.

Hottmann, C.E. and Johnson, R.K. (1965). Estimation of Formation Pressures from Log-Derived Shale Properties. Journal of Petroleum Technology, 17 (6): 717-722. DOI:10.2118/1110-PA

Klein, J.D. (1993) Induction Log Anisotropy Corrections. The Log Analyst, 34(2), 18-27.

Kuznetsova, A., Almeida, J.A., Legoinha,P. (2014) Stochastic Simulation of the Morphology of Fluvial Sand Channel Reservoirs. Mathematics of Planet Earth, Lecture Notes in Earth System Sciences, 639-642.

Luis, A., Almeida, J.A. (1996) Stochastic characterisation of fluvial sand channels. Geostatistics Wollongong'96, Vol.1, eds. E.Y. Baafi and N.A. Schofield, 477-488.

Moran, J.H. and Gianzero, S. (1979) Effects of formation anisotropy on resistivity-logging measurements. Geophysics, 44 (7), 1266-1286. DOI:10.1190/1.1441006.

Mouchet, J.P. and Mitchell, A. (1989) Abnormal Pressures While Drilling: Origins, Prediction, Detection, Evaluation. Manuels techniques elf Aquitaine, Boussens, FR.

Quental, P., Almeida, J.A., Simões, M. (2012) Construction of high-resolution stochastic geological models and optimal upscaling to a simplified layer-type hydrogeological model. Advances in Water Resources 39, 18–32.

Swarbrick, R.E. and Osborne, M.J. (1998) Mechanisms that Generate Abnormal Pressures: an Overview. AAPG Memoir 70: Abnormal Pressures in Hydrocarbon Environments (Edited by B.E. Law, G.F. Ulmishek, and V.I. Slavin), Chapter 2, 13-34.

Terzaghi, K., Peck, R.B. and Mesri, G. (1996) Soil Mechanics in Engineering Practice. John Wiley & Sons, 3rd edition, 549p.

Zhang, J. (2011) Pore Pressure Prediction from Well Logs: Methods, Modifications, and New Approaches. Earth-Science Reviews, 108 (1–2), 50–63.

Zhang, J. and Roegiers, J.-C. (2005) Double Porosity Finite Element Method for Borehole Modeling. Rock Mechanics and Rock Engineering, 38(3), 217-242.

Web references

[1] http://www.investopedia.com/terms/e/exploratory-well.asp (21/01/2014)

[2] http://www.wisegeek.com/what-is-wireline-logging.htm (21/01/2014)

[3] http://iodp.ldeo.columbia.edu/TOOLS_LABS/LWD/lwd_arc.html (21/01/2014).

[4] http://www.qgc.com.au/qclng-project/in-the-surat-basin/exploring-for-gas/exploration-wells.aspx (21/01/2014)

[5] http://www.premier-oil.com/premieroil/glossary (21/01/2014)

[6] http://www.slb.com/services/drilling/mwd_lwd/ppl/arcvision.aspx (29/01/2014)

8. Annex

Joia Well

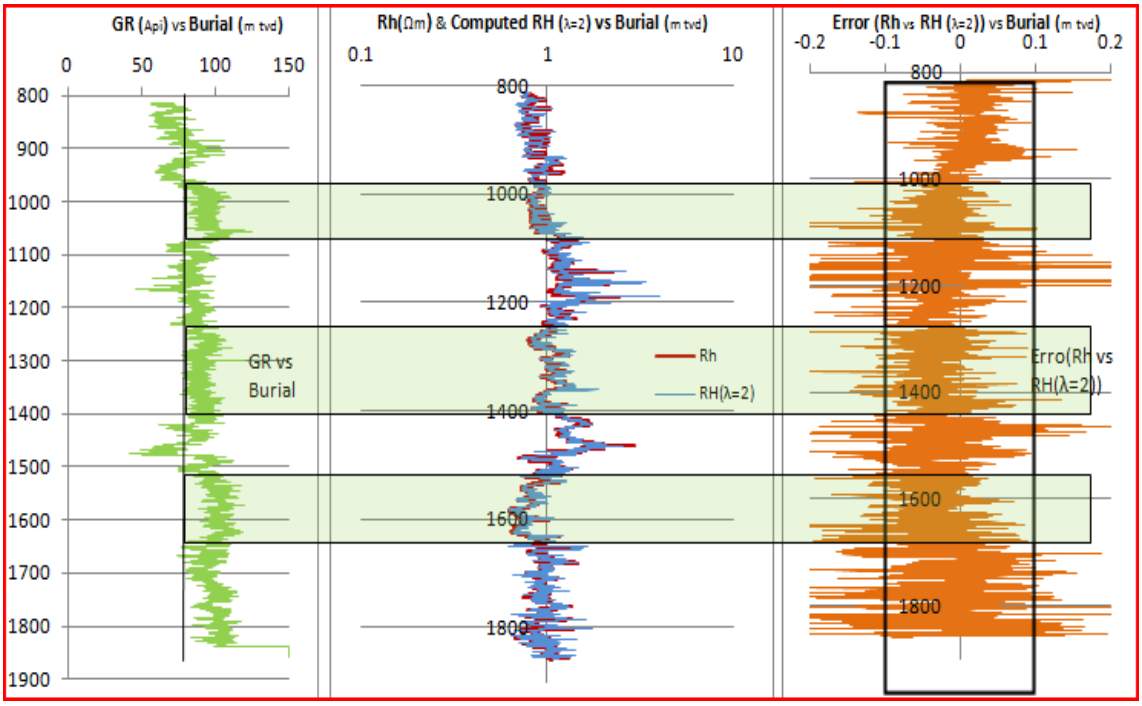

Figure 8.1 Joia Well. Validation of the equation 5 using constant coefficient of anisotropy 2 and error associated.

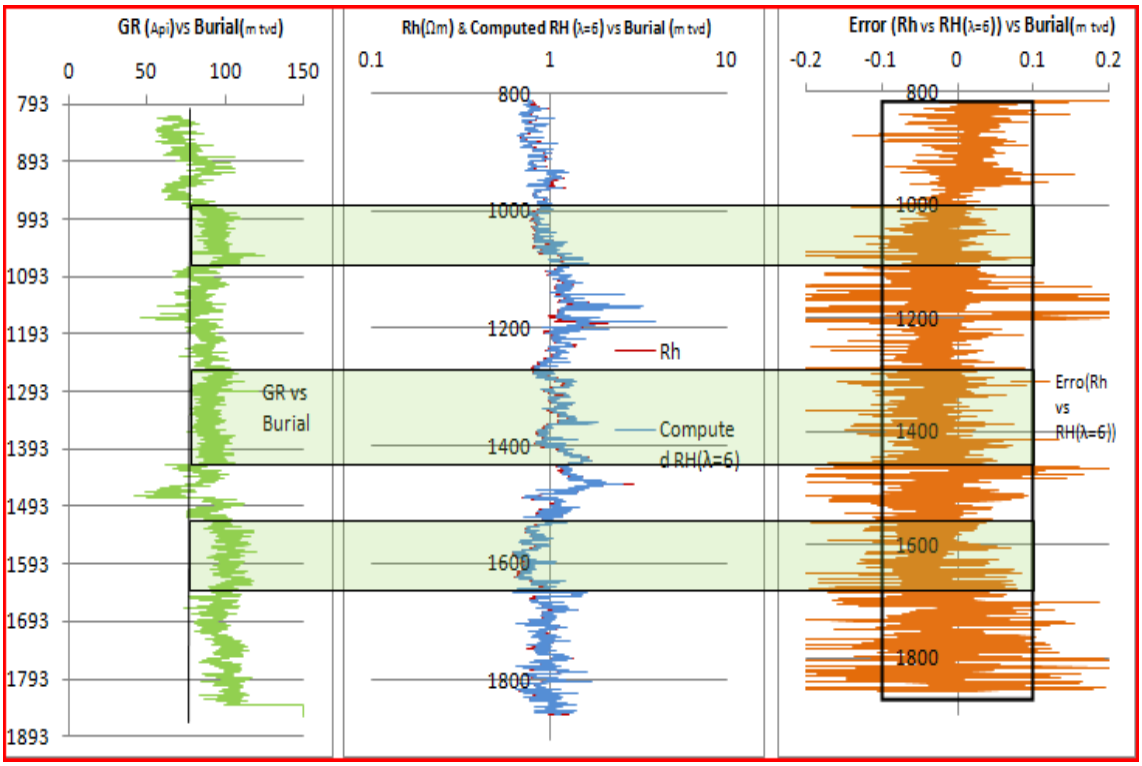

Figure 8.2 Joia Well. Validation of the equation 5 using constant coefficient of anisotropy 6 and error associated.

Obika Well

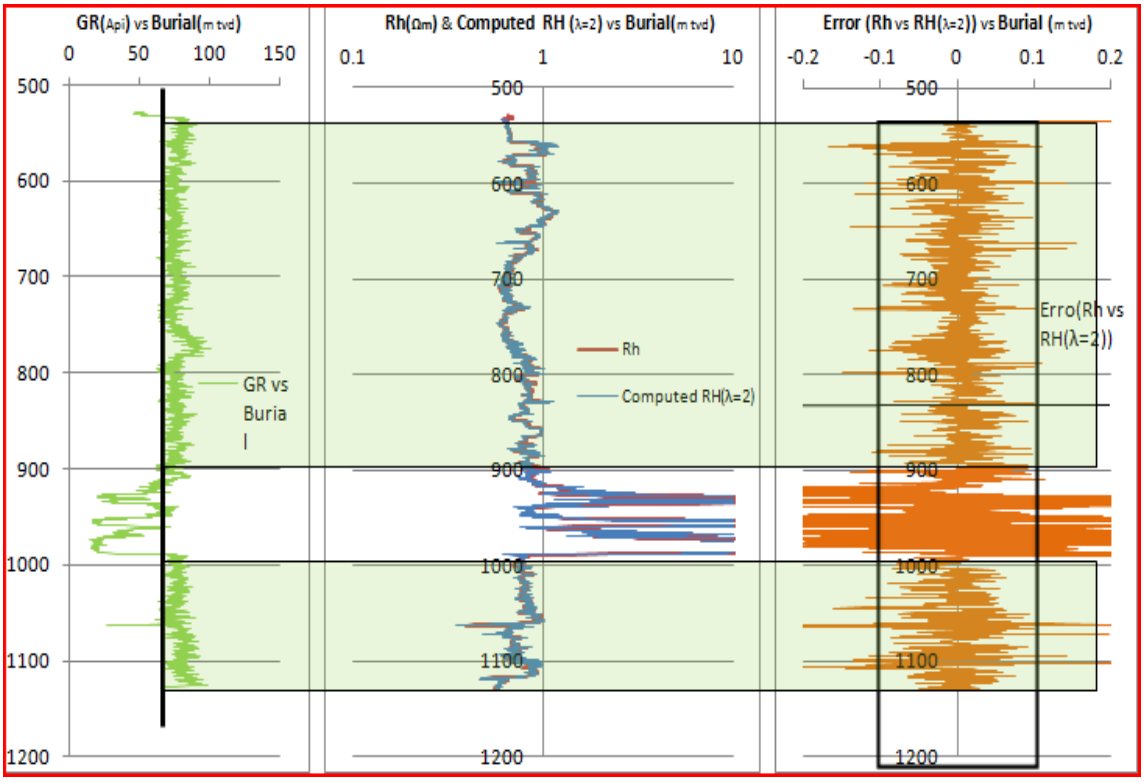

Figure 8.3 Obika Well. Validation of the equation 5 using constant coefficient of anisotropy 2 and error associated.

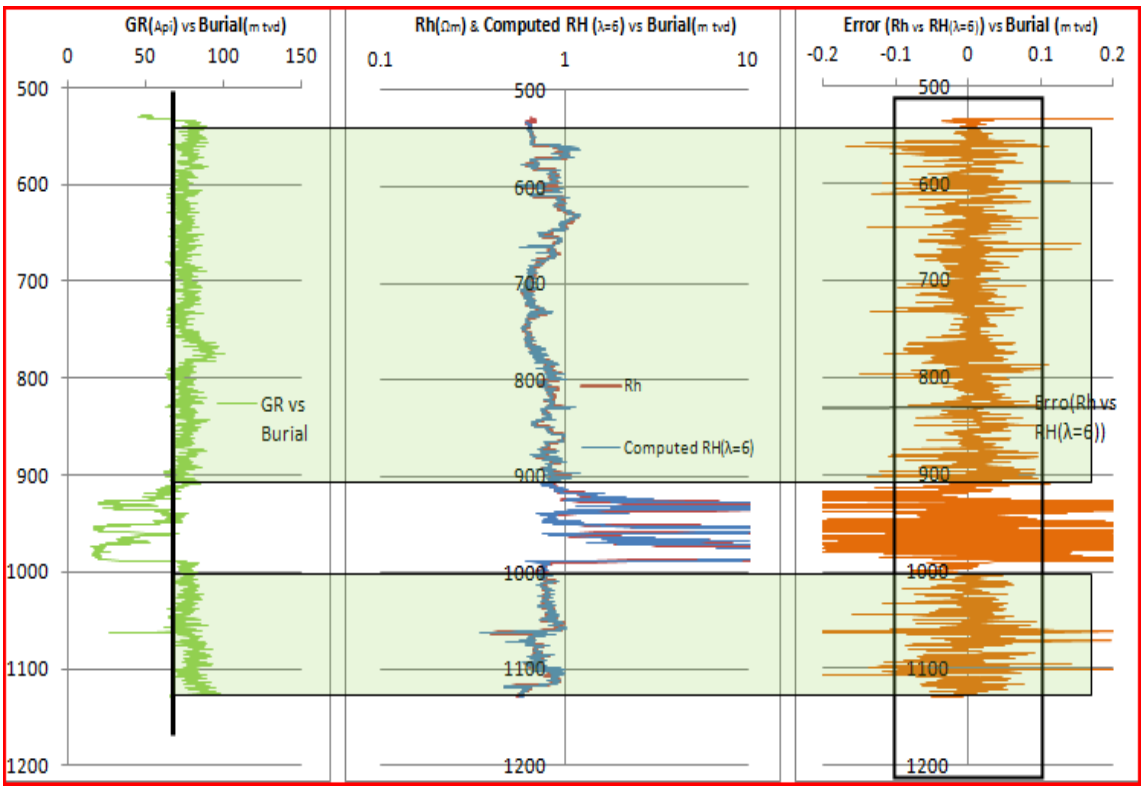

Figure 8.4 Obika Well. Validation of the equation 5 using constant coefficient of anisotropy 6 and error associated.

Moyo Well

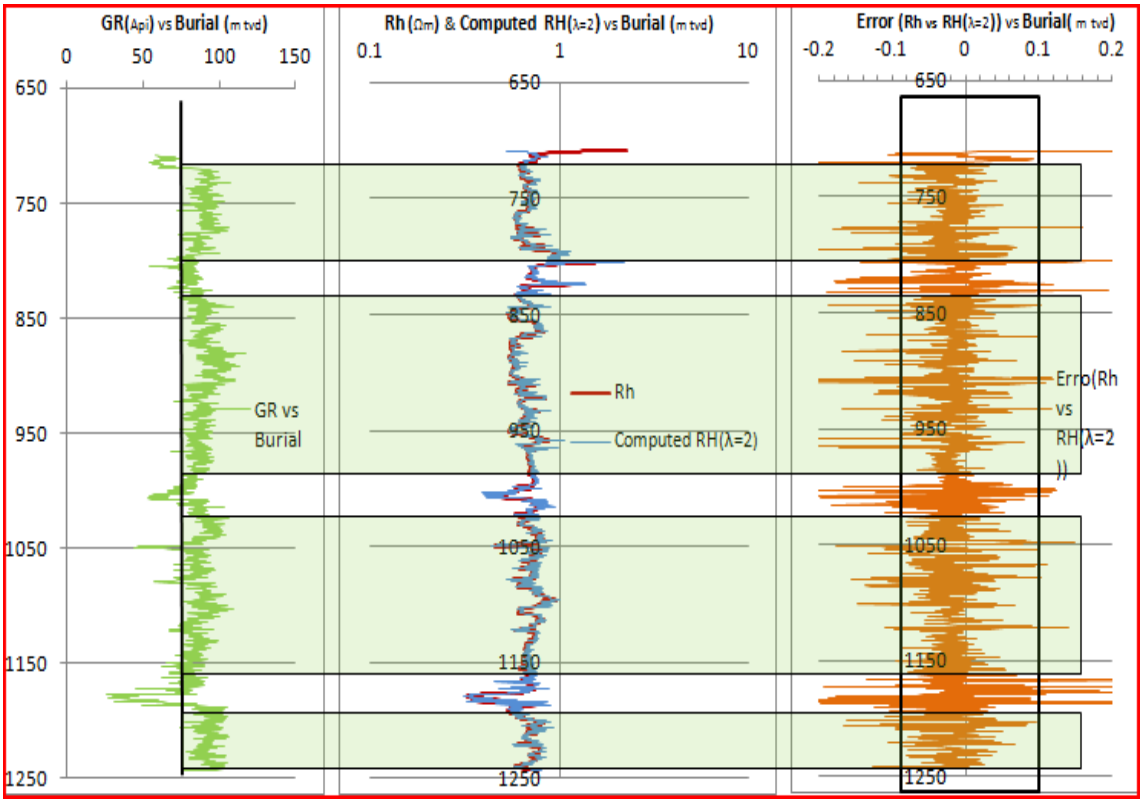

Figure 8.5 Moyo Well. Validation of the equation 5 using constant coefficient of anisotropy 2 and error associated.

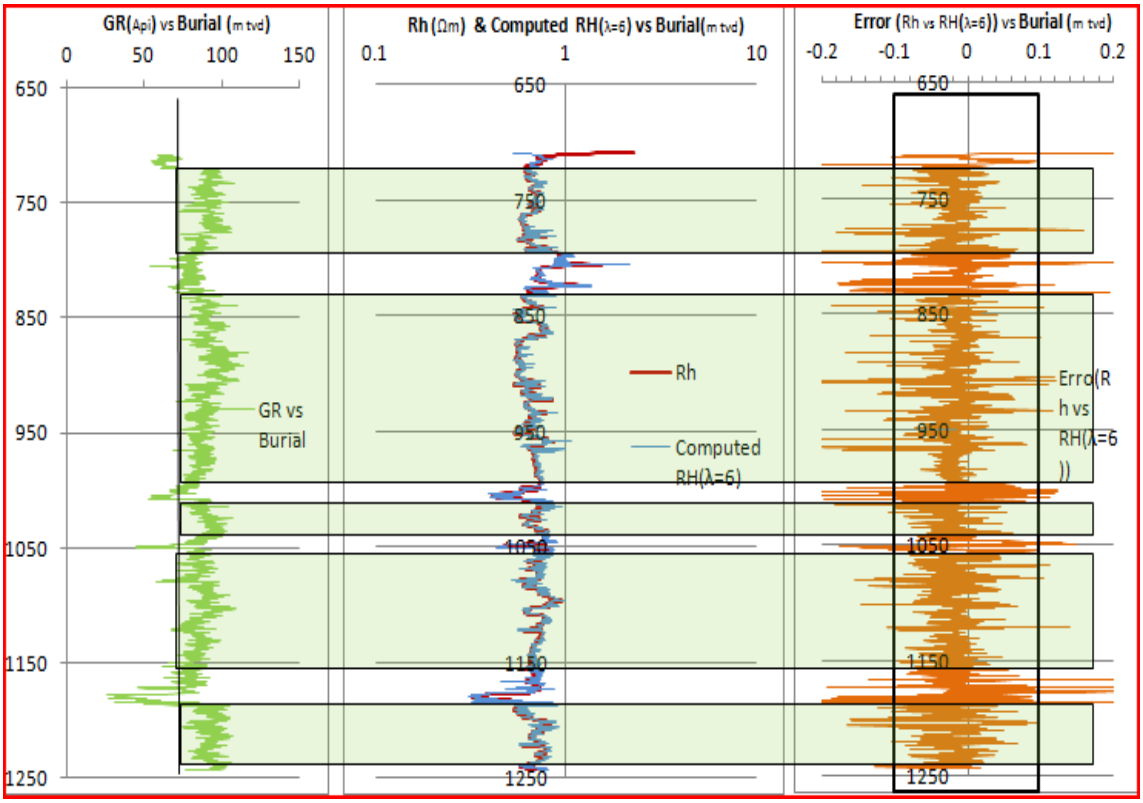

Figure 8.6 Moyo Well. Validation of the equation 5 using constant coefficient of anisotropy 6 and error associated.

Samalesso Well

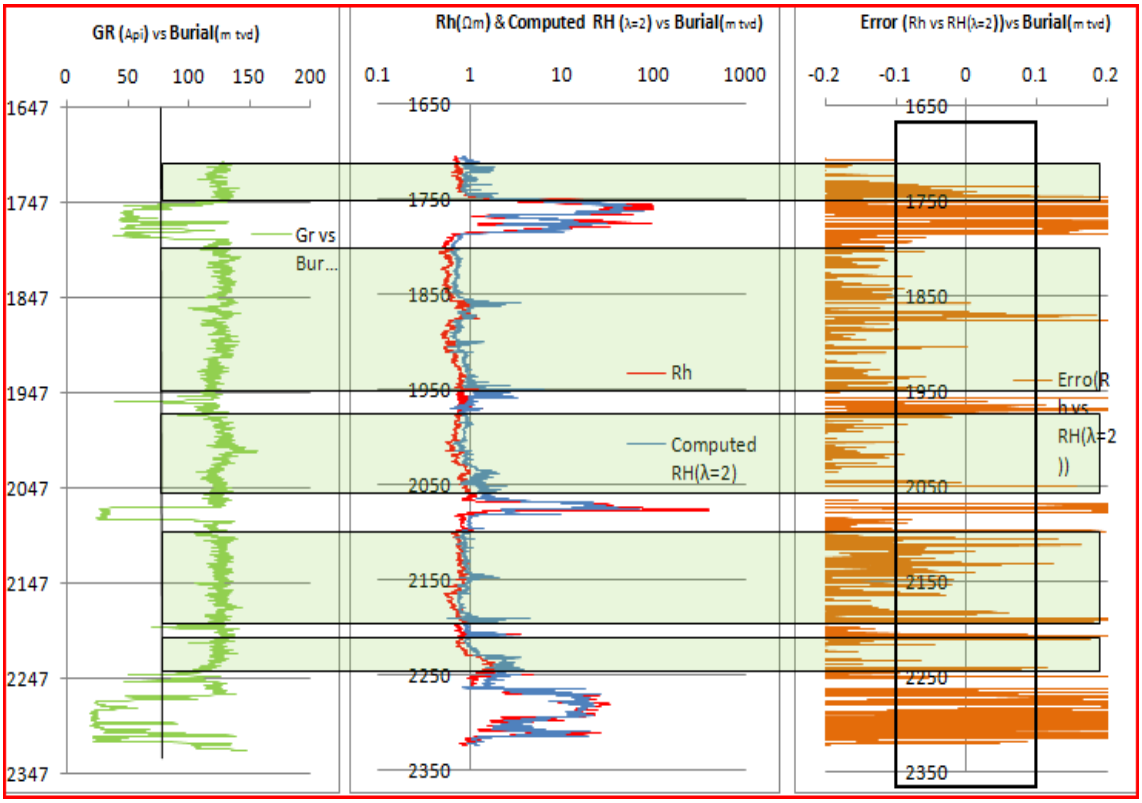

Figure 8.7 Samalesso Well. Validation of the equation 5 using constant coefficient of anisotropy 2 and error associated.

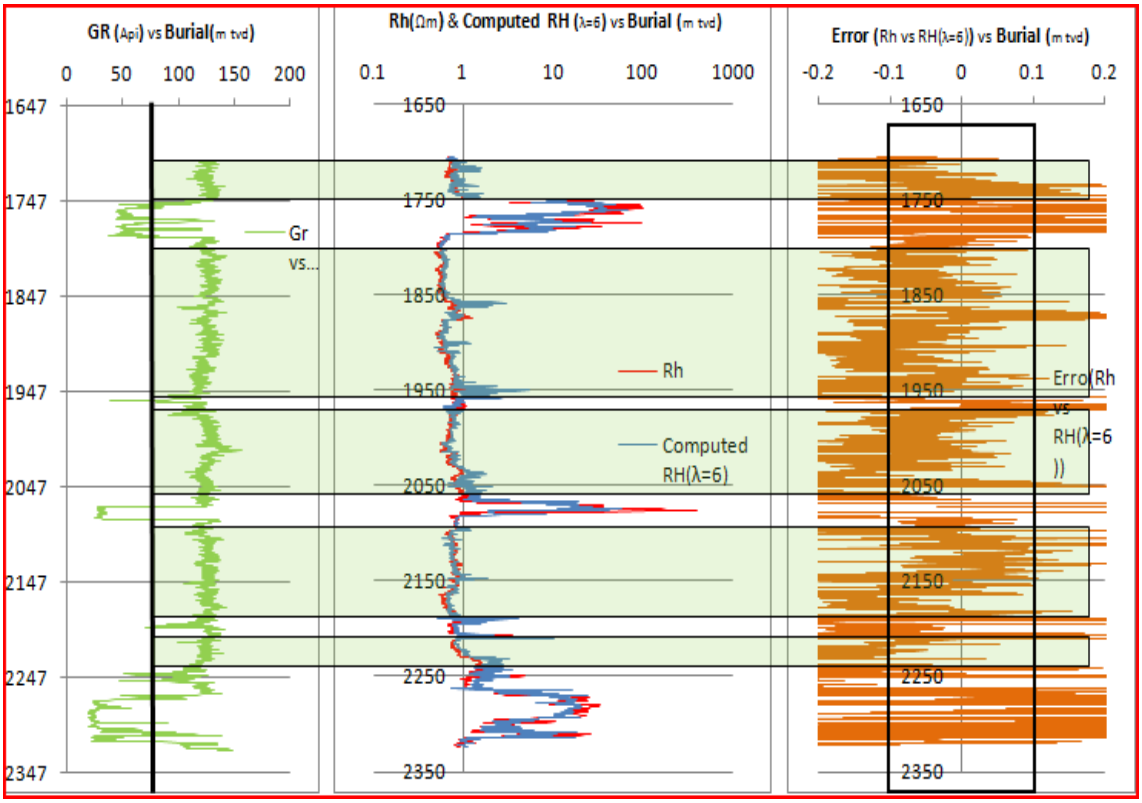

Figure 8.8 Samalesso Well. Validation of the equation 5 using constant coefficient of anisotropy 3 and error associated.

Lango Well

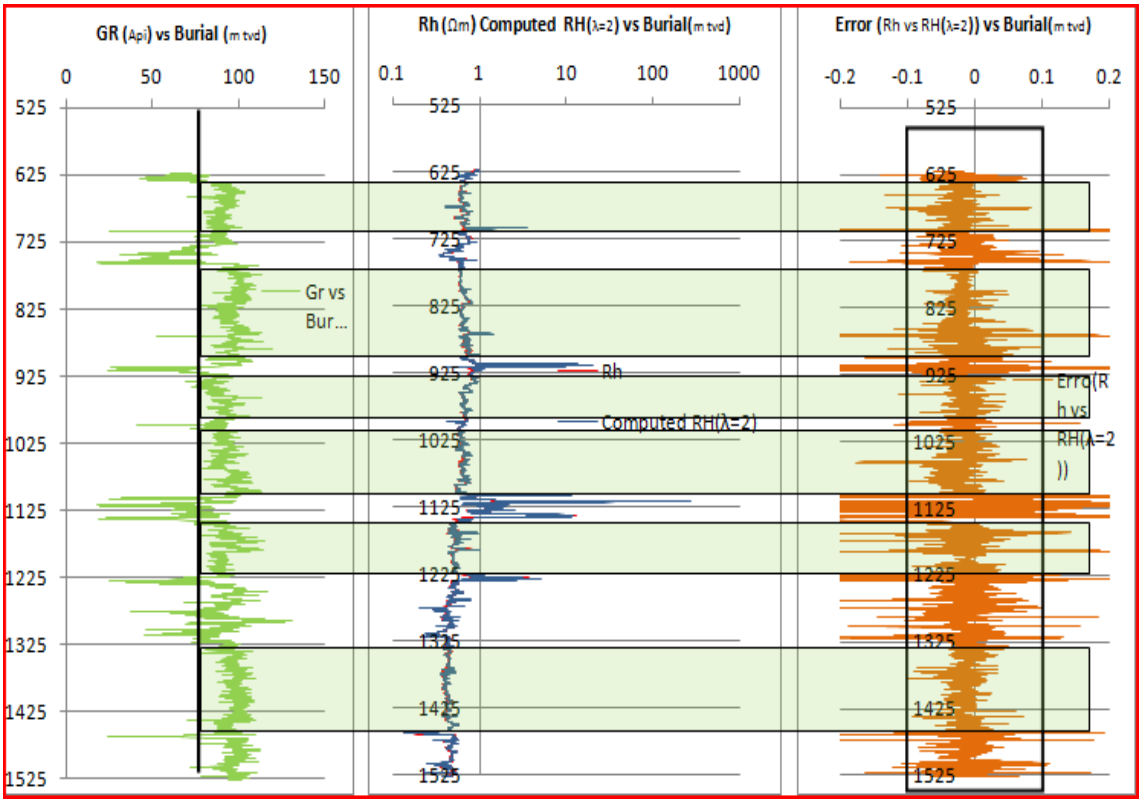

Figure 8.9 Validation of the equation 5 using constant coefficient of anisotropy 2 and error associated.

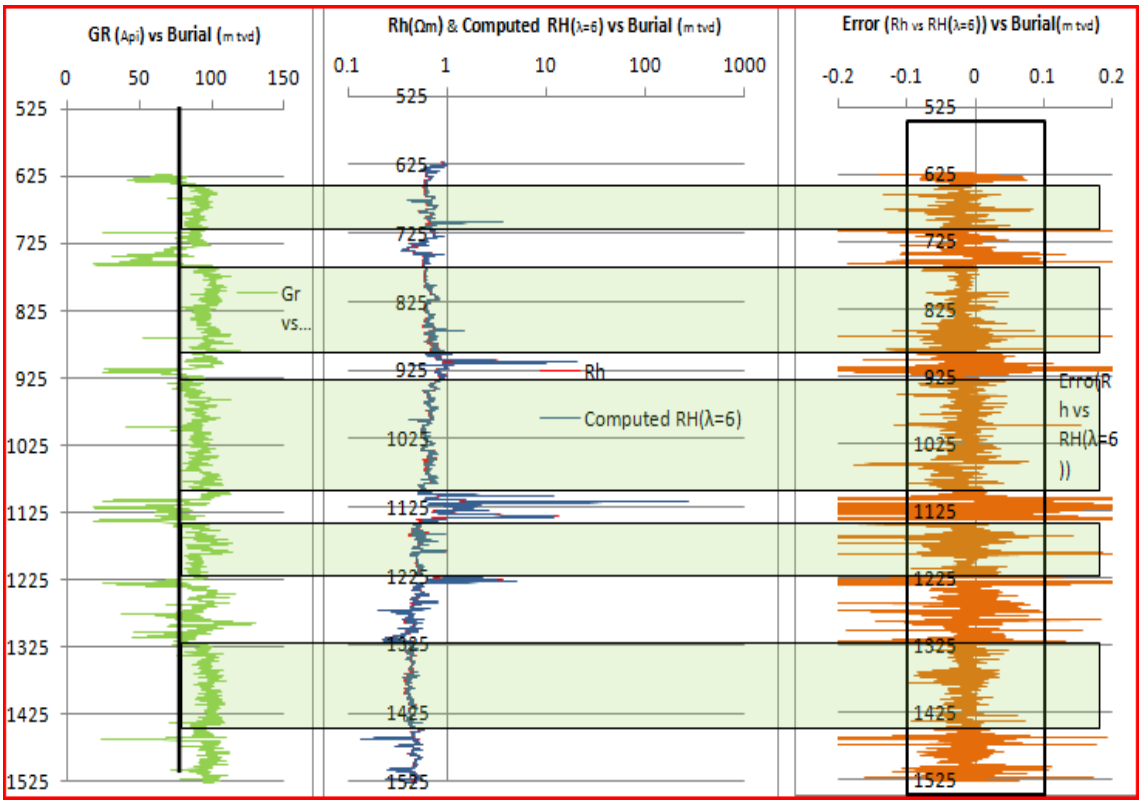

Figure 8.10 Lango Well. Validation of the equation 5 using constant coefficient of anisotropy 6 and error associated.

Global Error

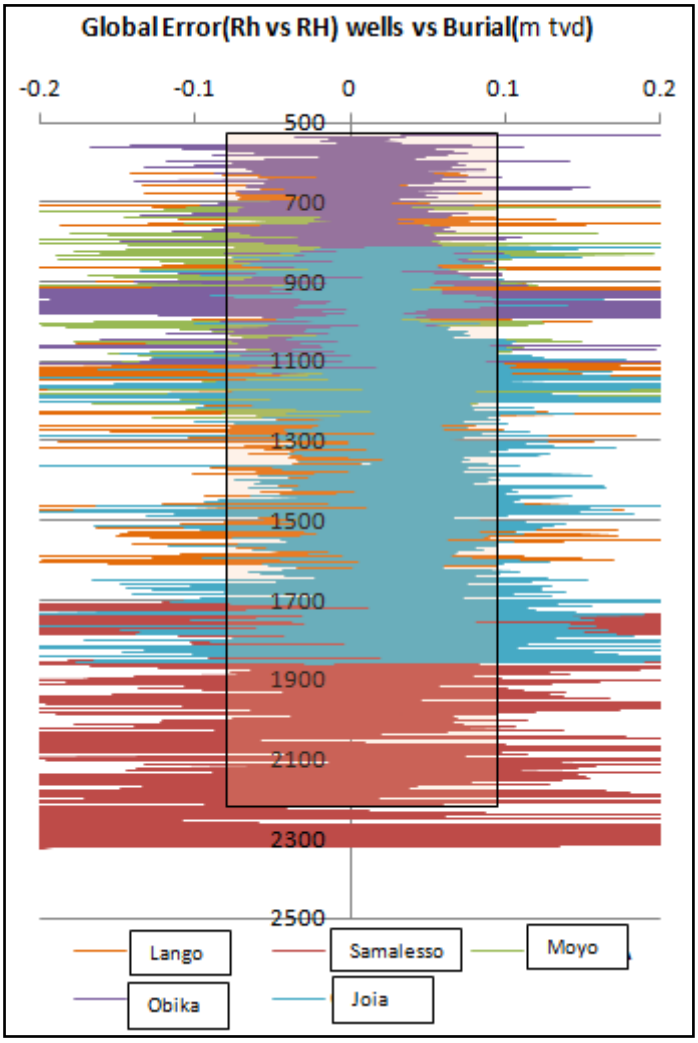

Figure 8.11 Global uncertainty of the correspondence between computed RH and measure resistivity.